Application of Solution State NMR to Structural Problems in Chemistry.

By

Ntai Martin Khoabane.

A thesis submitted in partial fulfilment of the requirements for the degree of Master of Science.

Department of Chemistry.

Durham University.

September, 2006.

Memorandum

The research presented in this thesis has been carried out at the Department of Chemisry of Durham University. None of this work has been submitted for any other degree.

Acknowledgements.

First and foremost I would like to thank the Lord almighty for the life he has given me.

My stay and study at Durham University was funded and supported by Canon Collins Trust to whom I am very thankful. I would also like to pass my gratitude to the National University of Lesotho for releasing me on staff development leave, my dependants' allowance, and funding my travel both ways.

I would like to thank my supervisory team: Dr. Alan M. Kenwright for his supervision and training and demonstrated kindness and patience. He motivated and encouradme during this period. I am also grateful to him for coming up with original ideas of a project on which I worked.

Dr. John Sanderson cannot be forgotten for his co-supervisory role. I am also grateful to Dr. Elizabeth Grayson for the supervision in chemistry and for the protection and deprotection of the mannoside compounds. Dr. Louise Natrajan, I thank you for the lanthanide complexes I worked on. I would also like to thank Mr. Ian McKeag and Mrs Catherine Heffernan who contributed a lot to my training in solution state NMR.

Other groups of people who contributed to my training need to be mentioned: all my lectures in the taught modules, the mass spectrometry facility and all the Chemistry Department staff.

Last but not least my family members. Most importantly my wife and son who suffered the loneliness of my being thousands of miles away from them without complaint.

Abstract

Nuclear Magnetic Resonance (NMR) spectroscopy is a robust, non invasive technique applicable in structure determination as well as in the study of dynamic behaviour of chemical compounds. This thesis is in two sections, the first dealing mainly with a structure determination application of NMR and the second dealing mainly with a study of dynamic behaviour.

Section 1

NMR characterisation of carbohydrates has proved challenging because of the limited chemical shift ranges of both the proton and carbon signals. The broad signals due to the labile hydroxyl protons cause further complications by overlapping proton signals from the ring. Protecting group chemistry is vital in the preparation and manipulation of synthetic carbohydrates and can potentially help with the assignment of the (otherwise extremely complicated) NMR spectra of carbohydrates. However, the widely used benzyl protecting group can make the spectrum more difficult to interpret because the benzyl CH_2 proton signals often come in the same region of the spectrum as the anomeric protons, usually used as reporter groups of carbohydrates and the benzyl CH_2 carbon signals come in the same region as the carbohydrate ring carbons. This section reports the invetsigation and application of a family of alternative protecting groups, namely various fluorobenzyl groups, which have not been used in carbohydrate chemistry before. With pentafluorobenzyl, the proton chemical shift dispersion is improved, and the CH_2 and carbohydrate ring carbon signals are shifted to lower frequency, considerably simplifying the task of assigning the carbon spectrum, facilitating the interpretation of all ^{1}H-^{13}C correlation experiments (HSQC, HMQC, HMBC).

Section 2

Cyclen complexes of lanthanide (III) ions have found use in magnetic resonance imaging (MRI), luminescence imaging and assay studies. In particular, europium (III) complexes have potential in anlytical, forensic, and biomedical applications based on their impressive emissive properties. However, the emissive properties are modulated by the thermodynamic stability and kinetic inertness of the complexes. For biomedical applications, chelation is necessary to avoid europium toxicity that may be triggerd by accidental dissociation of the complex and release of the metal *in vivo*. A new cyclen europium(III) complex with pyridyl pendant ligands instead of the usual acetate groups has been synthesised by a group at Manchester University. The pyridyl ligands confer higher emmisive intensities to the complex, to enable applicability of the complex in time gated measurements. The chemical structure determination of the compound was accomplished by ^{1}H, ^{13}C, COSY, HMQC / HSQC and EXSY NMR experiments. Selective inversion experiments data were evaluated using the CIFIT simulation program, and showed that in aqueous solutions from -0.2º C to 107.6º C the dominant dynamic process is flipping of the pendant (pyridyl) arms, and isomerism is biased towards the twisted square antiprism (TSAP). .

Contents

SECTION 1

"The chemistry and biology of carbohydrates has been a Cindarella field: an area that involves much work but, alas, does not get to show off at the ball with her cousins, the genomes and proteins"[1]

1 Introduction.

1.1. Description of saccharides, distribution, properties and function

Carbohydrates are one of the major classes of compounds, making up more than 50% of the dry weight of the earth's biomass. Their role in energy transfer and storage, metabolic intermediates provision, support and protection in living systems have been well studied and established.[2-4]

Of current interest to the biochemical fraternity are glycoconjugates, in which oligomeric carbohydrate subunits (glycans) are attached to proteins and lipids to form glycoproteins and glycolipids. The glycoconjugates are found on cell surfaces. An immense number of cell to cell interactions involve the interaction of the oligosaccharide of a glycoprotein (acting as a ligand) on the surface of one cell and a receptor protein (lectin) on the surface of the other. Such a cell to cell interaction triggers biological events such as fertilization, viral infection and the immune response to mention a few.[5-7]

The cell surface bound glycoconjugates interact with receptor proteins called lectins.By having receptor sites to which glycoconjugates bind, lectins are thought to "read and understand the messages" encoded on the glycoconjugates.[8, 9] The receptor-ligand binding is specific and is shown in Scheme 1.

Natural glycoconjugate amounts are very small and are of low chemical stability.[5] To thoroughly study, understand and exploit these biochemical processes and interactions in pharmaceutical therapeutics, scientists need to synthesise, in sufficient amounts, and characterise glycoconjugates to mimic the receptor-ligand interactions occurring *in vivo*.[5, 6] Recently, due to the emerging antibiotic resistance, scientists have resorted to using certain peptides as antibiotics that potentially bind to bacterial cell surface carbohydrates intefering with the cell signalling mechanisms that sustain their survival. [10]

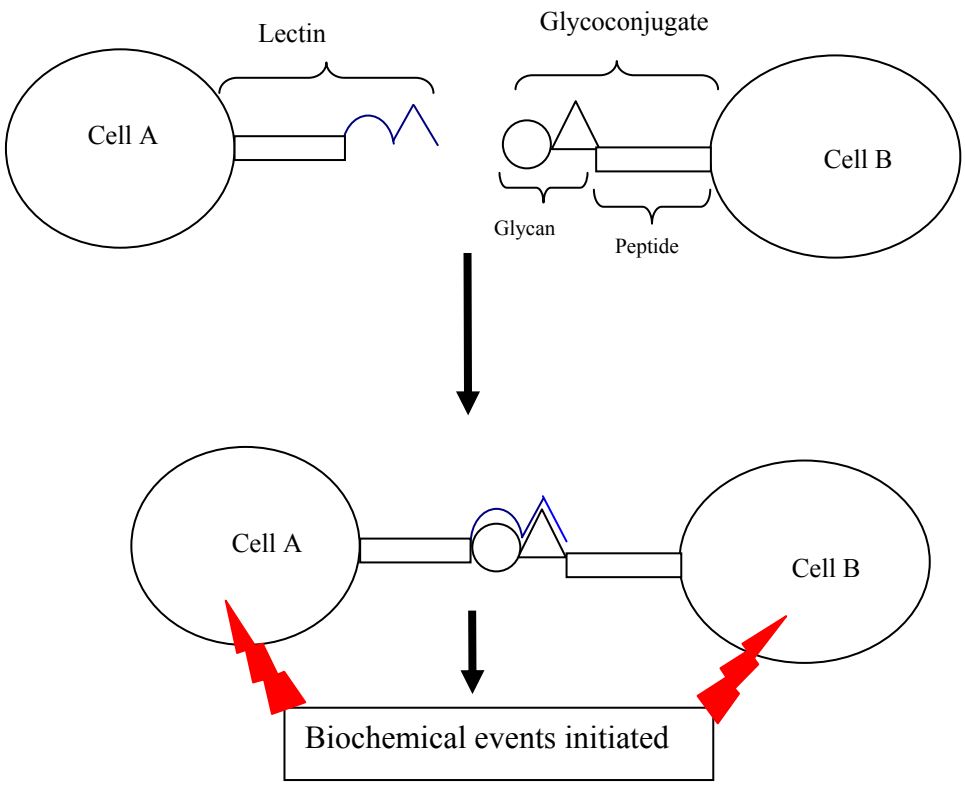

Scheme 1: A schematic showing cell to cell interaction leading to biological events.

Carbohydrates have high structural diversity. This arises from different the configurational, conformational and linkage possibilities available to them. Any chiral center can have the hydroxyl group in either the axial or equatorial configuration. The hydroxyl at carbon 1 of glucose can be in either the axial or equatorial orientation giving rise to an α or β anomer (Figure 1). Analogously α or β linkages can be formed between two monosaccharides in an oligosaccharide. A different orientation at carbon 2 of glucose gives rise to mannose. Mannose is a C2 epimer of glucose (Figure 5).

α-D-glucose β-D- glucose

Figure 1: The figure shows the different orientations that can be adopted by a hydroxyl group at carbon 1, leading to either an α or β anomer.

The cyclic monomers can adopt either of the two conformers; the $^4C_1$ and $^1C_4$. For protected glucose, galactose and mannose, the $^4C_1$ is preferred (Figure 2). Protected rhamnose, on the other hand, favours the $^1C_4$ conformation.

Glucose $^4C_1$ conformer Rhamnose $^1C_4$

Figure 2: The figure shows conformations preferred by protected glucose ($^4C_1$ conformation minimizes crowding by having maximum number of equatorial substituents) and protected rhamnose ($^1C_4$).

Any two monomers can be linked via several different positions. For example, monomers can link via a 1-2, 1-3, 1-4, or 1-6 linkage.1-4 and 1-6 glycosidic linkages are shown in Figure 3 as an example. In addition, linkage stereochemistry can be α or β.

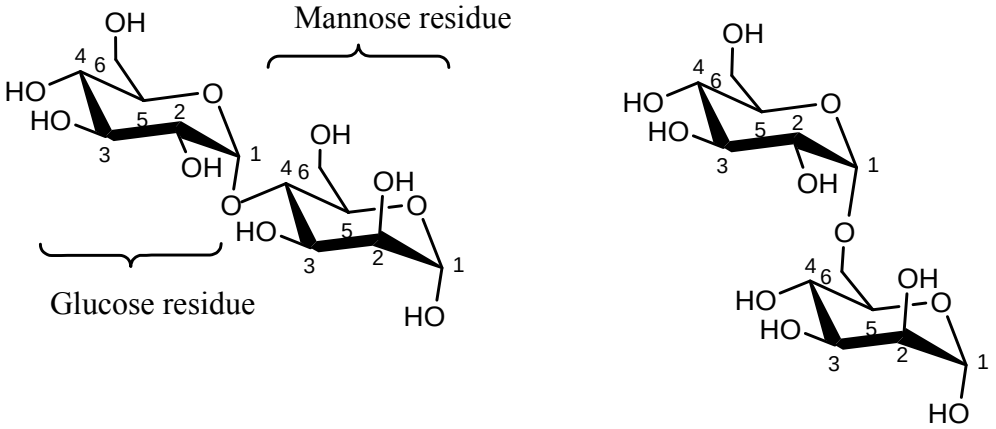

Figure 3: An α 1-4 and α 1-6 linkage between glucose and mannose. The figure also illustrates the difference in stereochemistry at position 2 of the monomers, leading to glucose and mannose subunits.

A problem in oligosaccharide chemistry is synthesizing molecules with the desired linkage, stereochemistry and composition, given the diversity of possible linkages and stereochemistry. Hence a need for Nuclear Magnetic Resonance (NMR) to find out if the desired oligosaccharide has been synthesised.

1.2. Structural determination of sacchrides.

X-ray crystallography is a technique in which electromagnetic radiation in the region 10 to 0.01 nanometers is bombarded through a solid substance to produce a pattern, providing information about the lattice of the closely spaced atoms, and leads to molecular structure. Because of the poor crystal forming capabilities, many oligo-saccharides are better analysed by powder diffraction. A disadvantage with this technique is the ability to provide information about only one conformation at a time. [11]

Mass spectrometry is limited to molecular weight determination. [12, 13] Recently, the scope of MS has been extended to structural characterization of oligosaccharides. [12-14] However, this extension comes at a price. Several techniques have to be combined to achieve a complete characterization. MALDI is used together with methylation and exoglycosidase. These involve hydrolysis and separating the oligosaccharide fragments by GC/MS before MALDI and ESMS are used. Thus mass spectrometry is not suitable for routine use. An advantage with mass spectrometry is its ability to determine molecular weights from samples in the microgram range.

Nuclear Magnetic Resonance spectroscopy, NMR, is a non-invasive, non-destructive and robust tool for chemical structure determination. It is also capable of simultaneous determination of compounds in mixtures. Several parameters associated with NMR aid in the complete chemical structure determination. Chemical shifts give information about the different chemical environments present in a molecule. Coupling constants help to establish connectivity between the different chemical environments in a molecule. This leads to realization of different fragments contained if the coupling network is not continuous. The Nuclear Overhauser Enhancement (NOE) together with the coupling constants help establish the stereochemistry, showing the spatial arrangement of different groups with respect to each other.

There are a number of problems making NMR application in carbohydrate chemistry not so attractive. The similar chemical environments of non-anomeric spins, differing only a

little in their coupling patterns and stereochemistry means that the proton spectra are highly crowded within a region less than 1 ppm. This is aggravated by the presence of the exchangeable protons on the hydroxyl groups, causing broad signals which overlap the narrow closely spaced lines of the ring proton signals.

The problem is not so bad in the carbon-13 spectra of carbohydrates, which cover less than 20 ppm [11] of *ca.* 200 ppm of the total carbon-13 spectral width. The main problem is poor sensitivity, requiring tens of milligrams of sample. Solubility often puts the ultimate limit to carbon-13 acquisition.

1.3. Two-dimensional spectroscopy as an aid for spectral assignment.

Carbon-13 NMR is limited by the low natural abundance of the NMR-active nuclei at 1%. Relatively large amounts of sample are needed to acquire decent ^{13}C NMR spectra, but this may be limited by solubility. Heteronuclear correlation experiments like Heteronuclear Multiple Quantum Coherence (HMQC) combine the favourable C-13 spectral dispersion with the higher proton sensitivity to unravel molecular structure. [15] This aids the assignment and confirmation of highly overlapped proton spectra.

There is also another very similar technique, Heteronuclear Single Quantum Coherence (HSQC). The difference is that with the former multiple quantum coherences are used while in the latter single quantum coherences are used. [15-17] Coherences are magnetizations. HMQC is less sensitive to experimental imperfections and miscalibrations while HSQC is easily affected, especially when applied to the low natural abundance nitrogen-15 correlation. Pulse field gradients have been reported and successfully implemented in these pulse sequences to remove artifacts associated with these two experiments. The data provided by HMQC and HSQC have since differed in the finer details which are beyond the scope of this project. HSQC is better for large biological molecules while HMQC is a method of choice for small organic molecules. [18]

The simplified version of an HMQC experiment is shown in Figure 4. The magnetization, (also referred to as coherence) of the highly sensitive proton is transferred to the carbon-13 spins, is then spin labelled with the carbon-13 frequency during evolution time, t_1, then transferred back to the proton spin system for detection.

The proton spins are exited by a 90º Rf pulse, which tips the magnetization away from equilibrium. This is then followed by an evolution time, τ, during which the heteronuclear coupling evolves, generating antiphase magnetization. The evolution time is set such that it allows evolution of coupling. Typically, an optimum value of $\tau = 1/(2 .{}^1J_{CH})$ is usually set. A second Rf pulse (B) applied to the carbon-13 spins, transfers the proton antiphase magnetization to the carbon via scalar coupling. Then evolution time, t_1, follows during which the antiphase magnetisation is spin labelled with carbon-13 spin frequency offset.

Another 90º pulse (D) is applied to the carbon-13, transferring the carbon-13 frequency spin labeled magnetization back to the proton spin system. This is followed by a second delay, τ, during which the antiphase coherence evolves into the in-phase coherence. At exactly halfway through the application of the two carbon-13 pulses, a 180º pulse (F) is applied to the proton spins. This serves to refocus evolution of the proton offset so that the excited magnetization does not evolve under the proton spin offset, leaving the carbon-13 spin offset to dominate. In addition, this filters out the proton signals which are not scalar coupled to carbon-13 nuclei spins.

The spectrum is acquired by a proton detection mode, while simultaneously applying decoupling to carbon-13, so as to maintain the usual high intensity singlets.

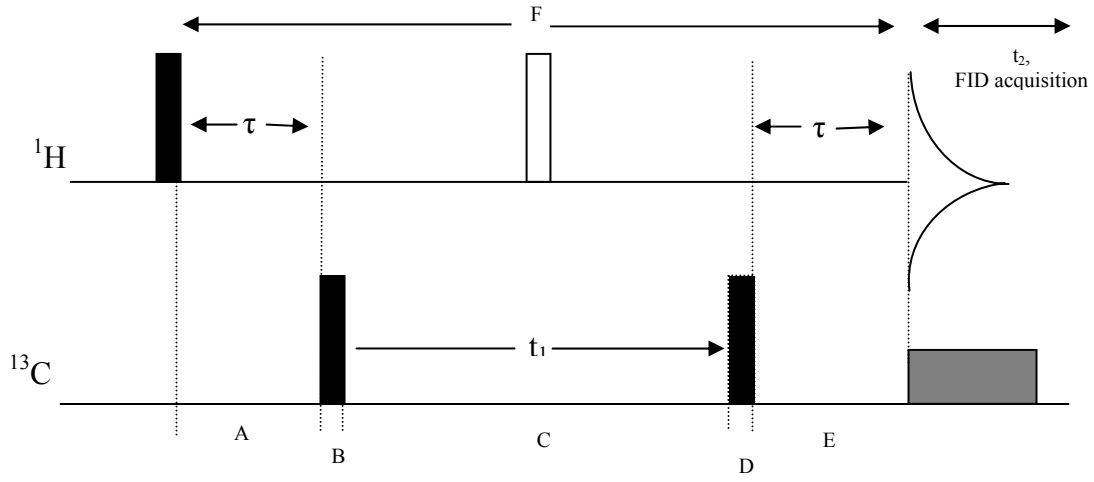

Figure 4: A schematic diagram of the HMQC experiment. The black rectangles represent 90º pulses and the grey rectangle shows the decoupler pulse. Adapted from Understanding NMR Spectroscopy. [17]

Heteronuclear Multiple Bond Correlation (HMBC), reports two and three bonds correlation. It is very similar to HMQC, the only difference being that the second evolution period, τ, and the refocusing pulse are absent (Figure 5). Signals are detected immediately after the t_1 period without using broad band decoupling. Broad band decoupling is not used because anti-phase coherences are detected this time, decoupling will squash the anti-phase signals to zero. HMBC records signals due to evolution of multiple bonds, with relatively small coupling constants, typically ^{n}J= 5 - 10 Hz are detected. HMQC records evolution of single bond coupling, with very large coupling constants, ^{1}J= 100-200 Hz.

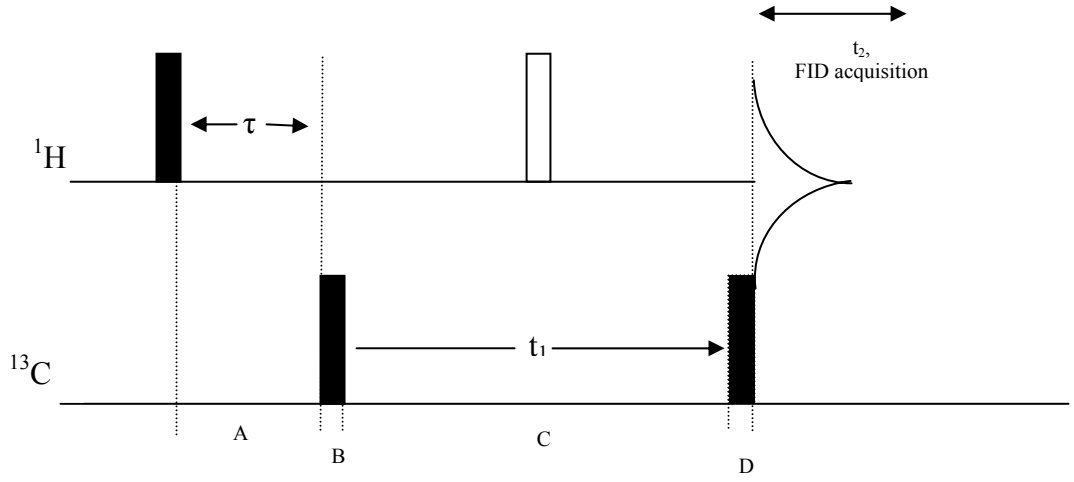

Figure 5: The HMBC pulse sequence. The sequence is very similar to HMQC, except that there is no broad band decoupling, the second evolution time, τ, and the refocusing pulse. Coupling evolves under long range heteronuclear bonds. Adapted from Understanding NMR Spectroscopy. [17]

Homonuclear two dimensional techniques such as Correlated Spectroscopy, COSY, aid in tracing out the coupling network in a molecule. [19] The high proton sensitivity makes sure that sample size is not a problem, and a decent spectrum can be acquired within ten to twenty minutes. This is a handy tool to begin assignments when the chemical shift of any one of the protons can be assigned by other means. However, proton crowding may hamper its utility, and very similar geminal and vicinal coupling constants can lead to ambiguous assignments. Combined with any of the heteronuclear techniques mentioned above, assignments are simpler, and ambiguities can be straightened out.

The COSY pulse sequence is the simplest commonly used two dimensional (2D) sequence, utilizing only two Rf pulses as shown in Figure 6 below. The *z*-magnetization is subjected to a preparative 90º pulse. The resulting magnetization evolves for time t_1 during the evolution period. Evolution of coupling takes place between any two scalar coupled spin systems. A 90º read pulse is applied, flipping the magnetization along the *x*-*y* detector plane during which detection occurs, t_2. The procedure is repeated several times systematically incrementing t_1 for each scan.

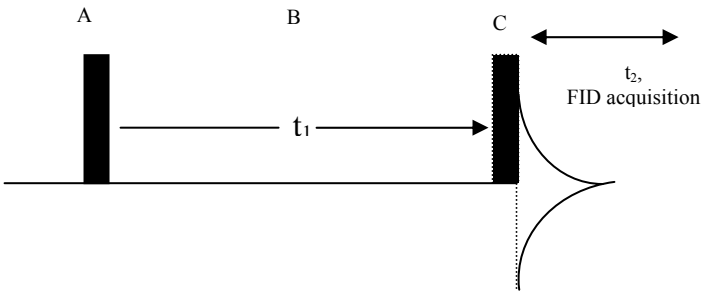

Figure 6: The COSY pulse sequence. Adapted from Understanding NMR Spectroscopy. [17]

A series of free induction decays (FID) as a function of t_1 increments is acquired and stored in computer memory. These time domain signals are Fourier Transformed into the frequency domain which is then plotted on the f_1 and f_2 axes from the t_1 and t_2 data respectively. Two types of peaks are produced, the diagonal and the cross peaks.

A peak with the same coordinates along the f_1 and f_2 on the spectrum results in a diagonal peak. If the coordinates are not the same on both axes, this leads to a cross peak. The cross peak correlates coupling partners. This is shown schematically in Figure 7 and is the basis for interpretation of a COSY spectrum.

Supposing we have a four spin system, A,B,C,D. If there is scalar coupling between A and D, a cross peak modulated at the frequency of A (ν_1) in the f_2 and that of D (ν_2) in the f_1 will result showing coupling between the two spins. Spins with no coupling will develop peaks only at frequencies $\nu_n = \nu_n$, the diagonal peaks.

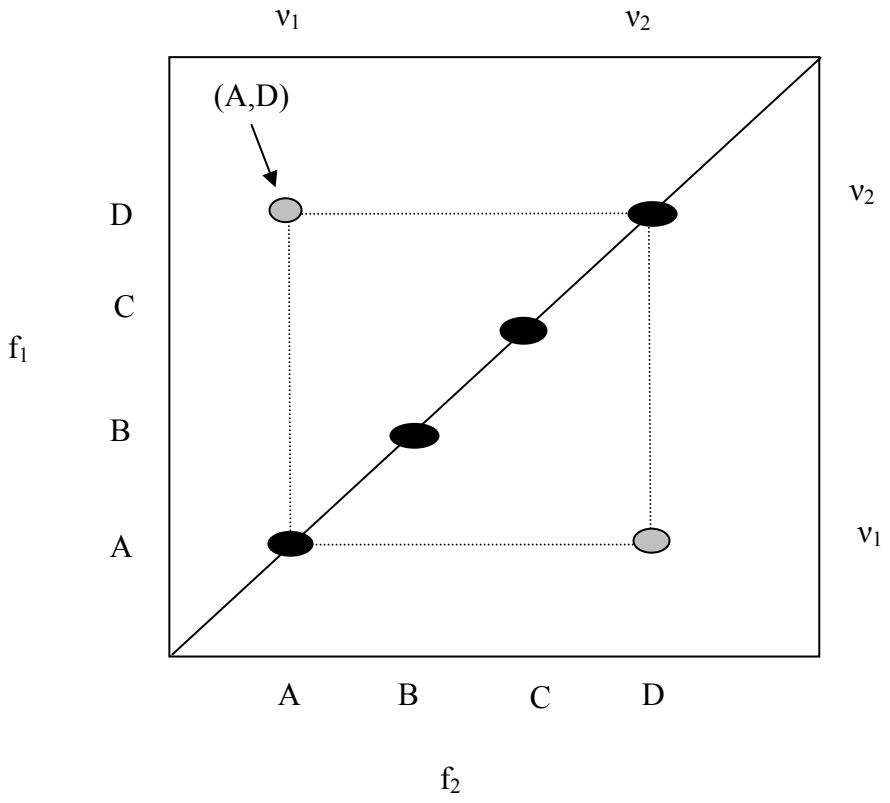

Figure 7: The COSY pulse sequence. Adapted from Understanding NMR Spectroscopy. [17]

Tipping magnetization of spin A, and setting in the evolution time, t_1, allows spin A magnetization to evolve under its offset (ν_1) and under its coupling to spin D. During t_1, spin A magnetization also becomes anti-phase. The second pulse transfers the anti-phase spin A magnetization to spin B through scalar coupling. This produces the cross peak (A,D), modulated at the frequency of spin A (ν_1) in the f_2 and that of spin D (ν_2) in the f_1. If the coupling constant is zero, no transfer of anti-phase spin A magnetization to spin D, and hence no cross peak. For those spins which do not evolve coupling between them during t_1, no COSY correlation is seen. Only the diagonal peaks will show up, at frequencies corresponding to the one dimensional spectra of the spins ($\nu_n = \nu_n$ for A,B,C,D). The optimum value of t_1 is when $t_1 = 1/2J$.

1.4. NMR methods previously applied in carbohydrate chemical structure determination.

The structural diversity *(vide supra)* of carbohydrates impinges on the already limited proton dispersion, by introducing a varied array of closely spaced chemical shifts and coupling constants, rendering carbohydrate NMR interpretation very difficult. [1]

A number of attempts have been made in simplifying carbohydrate NMR spectral interpretation.

Chemical methods have been tried to solve the problem of spectral overlap in carbohydrates. [20] Free carbohydrates are soluble in deuterium oxide (D_2O) and dimethyl sulfoxide (DMSO). Solutions for NMR have been prepared in D_2O in which there was exchange with the hydroxyl of the carbohydrate. This removed the broad overlapping peak due to exchange but introduced an HOD peak which sometimes obscured the anomeric proton. DMSO has since proved to be a better solvent [21] as its carbohydrate spectra are well resolved.

Sometimes temperature and pH were used to move the HOD peak out of the spectral range of the ring protons. Carbohydrates were also converted to their methyl or trimethyl silyl ethers to remove the hydroxyl groups from the molecules.

The proton two dimensional J-resolved measurement on carbohydrates was reported by Hall and coworkers. [22, 23] In their work, they showed that this technique was able to separate the chemical shift effect from the scalar coupling, bringing good resolution. This was a good result for the highly overlapped carbohydrate proton spectra. However, the technique did not address the problem of assigning individual resonances. Matching of spin splittings and spin decoupling experiments become limited as a result. Resolution was enhanced by application [24] of Lorentzian and Gaussian transformation. Selective decoupling was also used for spectral assignment. The application of the technique was extended to underivatised sugars, as a result. However, the disadvantage is that this can only apply to proton spectra.

Two dimensional homonuclear experiments like COSY and SECSY (Spin Echo Correlated Spectroscopy) were first reported and applied to carbohydrates by Bernstein [19] and coworkers. These were modified versions of the 2D J resolved spin echo experiments which comprised three distinct parts: preparation, evolution, mixing (*vide supra*). Mixing is placed in the middle of evolution in SECSY.

As applied on trideuteriomethyl 2,3,4,6- tetra-*O* (triduterioacetyl) α-D-glucopyranoside, these techniques showed great promise. Connectivity and coupling is established by inspection. High resolution combined with good signal to noise ratio make the technique robust. Armed with symmetrization data processing, signal to noise ratios become superb. Introduction of pulse field gradients made these experiments fast, where acquisition and processing can be accomplished in about ten minutes with gradients as opposed to one hour when phase cycling was used.

There are problems they cannot solve however. Cross peaks are difficult to see when linewidths are wider than coupling constants. Cross peaks close to the diagonal are sometimes difficult to resolve and extract coupling information from them.

Blundell and coworkers [25] acquired spectra of a free hexasaccharide (glycosaminoglycan hyaluronan) at 900 MHz field. They showed that higher magnetic fields have an advantage of good dispersion, high resolution and signal to noise. Higher magnetic fields also eliminated the coupling-associated distortions and artifacts. However, the cost-benefit analysis is not great here. A resolution enhancements factor of 1.5 is achieved at costs 2 -3 times higher, in terms of facilities, which are greater than the enhancement. A 900 MHz, instrument is costly in terms of money and space needed to accommodate it.

Use of transform techniques other than [26] the Fourier transform aid in spectral resolution. It was demonstrated by Armstrong and coworkers that when a Filter Diagonalization Method (F.D.M.) processing method was used, improved spectral resolution resulted. Another advantage was that the method does not require phase sensitive data and reduces the data size to 1/8. An isotag is used, from which magnetization is transferred to the ring

protons, increasing their spectral range. A drawback with the technique is a need for more computing power to cater for the more complex transformation. A very complex pulse sequence is also used.

Dynamic Nuclear Polarisation (DNP) has recently been introduced in the NMR sensitivity arsenal available to spectroscopists, yielding theoretical signal to noise ratio enhancements of up to 10,000 times. It is marketed as Hypersense^{TM} by Oxford Instruments. It offers great promise in sensitivity enahancement for the low abundance C-13 spectroscopy, making possible some of the experiments like two dimensional INADEQUATE, which were sensitivity limited.

Uhrin *et al* ,[27] attempted to establish the structure of glucose by tracing the carbon-carbon connectivities using the above-mentioned technique, hence the coupling network. This was achieved by protecting the anomeric hydroxyl group with an enriched acetyl group, and then the polarization was transferred through the carbon-13 skeleton of the molecule using INADEQUATE pulse sequence. A drawback associated with the technique is that the polarization enhancement is done in a separate magnet, and the analyte transfer to the NMR magnet takes about four seconds. Most of the polarisation is lost by the time the sample is in the NMR magnet, especially for small molecules like oligosaccharides.

1.5. Protecting groups – implications for NMR.

Chemists are sometimes faced with the task of carrying out reactions at any one of the functional groups in polyfunctional compounds like carbohydrates. They have invariably resorted to protecting group chemistry [28, 29] to selectively carry out the reaction. The procedure consists of temporarily blocking the sites where reaction is not desired. Protecting groups are also used because they render the carbohydrates soluble in non-polar solvents and therefore extend the range of reactions which can be carried out on substrates.

Good protecting groups are chosen following a set of criteria. A good protecting group must selectively react with the intended site in very satisfactory yields. It must possess enough stability so as not to be accidentally removed while the reaction of interest is being carried out at the site of interest. After the reaction has been done, the protecting groups must be selectively removed in good yield. Use of deprotecting reagents which are readily available, non toxic and not reactive to the recovered functionality are highly desired. The protecting groups and reagents required for deprotection must not change the chemical reactivity and stereochemistry of the original compound. Acetyl, benzoyl, benzyl, chloroacetyl and pivolyl are among the most common protecting groups in carbohydrate chemistry. [28-30]

Catalytic hydrogenolysis, using palladium on charcoal is common for cleaving benzyl ethers. The cleavage is accomplished by reversible formation of a complex between the aromatic π system and the metal, which weakens the benzyl ether bond. Simultaneously, hydrogen is immobilized and activated by the solid catalyst, with charcoal increasing the reaction surface area. The weak benzyl ether bond is thus brought closer to the hydrogen atoms, resulting in bond cleavage to form toluene and an alcohol.[28]

In this work 2,3,4,5,6 –pentafluorobenzyl bromide was initially assessed as a protecting group to be used in place of benzyl bromide as an aid for spectral assignment of carbohydrates. Since the ease with which deprotection is effected is a crucial criterion in protecting group chemistry, several other benzyl groups, with varying degrees of fluorination were also tried when we realized that the pentafluorobenzyl group could not be removed easily from the sugar ring.

We hoped that when pentafluorobenzyl bromide was used, spectral assignment would be simplified by reducing overlap of both the proton and carbon-13 spectra. We believed that the pentafluoro group would shift the benzyl methylene carbon-13 signals to lower frequencies, avoiding overlap with the sugar ring signals. This is because we realized that fluorination of the free benzyl bromide moved the methylene carbon-13 signal to 15.97

ppm as opposed to a protonated benzyl bromide, having the methylene carbon-13 signal at 33.49 ppm. [31]

Pentafluorobenzyl bromide has been used for extractive alkylation [32, 33] in gas chromatography. It has been used to derivatise functional groups such as the carboxylic acids, phenols and mercaptans for electron capture detection in chromatography. The electron rich fluorine enhances the sensitivities by electron capture detection.

2 Results and discussion

2.1. Glucopyranoside spectral asignment by proton, carbon-13, and two dimensional techniques. Molecular weight confirmation by mass spectrometry.

The proton and carbon-13 ring assignments of the different synthesized derivatives were done by a combination of ^{1}H, ^{13}C, COSY, HMQC, and HMBC. The proton and carbon-13 assignment of ethyl 2,3,4,6-tetra-*O*-pentafluorobenzyl-β-D-glucopyranoside ***(3)*** will be discussed in detail as an illustration of the assignment process. The α anomer assignment is summarised in the experimental section. The numbering scheme used is shown in Figure 8.

A key point for signal assignment of **(3)** is the identification of the anomeric proton signal (4.30 ppm, doublet, $^{3}J = 7.8$ Hz), of the β anomer (Figure 9). This was identified from the carbon-13 anomeric carbon (appearing at high frequency and easily identified from other ring signals) and the HMQC correlation (Figure 11). In addition, the methyl protons were identified from the splitting pattern (triplet) and the integration ratios of the methyl to the anomeric proton give a value of 3:1, confirming assignment of the methyl protons (1.26 ppm).

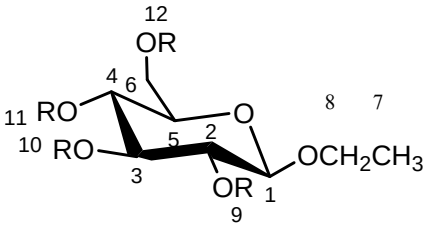

(1) R = H

(2) R = 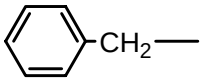 (Bn)

(3) R = 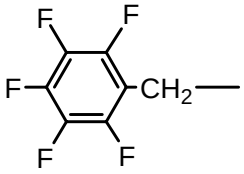 (PFBn)

Figure 8: The structure of ethyl glucoside, showing the numbering scheme used. PFBn is the 2,3,4,5,6 pentafluorobenzyl and Bn is the benzyl protecting group. Only the β anomer is shown for demonstration purposes.

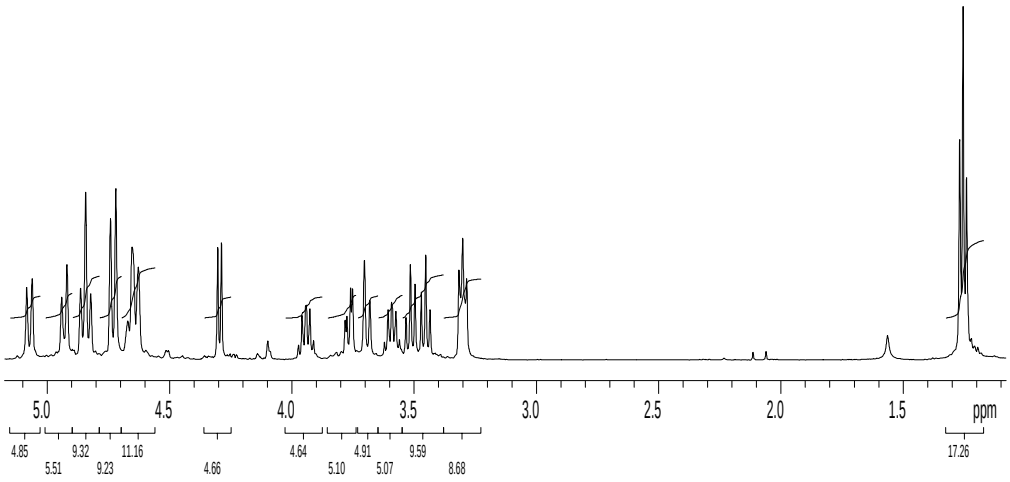

Figure 9: Proton spectra of **(3)**. Integrals are shown. (500 MHz, $CDCl_3$)

The COSY spectrum (Figure 10) shows a correlation between the anomeric proton H1 (4.30 ppm) and H2 (3.30 ppm). H2 further shows a correlation to H3 (3.45 ppm) next to it, which further shows another correlation to H4 (3.52 ppm). There is also a set of pentets at 3.59 and 3.94 ppm which correlate among themselves and to the methyl protons H7 (1.26 ppm), showing these to be methylene protons, H8.

By virtue of being on a carbon adjacent to a chiral centre, H6 and H6' show two doublets at 3.69 and 3.76 ppm. The peaks are also characterized by a 'roofing effect' showing that they are similar protons with very close chemical shifts. In addition the sum of integration of the two signals gives a value that is twice the value of the anomeric proton. H6's have a further correlation with the signal that was assigned H2, and the integration value of the peak at H2 is 2, showing that the shift must have two overlapping one-proton signals as evidenced by the complex splitting into a triplet. This was handy in assigning carbon-13 of C5 by HMQC (*vide infra*).

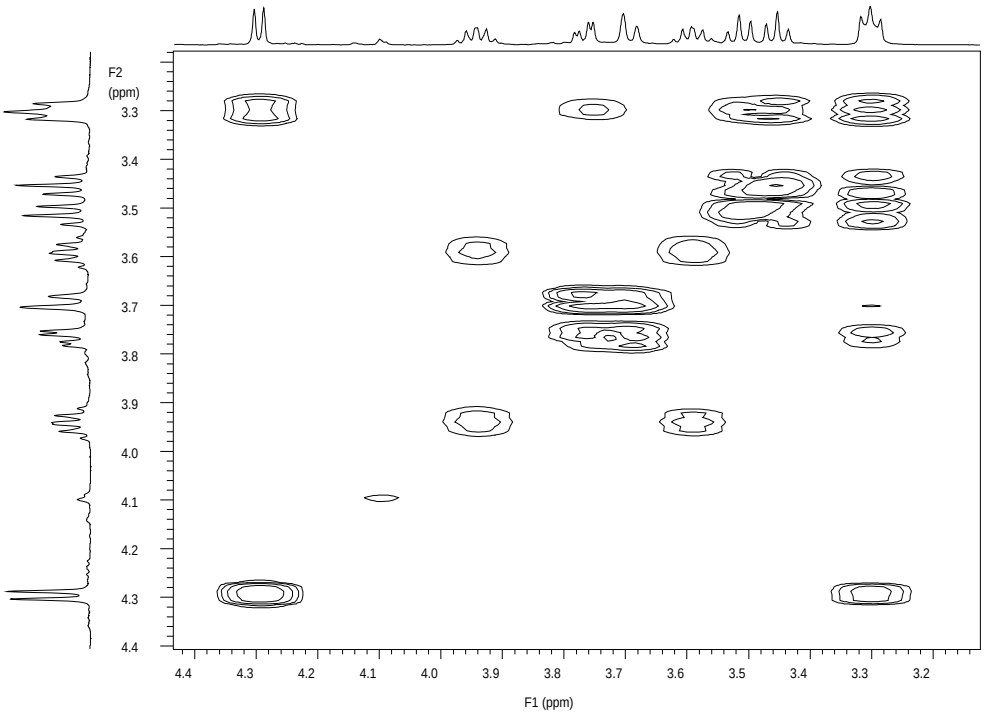

Figure 10: COSY spectrum of **(3)**. (500 MHz, $CDCl_3$). A full spectrum is in the appendix, Figure A1.

From the HMQC (Figure 11) the CH fragments were easily identified for C1 (103.2 ppm), C6 (69.2 ppm), C7 (66.0 ppm) and C8 (15.2 ppm). Following the proton assignments made in the COSY, C6 assignment was made easier by the fact that it showed correlation to two proton signals which are very close to each other. C6 is the only ring carbon with two protons attached. By the same token the C8 CH fragment was assigned whereby C8 correlated to two pentets (H8) previously assigned in the COSY.

C2 and C5 showed a fragment with H2 and H5 at 3.30 ppm. The exact shifts of C2 and C5 were determined using the empirical predictions for sp^3 carbons (CH_3, CH_2, CH) attached to the alkyl groups and other functional groups. C5 exhibited a chemical shift of 74.6 ppm and C2 at 82.4 ppm, further proving the COSY assignments for H2 and H5.

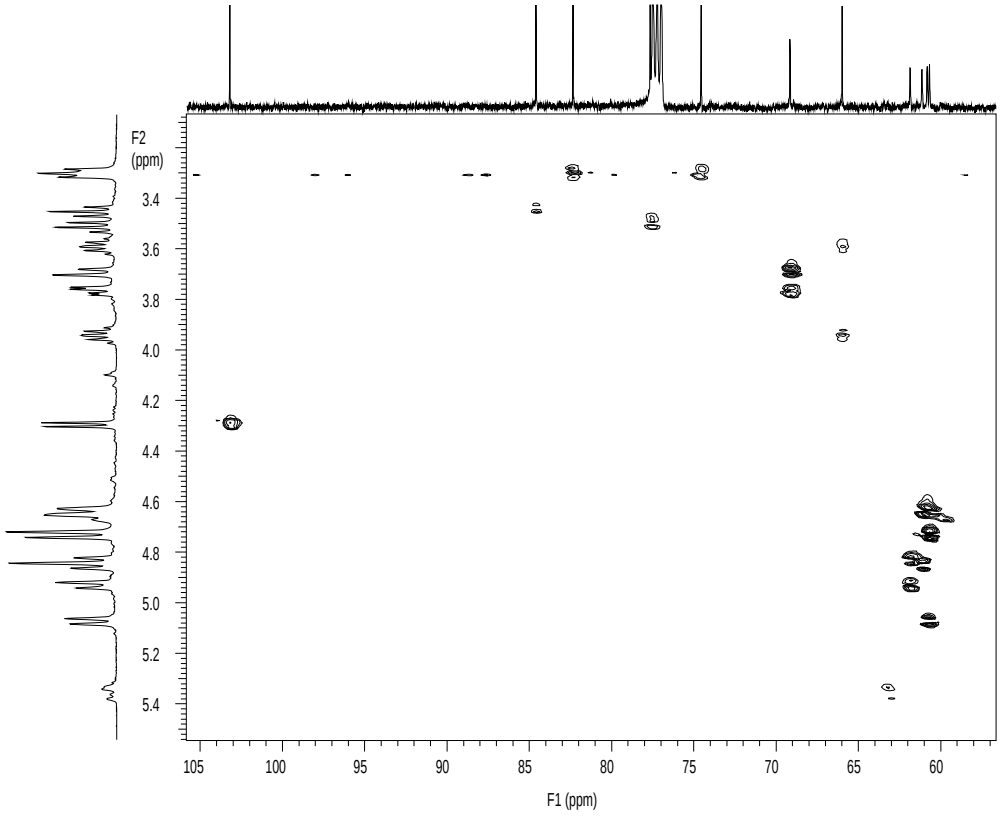

Figure 11: HMQC spectrum of **(3)**. (500 MHz, $CDCl_3$). A full spectrum is in the appendix, Figure A2.

To assign C3 and C4, HMBC (Figure 12) was used. It showed a 3-bond correlation between C3 (84.6 ppm) and H5. There was a further 2-bond C3 to H4 correlation. To further confirm, there is a 3-bond correlation with H1; the anomeric proton and a 2-bond correlation with H2. C4 at 77.7 ppm, beneath the solvent multiplet, exhibits a 3-bond correlation to H6 and a 2-bond correlation to H3. Following these HMBC assignments, the HMQC assignments were made which helped to decide the shifts of H3 at 3.45 ppm and H4 at 3.52 ppm, making the ring moiety assignment complete.

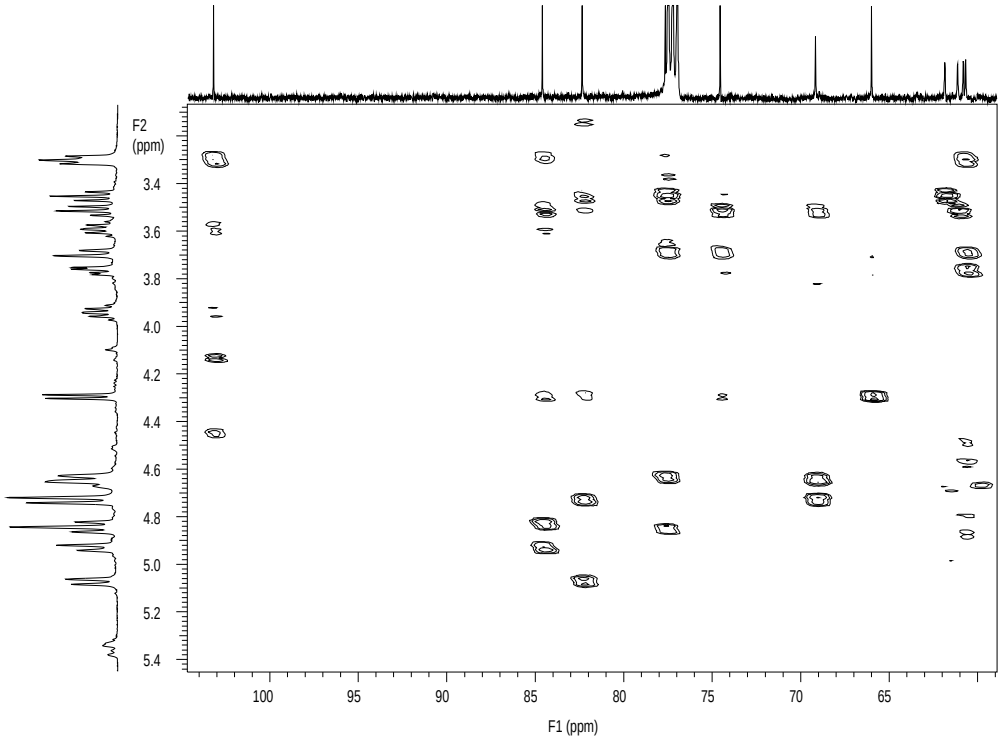

Figure 12: HMBC spectrum of **(3)**. (500 MHz, $CDCl_3$).

From HMBC, the CH_2 proton assignments of the pentafluorobenzyl groups were accomplished. C6 has a three bond correlation with two proton signals at 4.66 and 4.74 ppm, assigning these to H-12 CH_2. C4 correlates with signals at 4.64 and 4.86 ppm assigning these protons to H-11. C2 correlates with signals at 4.74 and 5.08 ppm and

assigns these signals to H-9. A correlation between C3 and two proton signals at 4.83 and 4.93 ppm assigns these proton signals to H-10.

The proton signal assignments from HMBC correlations made above were used to assign the CH_2 carbon signals on the pentafluorobenzyl group using HMQC (Figure11). The following assignments were made C9 (60.8 ppm), C10 (61.9 ppm), C11 (61.2 ppm) and C12 (60.7 ppm) from the CH fragments. These were confirmed by HMBC CH fragments between the pentafluorobenzyl CH_2 carbon assignments and the ring proton assignments. The integration of proton signals, *ca* 20, is consistent with a proton count on the known molecular formula of **(3)** (Figure 9)**.** The ^{13}C spectrum shows twelve carbon-13 signals consistent with the eight carbons on the ring, the ethoxy and four methylene carbons from the pentafluoro benzyl group as counted from the molecular formula (Figure 13). The high resolution *m/z* value of 951.0838 $[M + 23]^+$ further confirms that four pentafluorobenzyl groups have replaced all the protons from the glucoside.

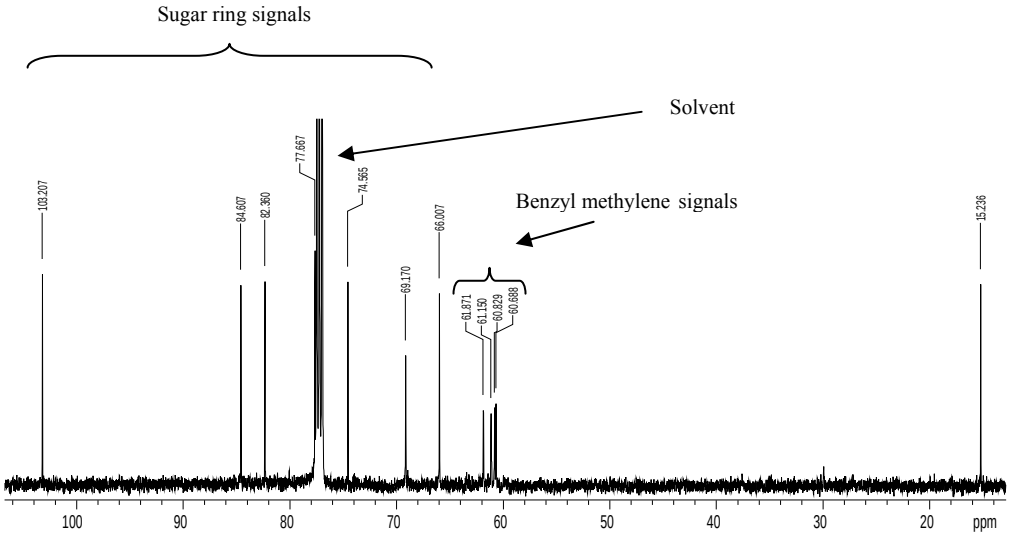

Figure 13: Carbon-13 spectrum of **(3)**, (125 MHz, $CDCl_3$), showing 8 carbon sugar signals and 4 protecting group methylene signals. Methylene signals do not overlap with the sugar signals.

Figure 14 below shows the crowding that arises when a normal benzyl group is used as a protecting group. Methylene benzyl carbon signals appear in the same region as the sugar ring carbon signals while they are clearly separated when a pentafluorobenzyl is used as shown in Figure 13.

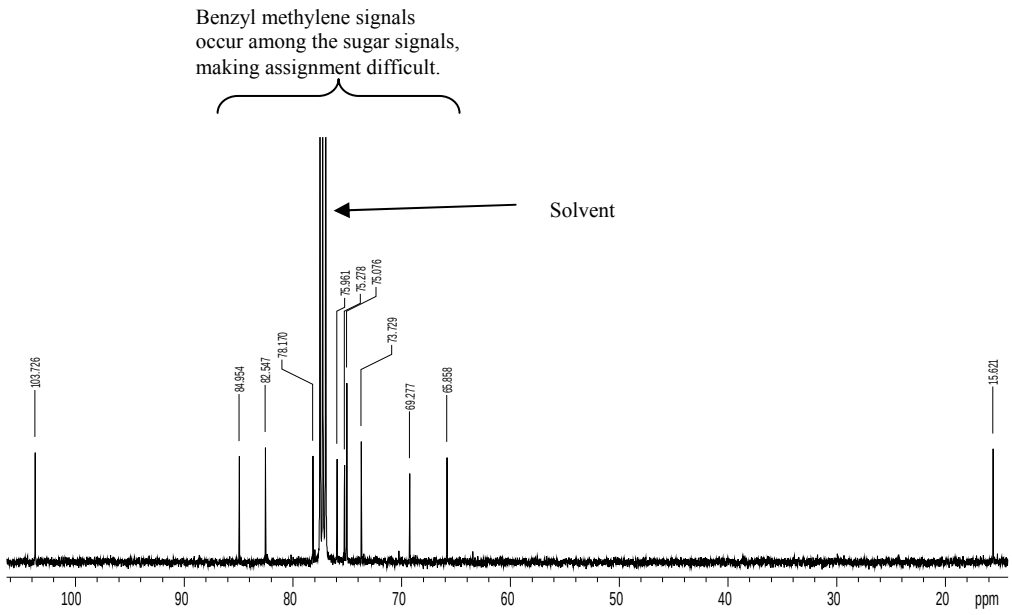

Figure 14: Carbon-13 spectrum of **(2)**, (125 MHz, $CDCl_3$), showing the methylene signals occurring in the same spectral range as the sugar carbon signals.

2.2. Mannopyranoside spectral asignment by proton, carbon-13, and two dimensional techniques. Molecular weight confirmation by mass spectrometry.

The proton and carbon-13 ring assignments of the different synthesized derivatives were done by a combination of ^{1}H, ^{13}C, COSY, HSQC, and HMBC. The proton and carbon-13 assignment of Methyl 2,3,4,6-Tetra-O-Pentafluorobenzyl-α-D-mannopyranoside **(6)** will be discussed in detail as an illustration of the assignment process. The numbering scheme used is shown in Figure 15.

The key in assigning the spectra of **(6)** was the identification of the anomeric proton at 4.62 ppm (d, ^{3}J = 1.5 Hz) and the methoxy protons, at 3.04 ppm, a singlet. This was identified from the carbon-13 anomeric carbon (appearing at high frequency and easily identified from other ring signals) and the HSQC correlation The methoxy protons appear at higher frequencies by virtue of being deshielded by the electronegative oxygen. Integration of the spectrum helped to show that these protons are in a 1:3 ratio further proving their identity (Figure 16). The numbering scheme of **(6)** is shown in figure 15.

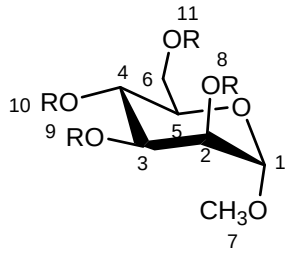

(4) R = H

(5) R = 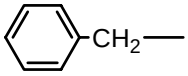 (Bn)

(6) R = 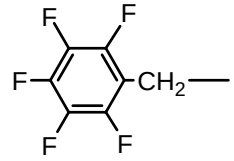 (PFBn)

(7) R = 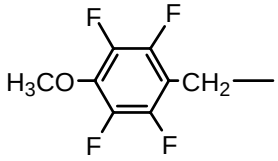 (TFOMeBn)

(8) R = 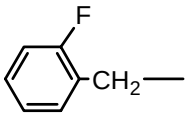 (MFBn)

(9) R = 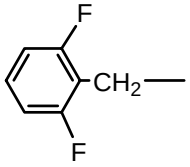 (DFBn)

(10) R = 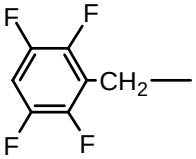 (TFBn)

Figure 15: The structure of methyl mannopyranoside derivatives, showing the numbering scheme used. R is the relevant protecting group.

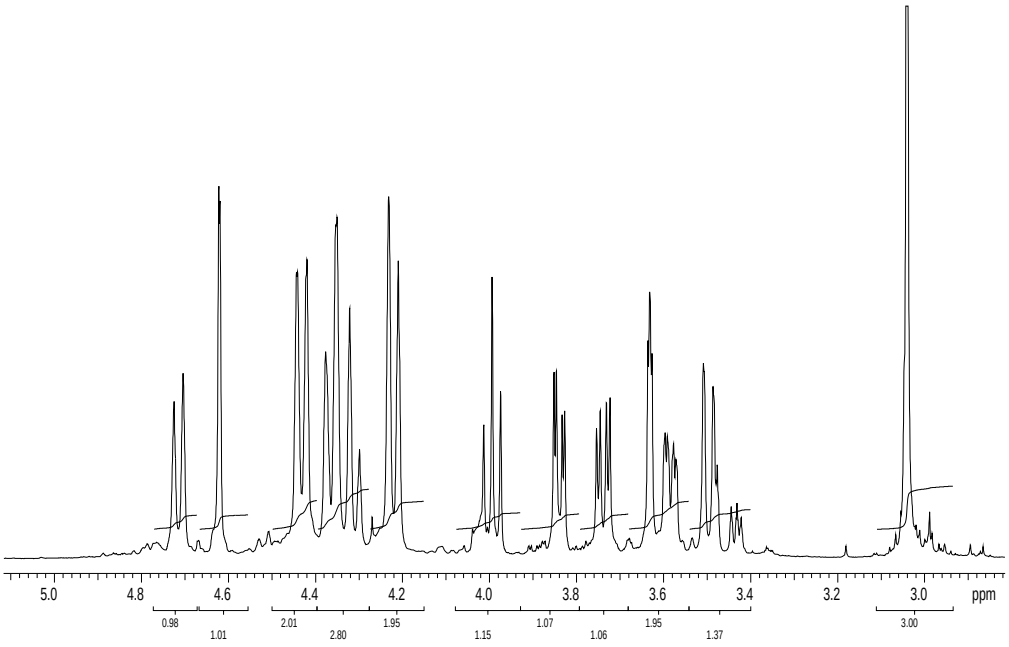

Figure 16: Proton spectrum of **(6)**, showing integration. (500 MHz, C_6D_6).

Using COSY (Figure 17) a corellation between the anomeric proton H1 (4.62 ppm) and H2 (3.63 ppm) was mapped out and the correlation was further followed from H2 and H3 (3.84 ppm), H3 and H4 (3.99 ppm), H4 and H5 (3.59 ppm), H5 and H6 and H6 (3.74 ppm) to another H6 (3.49 ppm).

The assignments made based on the COSY, were tested and confirmed using HSQC (Figure 18) and HMBC (Figure 19) while simultaneously assigning the carbon-13. A 3-bond corellation between H1 and C7 was found, thus helping to assign C7 (54.5 ppm) which was shown to be consistent by an HSQC H7-C7 fragment. In addition, C7 chemical shift is consistent with being in a deshielded methoxy group.

H1 was also used to map C3 (81.1 ppm) from a 3 bond HMBC which was further proved by the presence of a H3-C3 HSQC fragment.

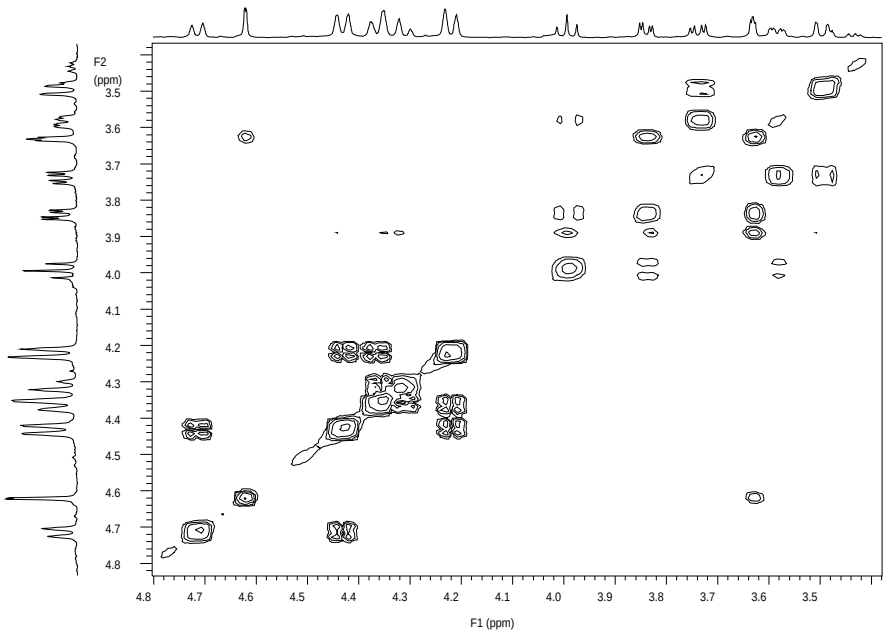

Figure 17: COSY spectrum of **(6)**. (500 MHz, C_6D_6).

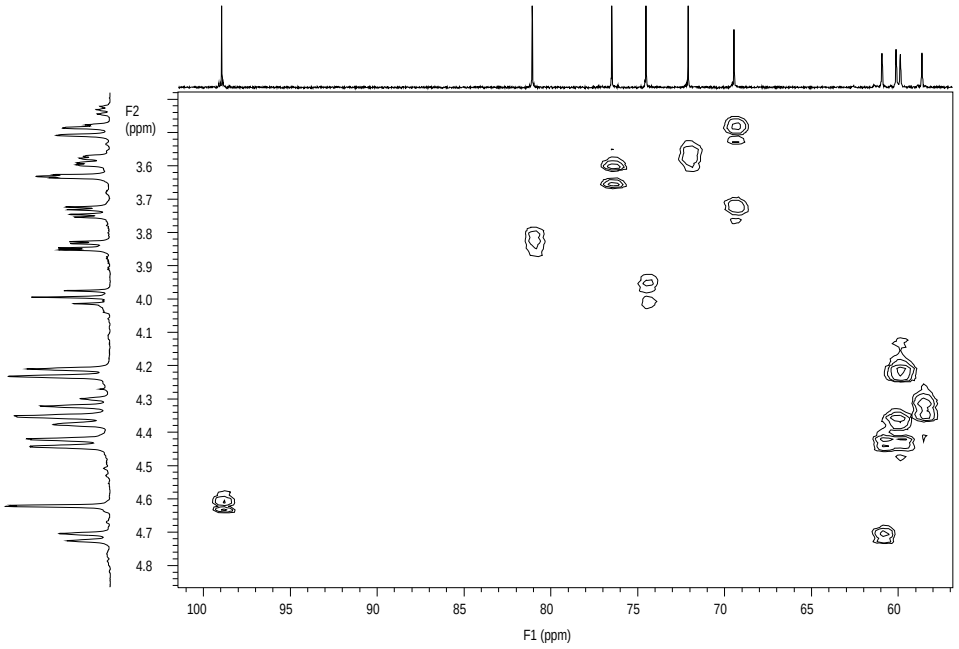

Figure 18: HSQC spectra of **(6)**. (500 MHz, C_6D_6). A full spectrum is in the appendix, Figure A3.

Having assigned the shift of C7 and H7, the C1 chemical shift (98.9 ppm) was mapped from a 3 bond correlation with the methoxy protons. Moreover, the shift is consistent with the general position of anomeric carbons being the only ones in the ring attached to two oxygens, and therefore more deshielded. The α anomeric carbons are usually found slightly below 100 ppm.

C6 was identified with the aid of HSQC. Two H6 showed a correllation with a carbon line at 69.5 ppm which was assigned to C6 by a mere fact that it appeared at the lowest frequency of the sugar carbons as it had shielding from two protons. HMBC revealed it to have a 3 bond correllation with two protons which were not among the ring protons; these are the CH_2 of the pentafluorobenzyl which helped to identify those protons.

HSQC was used to map out the rest of the ring carbons C2 (76.5 ppm), C4 (74.5 ppm), C5 (72.1 ppm), using the CH fragments with HMBC further confirming the asignmens.

With the ring carbons assigned, the CH_2 protons of the derivitising agent were assigned by following the HMBC correlations. The carbon nuclei of the CH_2 were also followed from the HMBC using the protons previously assigned by COSY and confirmed using HMBC and HSQC. These carbons appeared at lower frequencies than the ring carbons because of the anisotropic shielding they experience by their close proximity to the electron-rich pentafluorobenzyl group.

Overall integration of the proton spectrum showed a total of 18 protons consistent with the molecular formula of the compound (Figure 16). Eleven carbon signals are also seen for the sugar moiety and the CH_2 of the pentafluorobenzyl groups, further confirming the assignment (Figure 20). The high resolution electrospray mass spectrum confirms the capping of all the sugar hydroxyl groups. It shows a peak corresponding to a m/z 937.0676 $[M + 23]^+$, further supporting the NMR integrals and assignment.

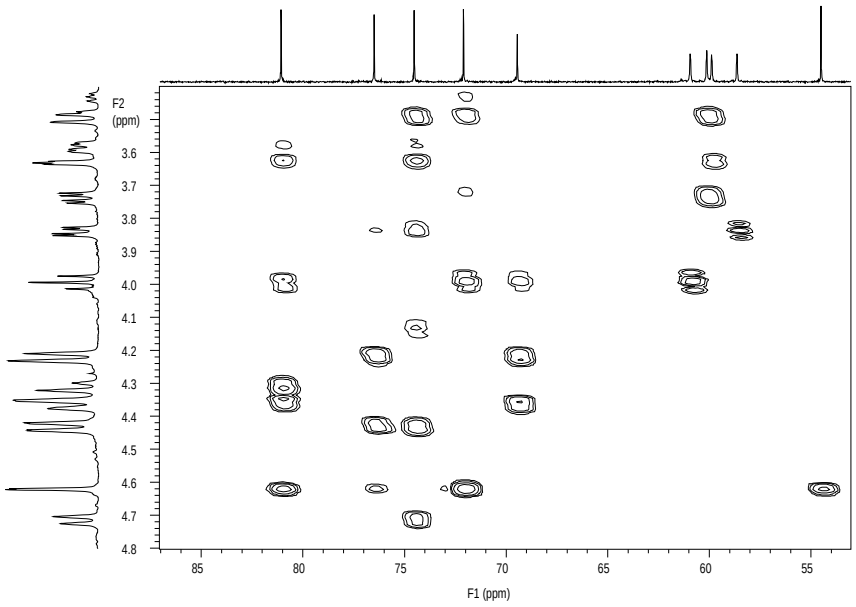

Figure 19: HMBC spectrum of **(6)**. (500 MHz, C_6D_6).

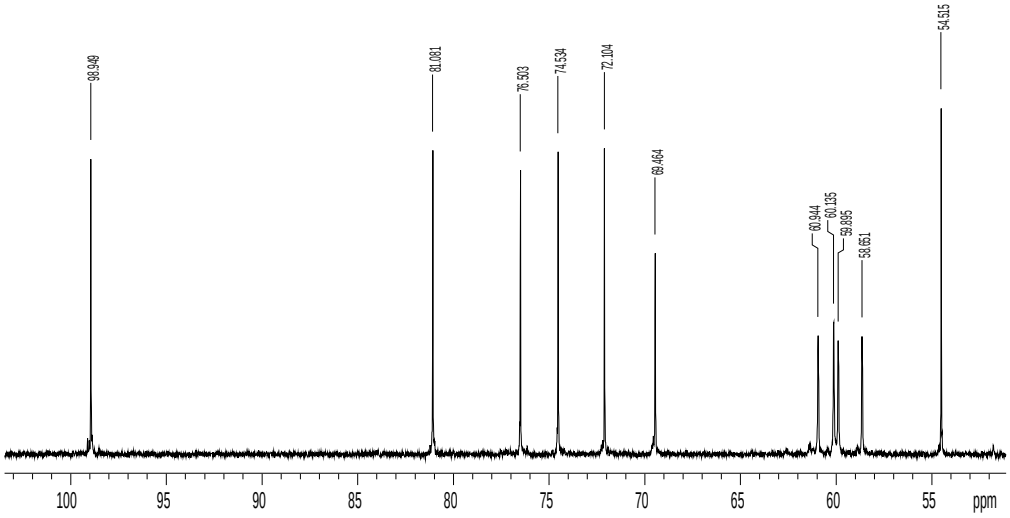

Figure 20: Carbon-13 spectrum of **(6)**. (125 MHz, C_6D_6). Sugar ring carbon signals (5) are separated from the protecting group methylene signals (4).

2.3. Fluorine-19 spectral assignments

A complete assignment of the protected saccharide molecules was pursued by trying to assign the different fluorine signals on the different sugar *O*-positions. This was accomplished by selective decoupling of the *ortho* fluorine signals because the coupling constants between the fluorines and both the benzyl carbons and protons were too small to allow successful two-dimensional fluorine-proton or fluorine carbon long-range correlation experiments. Nevertheless, residual couplings to the fluorines were visible in the relevant spectra. For example, the linewidths of the PFBn derivatised methylene carbons in the carbon spectra (Figure 13 and 20) are wider than the sugar carbon signals.

Selective decoupling ("spin tickling") is a technique in which a second Rf frequency (γB_2), is made to resonate directly and selectively on the position of the resonance frequency of interest. [15, 16] This second Rf frequency, called the decoupler frequency, causes the two spin states (α and β) responsible for splitting to oscillate at a frequency greater than the coupling constant leading to a collapse of the multiplet into a singlet. For selective decoupling, the decoupler power has to be very low in order for the decoupling not to spill into the adjacent resonances, causing undesired broadband decoupling, hence "spin tickling".

The *ortho* fluorine atoms are involved in a long-range coupling with the methylene protons of the pentafluoro group because of their spatial proximity. A major problem with fluorine is its extensive scalar coupling which extends to spin systems four bonds away. This is evidenced by splitting of the methylene multiplets into doublets of triplets in their fine structure. Another problem was that the *ortho* fluorine signals on different *O*-positions are extensively overlapped. This therefore meant that a highly selective experiment was needed to decouple the limited and smallest of the couplings.

Since the methylene assignments were done (*vide supra*) for **(3)** and **(6)**, they were used to assign the fluorine at the *ortho* position. There was hope that having done that, the

different pentafluoro groups could be traced to the oxygen positions of the protected hydroxyl groups on the sugar ring.

The dispersion between the ortho fluorine of **(3)** [α and β] allowed usage of a decoupler power at 3dB. When the **β** anomer fluorine peak at -143.95 ppm was "spin tickled", proton multiplets at 4.40 and 4.81 ppm, corresponding to the position at 9, as well as 4.69 and 4.80 ppm, corresponding to the position at 10 were enhanced. This showed that the fluorines peak at -143.95 ppm corresponds to the *ortho* group at 9 and 10. This is supported by integration ratio showing to be twice as much as in other fluorine peaks (Figure 21).

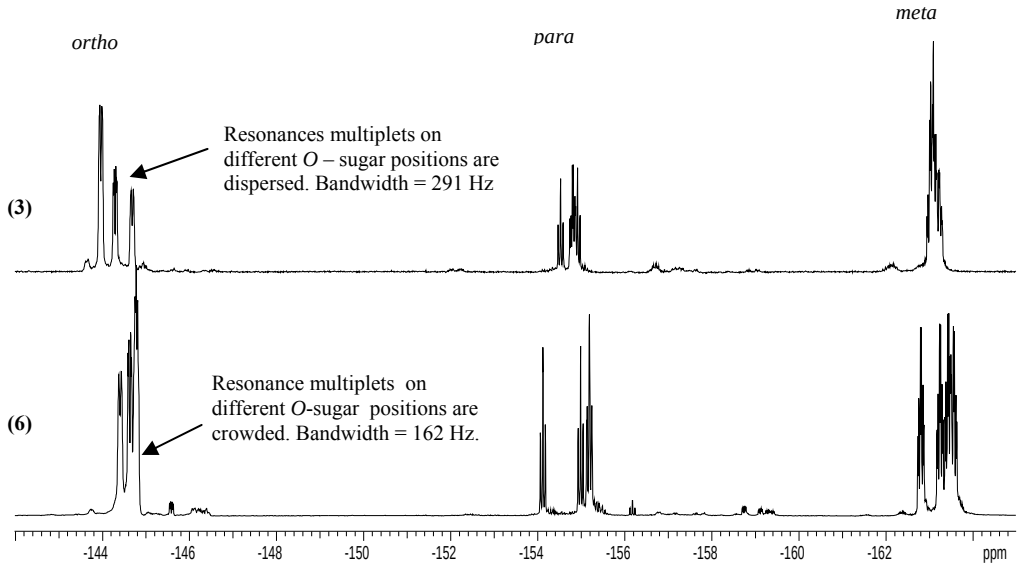

Figure 21: A stacked F-19 plot showing the fluorine spectra of **(3)** and **(6)**. In **(3)**, *ortho* multiplets are apart, selective decoupling was achieved by decoupler power at 3 dB. The crowded multiplets in **(6)** were only selectively decoupled with decoupler power at -12 dB, (376 MHz, C_6D_6)

"Tickling" at -144.24 ppm, the methylene multiplet at 4.28 ppm, corresponding to position 11, was enhanced; indicating that the fluorine peak belongs to the group attached at 11. The methylene peak at 12, 4.65 ppm, was enhanced on "tickling" the fluorine peak

at -144.64 ppm. The results for the α anomer of **(3)** and that of **(6)** are summarised in Table 1 and 2 respectively.

Table1: Selective decoupling results of the **α** anomer of **(3),** [500 MHz, C_6D_6).

Ortho F-19 peak "tickled" /ppm decoupler power =3dB	**Methylene protons enhanced/ ppm.**	**Conclusion**
-144.03	10	Ortho F-19 at 10
-144.46 (integration twice 11 or 10)	9, 12	Ortho F-19 at 9, 12.
-144.66	11	Ortho F-19 at 11

Note: The numbering scheme used in Table 1 is shown in Figure 8, page 19.

Table2: Selective decoupling results of **(6),** [500 MHz, C_6D_6). Poor dispersion called for usage of high attenuation (-12 dB).

Ortho F-19 peak "tickled" /ppm decoupler power =-12 dB	**Methylene protons enhanced/ ppm.**	**Conclusion**
-144.38	9	Ortho F-19 at 9
-144.60	11	Ortho F-19 at 11
-144.72 (integration twice 9 or 11)	8, 10	Ortho F-19 at 8, 10

Note: The numbering scheme used in Table 2 is shown in Figure 15, page 26.

The *ortho* position fluorines were used as leads to assignment of all other fluorine atoms using COSY. The signal at the *ortho* couples to the *meta* position next to it. The *meta* then correlates to the *para* position. Both the *ortho* and the *para* couples to the *meta*, confirming the assignment of the meta at around -163.31 ppm. The COSY spectrum of **(3)** illustrating the correlations is reported in Figure 22. The assignments of other compounds, except (8) [2-monofluoro] and (9) [2,6- difluoro] were done in a similar manner and are summarized in Table 3.

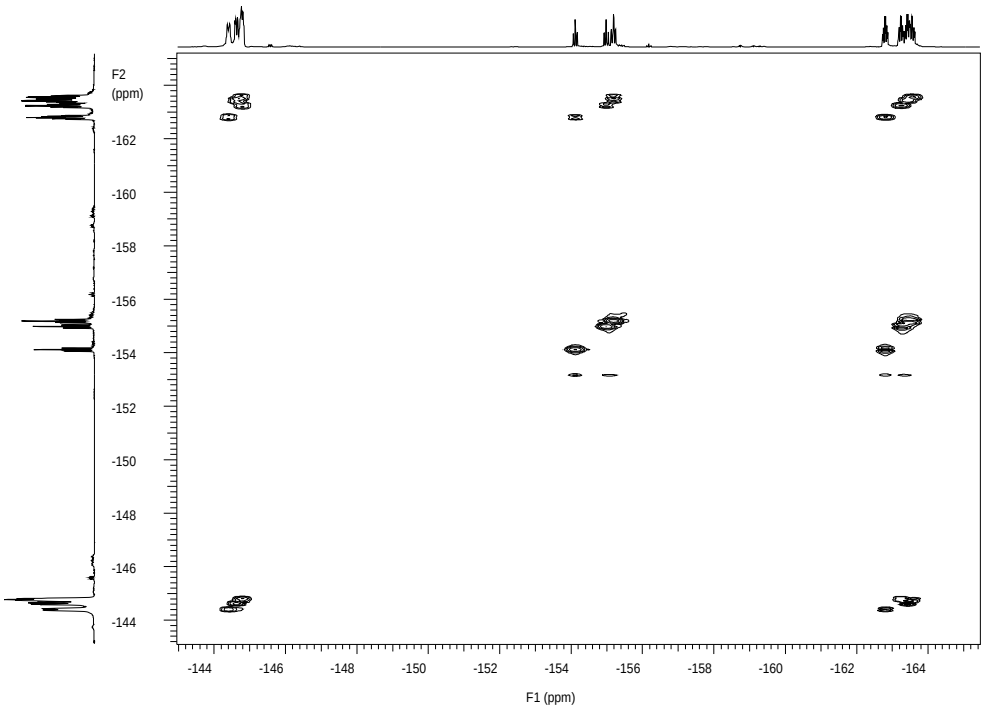

Figure 22: The F-19 COSY spectrum of **(6),** (376 MHz, C_6D_6)

Table 3: Summary of aromatic fluorine-19 assignments. (376 MHz, C_6D_6)

Compound	***ortho* /ppm**	***meta* / ppm**	***para* / ppm**
(3) β	-144.70 to -143.95	-163.31 to -162.91	-155.00 to -154.44
(6)	-144.72 to -144.38	-163.60 to -162.55	-155.22 to -154.04
(8)	-119.55 to -118.59	None	None
(9)	-115.22 to -115.05	None	None
(10)	-140.41 to -139.61	-144.80 to -144.38	None

Equivalent methods were used to assign the proton and carbon-13 spectra of all the other derivatives ((**2**), (**4**), **(5)**, **(7)**, **(8)**, **(9)**, **(10)**), and a comparative discussion of the results obtained is presented below.

2.4. Effect of the various protecting groups on the proton spectra.

A stacked plot of the proton spectra of the unprotected methyl-α-D- mannopyranoside and its protected analogues is presented in Figure 23. The sugar ring and the methylene proton regions are shown.

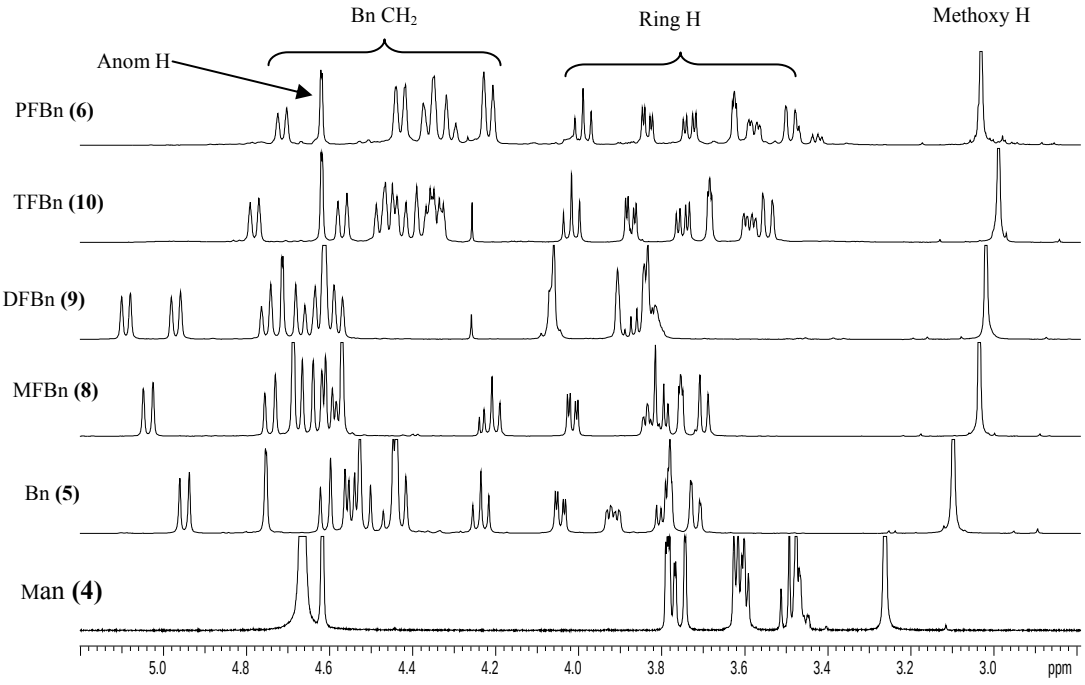

Figure 23: Stacked plot of 1H- NMR spectra of methyl-α-D-mannopyranoside (500 MHz, D_2O, δ/ppm) and its analogues with different protecting groups (500 MHz, C_6D_6, δ/ppm).

An interesting effect that is brought about by the degree of benzyl ring fluorination of the protecting group is shown. The proton spectrum dispersion of the sugar ring improves as the number of fluorine atoms on the benzyl ring increases. The anomeric position (*ca* 4.62 ppm, Anom H) is disregarded in this case since by virtue of being on a carbon connected to two oxygen atoms; it is more deshielded, and well separated from the other sugar ring protons. For the unprotected mannopyranoside (Man), the sugar ring protons cover some 0.34 ppm, a narrow range from 3.46 to 3.80 ppm. The dispersion increases gradually as the number of fluorine atoms on the aromatic ring increases. At the highest

extreme, where 2,3,4,5,6-pentafluorobenzyl (PFBn) has been used as a protecting group, the dispersion is the widest, covering some 0.50 ppm range from 3.50 to 4.00 ppm. The different ring proton resonances are free from overlap.

The methylene proton signals in the protected analogues occur at higher frequencies. They do not overlap with the proton ring signals as there is a clear demarcation between the two groups. The only exception is the anomeric proton signal which occurs among the methylene region. However, this is not a problem since it is easily distinguished from its coupling pattern, a doublet with a coupling constant (^{3}J) of about 1.5 Hz. The methylene signals are AB multiplets with coupling constants equal to or greater than 10 Hz.

An explanation of the shifts patterns and the dispersion is that they are caused by a combination and balance of fluorine anisotropy, inductive electron withdrawal effects and electronic effects. It is observed that introduction of a monofluorobenzyl (MFBn) group, shifts the resonances to higher frequencies with some little amount of dispersion. Tetrafluorobenzyl (TFBn) and pentafluorobenzyl (PFBn) gradually increase the dispersion, at the same time shifting the sugar ring protons to lower frequencies.

Introduction of MFBn deshields the protons by inductive electron withdrawal effects, thus pulling the resonances to higher frequencies. At the same time, the little anisotropy brought in with one fluorine atom on the benzyl, causes differential shifts of the resonances to higher frequencies. Increasing the number of fluorine atoms (TFBn and PFBn) increases the anisotropy, hence wider dispersion. However, the resonances shift to lower frequencies. Perhaps this can be explained by p-π interaction [34, 35] properties of fluorine. The strong electronegativity of fluorine means that it pulls the electrons from the electron-rich aromatic system towards itself, but the small fluorine atom with no empty orbitals cannot accommodate the acquired electron cloud. The now electron-rich p orbitals then feed back the electrons to the aromatic π-electron system via a p-π interaction, and the excess electron cloud is absorbed through the bonds to stabilize the whole system and hence increased ring current shielding on the protons as far as the sugar ring.

The DFBn deviation from the trend explained above may be due to the fact that the amount of p-π interaction is small and by virtue of the 2,6-positioning of the fluorine on the aromatic ring, the net magnitude of the dipoles developed cancel. This therefore leads to dominance of the electron withdrawal effects. The Bn groups also cause some dispersion mainly due to stereoelectronic effects, which are more pronounced for protons 3, 4 and 5 (see full assignment in the experimental section). The anomeric proton appears at roughly the same position in the spectra for mannopyranoside and with all the protecting groups except with MFBn and DFBn where it is shifted to higher frequencies.

The methylene protons of the benzyl groups are shifted to higher frequencies by deshielding caused by a combination of two factors. The first is hydrogen bonding with the fluorine at the ortho positions of the aromatic ring systems. From their position, it is highly likely that they undergo dipolar interaction with *o*-fluorine. They also stick out into the aromatic ring in a direction which lands them into the deshielding region of the ring current, thus along the ring plane. Dispersion increases with the number of fluorine atoms on the aromatic system, and the shift to lower frequencies is an interplay between the hydrogen bonding deshielding and the ring current shielding (*vide supra*).

The two benzyl methylene protons split each other into multiplets because of their proximity to a chiral centre on the sugar ring. The protons corresponding to the methylenes at position 10 have an interesting behaviour in which one of the multiplets is well separated from its partner and appears at frequencies above 4.7 ppm (Figure 16). The behaviour was probed by NOESY acquired on mannopyranoside protected with Bn in chloroform-*d* (Figure 24). It was observed that the methylene protons at 10 are engaged in a dipolar interaction with the ortho proton of the aromatic ring system at 11.

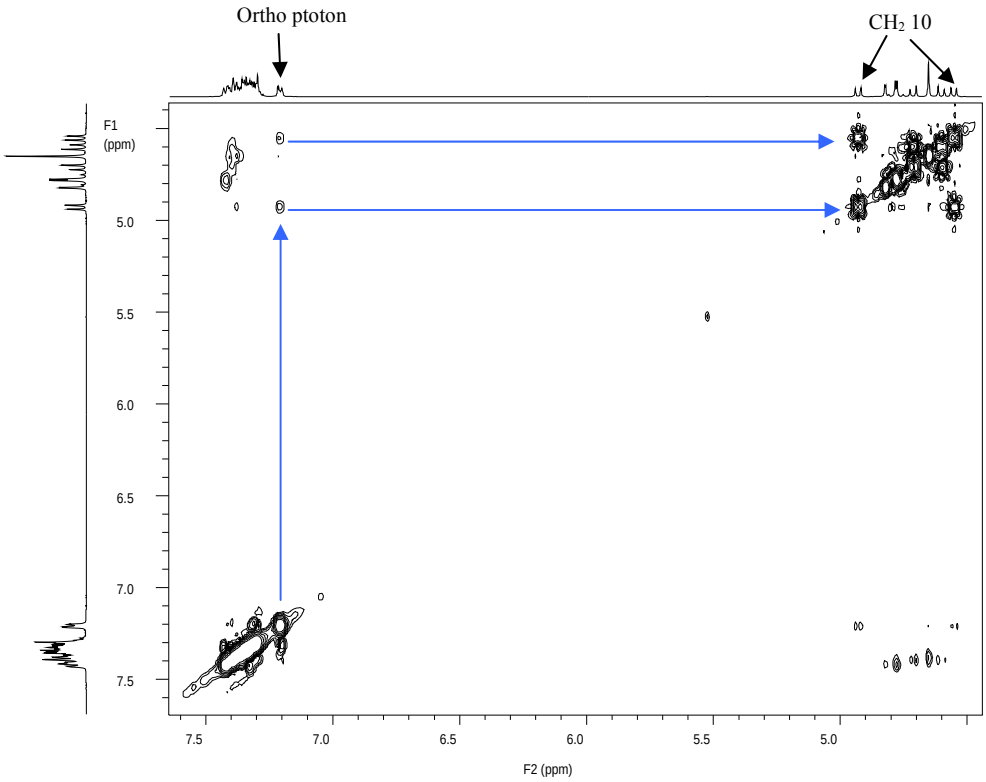

Figure 24: NOESY spectrum of Man Bn showing the dipolar interaction between the ortho proton and the methylene proton at position 10. (500 MHZ, $CDCl_3$, δ/ppm).

It is speculated that one of the methylene protons approaches the aromatic system at a direction along the deshielding plane of the ring and interacts with the ortho protons. This is shown in Figure 25. Since this behaviour is seen for all benzylated system, we believe the explanation applies to all of them.

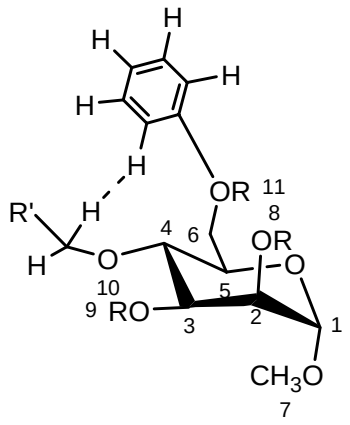

Figure 25: Diagram showing the proton dipolar interaction. The bonds are not to scale and steric repulsions have not been minimised.

2.5. Solvent effects on the proton resonances.

The solvent effect on the dispersion was studied on the PFBn protected beta anomer of glucoside. The proton spectra acquired in benzene-d_6 and chloroform-*d* were compared and are shown in Figure 26. The dispersion was as good as in the mannopyranoside protected with PFBn for the two cases. However, the spectrum in benzene exhibited a general shift to lower frequencies for all the resonances, with a slightly wider dispersion. Rapidly tumbling benzene-d_6 solvent molecules have π-electron functions shielding all the protons uniformly, causing a general lower frequency shift. Chloroform-*d* does not have the π-electron functions. Benzene-d_6 was therefore used for all the spectra acquired for its dispersion advantage.

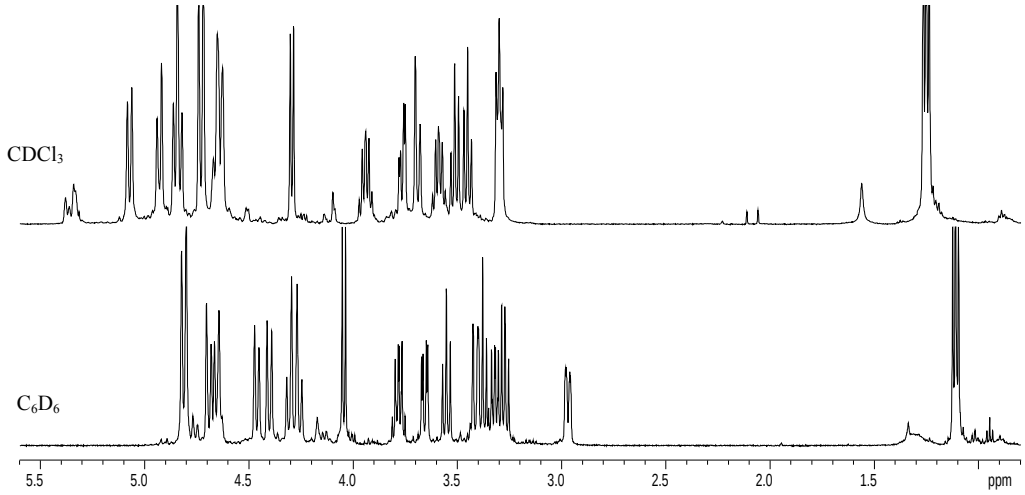

Figure 26: A 500 MHz stacked proton spectrum of **(3)** showing the solvent effect.

2.6. Effect of protecting groups on the carbon-13 of the sugar lines.

The effect of protection with different benzyl analogues on the carbon-13 spectra was studied, and the results are shown in Table 4. The carbon-13 lines assignment was done on a number of the mannopyranoside protected with the benzyl groups and compared to its unprotected version.

A striking observation is that protection with fluorinated benzyl groups simplifies spectral assignment. When an ordinary Bn group is used, the methylene carbon signals appear among the ring carbon signals; complicating assignment. Methylene signals appear in the *ca* 72 – 75 ppm range. Ring signals appear in the 70 – 80 ppm range causing some overlap.

Table 4: Carbon-13 line frequencies (125 MHz, δ/ppm), of Mannopyranoside (CD_3OD), and the derivatives protected with different benzyl analogues (C_6D_6).

ppm / C #	Protecting Group					
	None	Bn	MFBn	DFBn	TFBn	PFBn
1	101.6	99.4	99.2	99.5	99.0	99.0
2	70.9	75.7	76.2	76.8	76.6	76.5
3	71.4	80.8	81.0	81.5	81.3	81.1
4	67.4	75.5	75.3	75.7	74.9	74.5
5	73.3	72.7	72.5	72.5	72.2	72.1
6	61.8	70.0	70.1	70.4	69.7	69.5
7	54.0	54.4	54.3	54.3	54.5	54.5
8	-	73.0	66.9	60.8	60.3	59.9
9	-	72.1	65.5	59.4	59.2	58.7
10	-	75.0	68.6	61.8	61.4	60.9
11	-	73.4	66.7	60.6	60.6	60.1

On the other hand, with fluorinated benzyls, the methylene lines are shifted to lower frequencies, *ca* 58- 69 ppm, out of the way of the sugar ring lines, *ca* 70-82 ppm. The overlap between the two groups is minimized, simplifying spectral assignment by two dimensional techniques like HSQC/HMQC and HMBC. The low frequency shift is more pronounced when PFBn is used and less pronounced with MFBn.

Carbons lines of the positions at 2, 3, 4 and 6 of the sugar ring are shifted to higher frequencies by the electron withdrawal effect of the protecting groups. The stereoelectronic effects cause differential deshielding, as substantiated by carbon 2 and 3. In the unprotected mannopyranoside they have very similar frequencies, but with protection their separation is substantially increased. Carbons 1, 5 and 7 show very little shifts with protection. There are more intervening bonds between these spin systems and the deshielding centres. The intervening bonds may serve to neutralize the effects of the deshielding.

2.7. Removing the protecting group from the sugars.

A milestone in protecting group chemistry is reached when, having served their purpose, the groups can be removed to recover the original compound. [28, 29] From the assessment done above, an important observation made was that pentafluoro groups conveyed the best proton and carbon-13 dispersion of the sugar spectrum. The ease with which the pentafluoro groups could be removed was then studied. The deprotection using palladium on charcoal hydrogenolysis [28, 36, 37] was tried on ***(3)*** and proved to be a failure. A TLC plate showed one spot, an indication that there was no reaction, even after the reaction was carried on for days under acid catalysis.[38]

Deprotection by hydrogenolysis depends on the ability of π-system containing groups like benzyl to reversibly form complexes with transition metals, weakening and cleaving the benzyl ether bond formed during protection. Simultaneously, activation and immobilization of hydrogen on the catalyst surface therefore leads to formation of an alcohol and toluene from the benzyl fragment, hence deprotection.

Aromatic ring fluorination means that the benzyl CH_2 is deactivated by fluorine inductive electron withdrawal effects. [35] This acts through the γ-effect where fluorine mostly deactivates a γ-carbon. The electron cloud on the π-system is also decreased leading to poor formation of transition metal- benzyl complex.

To counter fluorine deactivation, 4-methoxy-2,3,5,6-tetrafluorobenzyl group was used, yielding good dispersion results but deprotection still failed. The hope was that the activating powers of a methoxy group [4] at the para position would enhance the benzyl ether cleavage.

Deprotection was tried with 2,6-difluorobenzyl group and a partial reaction was achieved after many days. The proton NMR spectrum of the deprotection product (Figure 27) is compared to the fully protected methyl mannopyranoside below (Figure 28). The unprotected methyl mannopyranoside (Man) was presented earlier on (Figure 23).

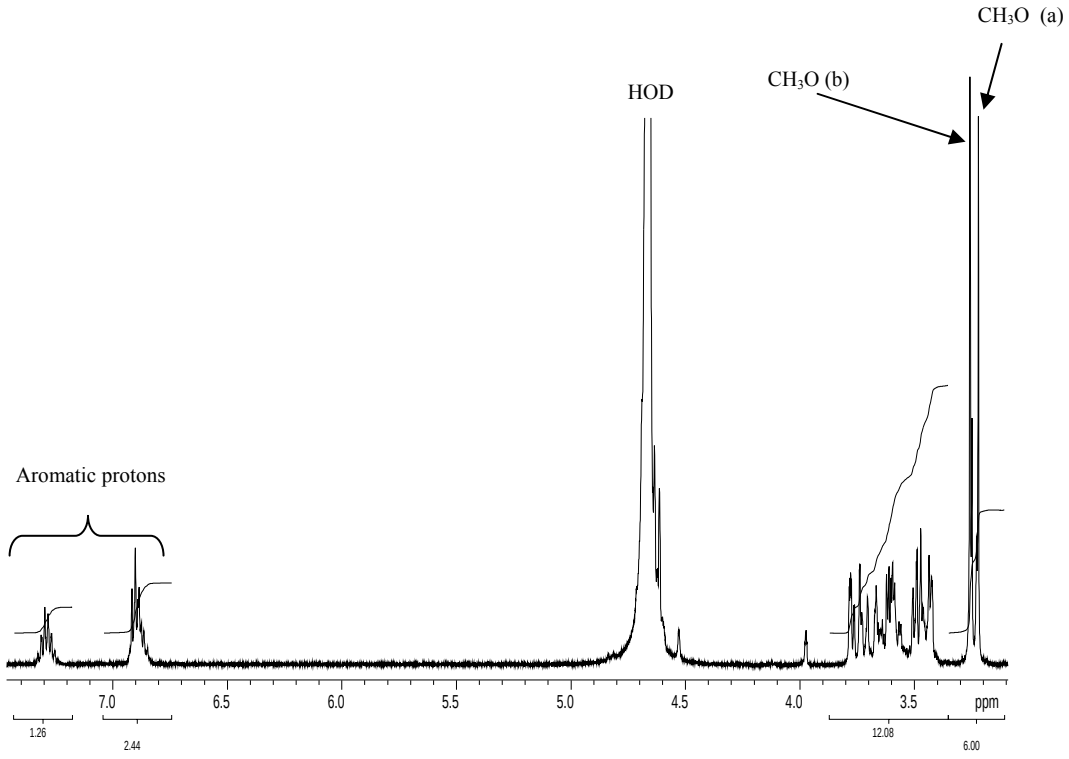

Figure 27: Proton NMR spectrum of the deprotection reaction product of methyl- mannopyranoside protected with difluorobenzyl group. (500 MHz, D_2O).

Comparison of the two spectra shows that deprotection was partial. This is evidenced by two methoxy signals in Figure 27, meaning there are two closely related species. Integration yields six methoxy protons and twelve sugar ring signals (two anomeric protons are buried under the solvent peak, leaving 2 x 6 ring protons). We would expect twelve aromatic protons as shown in Figure 28 (notice that one of the aromatic protons is buried under the solvent peak, showing eleven instead of twelve), but only three are present, showing that in one species, one difluorobenzyl group is still on. Mass spectrometry results support the NMR observation. There is a signal at m/z 217.1 $[M+23]^+$, corresponding to a fully deprotected adduct. A signal at m/z 343.1 corresponds to the methyl mannoside with one DFBn group still on. Electrospray mass spectrometry confirms the presence of a completely deprotected sugar. It also shows that there is a partially deprotected sugar.

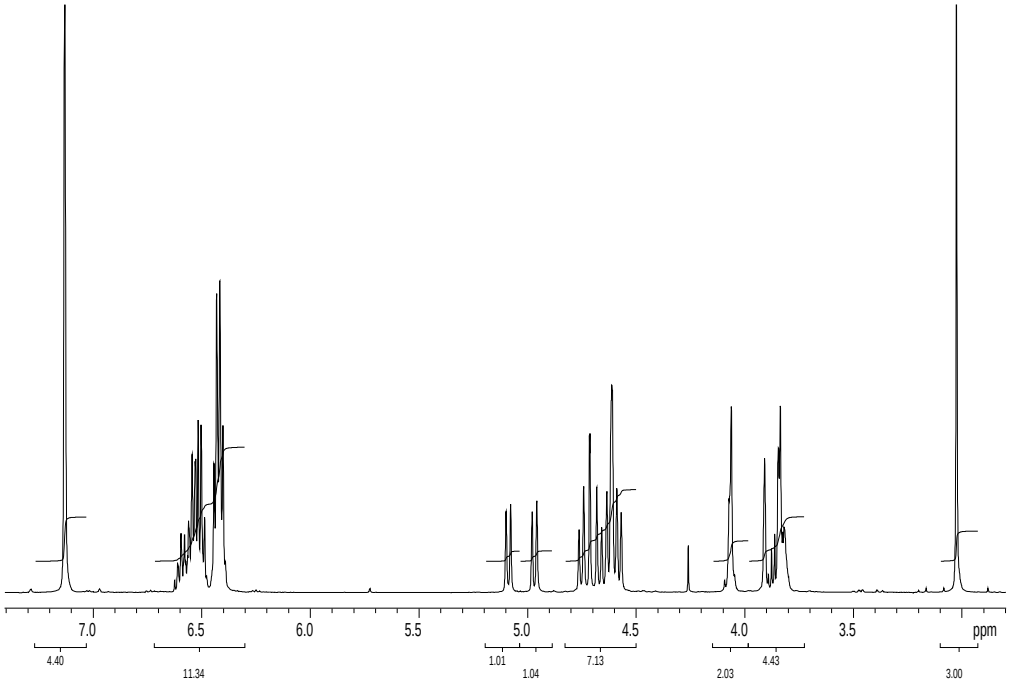

Figure 28: Proton NMR spectrum of methyl mannopyranoside protected with difluorobenzyl group (500MHz, C_6D_6).

3 Conclusions and future outlook.

3.1. Assesment of the spectral dispersion, protection and deprotection reactions.

Protection of the hydroxyl groups of all the sugars was successfully achieved as shown by evidence from the NMR proton, carbon-13, and fluorine-19 spectra. The mass spectra confirmed the capping by providing evidence of the molecular masses consistent with total tagging of all the hydroxyl groups.

The proton spectrum dispersion in the two sugars studied was immensely improved, when pentafluorobenzyl bromide was used as a protecting group, leading to an easier assignment of all the resonances. The other benzylated analogues (mono-, di-, tetra-) also simplified the assignments, but the dispersion was not as great as with the pentafluoro-group.

The carbon-13 spectrum assignment was equally simplified. The signals associated with the sugar carbons were pushed to higher frequencies, well away from the methylene carbons of the introduced fluoro benzyl groups, which were pushed to lower frequencies. Pentafluoro group caused the greatest separation. Comparison to benzylation with a normal benzyl group revealed that fluoro benzyl groups separated the sugar from the methylene carbons, while with benzyl groups the methylene signals were interspersed among the sugar signals, leading to crowding which complicates spectral assignment especially when two-dimensional heteronuclear correlation techniques are to be used.

A similar procedure for tagging the sugars with protecting groups was adopted for all the benzyl analogues. Normal benzyl had the best yields at 96%. Other yields of 88%, 64% and 20% for mono, tetra, and pentafluoro benzyl respectively indicated that pentafluoro benzylation was difficult to put into the sugar.

The failure of the deprotection of the sugar from the pentafluoro suggests that it would not be a very good group as it fails two of the criteria for a protecting group. [28, 29]

Benzene-d_6 generally shows better dispersion than chloroform-d_1. In addition, in the carbon-13 spectrum, the aromatic ring carbon-13 signals of the solvent (~128 ppm) are far away from the sugar signals (~60 – 80 ppm). The carbon-13 chloroform signal occurs in the region of the sugars (~77.2 ppm). It actually overlapped with one of the sugar signals. This suggests that benzene-d_6 is a solvent of choice. However, great caution should be exercised with benzene because of its high toxicity and carcinogenic effects.

The solvent effect should be considered on a case by case basis. For example the proton dispersion when DFBn was used as a derivative was very poor (Figure 23); however, making up the solution in chloroform-d_1 improved the proton dispersion. See Figure A3 in the appendix section for a comparison of the dispersion in the two solvents.

3.2. Future considerations of the project.

Future efforts should be concentrated on optimizing the deprotection. Since it has been shown that a difluoro benzyl can be removed, when the reaction is let to extend for longer periods of time, this gives hope that the deprotection is possible. Mild but very effective techniques of deprotection should be explored. Examples include reduction with dissolving metals. [39-41] Milder metals like calcium should be tried to avoid sugar ring cleavage by violent reactions. Another option may be light catalysed cleavage of benzyl ether bond by N-succinimide in the presence of calcium carbonate. [42] This procedure has been used successfully to cleave sterically hindered benzyl ethers as well as inert groups like phthalimides, glycosyl fluorides and sulfides.

Some suggestions concerning the assignments were based on speculations which need to be proven experimentally. One of them is the deshielding pattern of the methylene protons in fluoro benzyl protected sugars. A 3,5 difluoro group should be used instead of a 2,6 difluoro to study the trend of the methylene protons when the fluorine atoms are far away to exert dipolar interactions with these protons. If the methylene protons become deshielded to the same extent as when a 2,6 difluoro group is used, then the fluorine-proton dipolar interaction would be ruled out as a major factor shifting the methylene protons to higher frequencies.

The peculiar behavior of the methylene multiplets on position 10 was studied by NOESY. The result was that these multiplets were engaged in a dipolar interaction with the deshielding region of the aromatic system at 11. This was made on the assumption that the aromatic system was closer in space to the methylene protons. This needs to be verified using structure simulations programs giving the best fitted structure after energy minimizations have been done.

4 Experimental

4.1. Spectroscopic Characterization of the compounds.

NMR spectra were acquired mainly on Varian Inova-500 spectrometers (software VNMR 6.1C) operating at a proton frequency of 500MHz and a carbon-13 frequency of 125 MHz. A Bruker 5mm 1H/F19 dual probe was used for proton-fluorine decoupling experiments. [43-45] Fluorine COSY experiments were set up on a 400 MHz Varian Mercury with a 1 Broad Band channel and a proton only decoupler (software VNMR 6.1C). Mass spectra were acquired from Waters Micromass LCT, and Thermo Funigan LTQ FT spectrometer was used for high resolution mass spectra acquisitions.

4.2. Protection of glucose by benzylation.

Most of the reagents were used as purchased from Aldrich and included: glucose, methyl-α-D-mannopyranoside, methanol, methanesulfonic acid, sodium hydride; 60% dispersion in mineral oil, benzyl bromide (BnBr) and pentafluorobenzyl bromide(ArF_5CH_2Br). Dry ethanol and dimethyl formamide (DMF) were supplied by Fluka and sodium hydrogen carbonate by Lancaster. Dichloromethane (DCM), ethyl acetate and n-hexane were supplied by Fisher. The hexane was redistilled prior to use. Flash column chromatography (FCC) was perfomed on silica gel (40-63 micron 60A) supplied by Fluorochem and TLC on aluminium-supported silica gel ($60F_{254}$ by Merck) was visualised using a solution of phosphomolybdic acid:cerium sulphate.

Protected glucose analogues were prepared by treatment of ethyl glucoside with benzyl bromide analogues in the presence of a base.[36, 46, 47]

Ethyl glucoside***(1)*** :To a mixture of glucose (0.0500 g; 2.76 mmol) and dry ethanol (3.0 ml; 51.0 mmol) under nitrogen was added methanesulfonic acid (20 µl; 0.30 mmol). The resulting solution was refluxed at 100ºC overnight in an oil bath with stirring. The reaction mixture was cooled to room temperature after which the progress of the reaction

was checked by TLC (9:1; DCM-MeOH), which showed complete conversion of starting material into product. The methanesulfonic acid was neutralised with $NaHCO_3$ (0.050 g; 0.595 mmol) and ethanol was removed *in vacuo*.

The residue was purified by flash column chromatography on silica gel (9:1; DCM-MeOH) to give ethyl glucoside as a colourless oil (427 mg; 74%): ^1H NMR; 200 MHz in D_2O δ/ppm:1.04 (t, 3H ^3J=7.2 Hz, (H-7)), 3.0-3.8(m, 9H), 4.28(d, 1H, ^3J=8.3 Hz, H-1(β)), 4.45-4.69 (HOD) 4.75 (d, 1H, ^3J=3.9 Hz, H-1(α)).

Ethyl 2,3,4,6-Tetra-O-Benzyl-D-glucopyranoside***(2)***: To a mixture of ***(1)*** (0.151 g, 0.725 mmol) and DMF under argon (8.0 ml) was added benzyl bromide (0.680 ml; 5.50 mmol). The solution was cooled to 0 ºC in an ice bath, and sodium hydride (0.130 g; 5.80 mmol as a 60% dispersion in mineral oil) was added portionwise with stirring. The mixture was allowed to warm up gradually to room temperature and was stirred for 16 hours. TLC (9:1; DCM-MeOH) then showed that the reaction had gone to completion. Excess sodium hydride was quenched with methanol (1 ml).

Volatile materials were removed *in vacuo* and the residue purified by column chromatography using hexane (50 ml) to remove mineral oil, then 9:1; hexane-ethyl acetate to give ***(2)*** (132 mg, 32%) as a mixture of anomers. Further chromatographic purification furnished separate samples of ***(α-2)*** and ***(β-2)*** (α; 44 mg): ^1H NMR; 500 MHz in $CDCl_3$ δ/ppm: 1.27 (t, 3H, ^3J=7.0 Hz, H-7), 3.54 (m, 1H, H-8), 3.58 (m, 1H, H-2), 3.65 (m, 1H, H-6), 3.67 (m, 1H, H-4), 3.72 (m, 1H, H-8'), 3.76 (m, 1H, H-6'), 3.82 (m, 1H, H-5), 4.03, (t, 1H, ^3J=9.3 Hz, H-3), 4.50 (AB m, 2H, ^2J=10.4, 12.8 Hz, H-11, H-12), 4.64 (AB m, 1H, ^2J=12.1 Hz), 4.68 (AB m, 1H, ^2J=12.2 Hz), 4.79 (d, 1H, ^3J=3.4 Hz, H-1α), 4.82 (AB m, 1H, ^2J=12.5 Hz, H-9'), 4.84 (AB m, 1H, ^2J=10.8 Hz, H-10), 4.87 (AB m, 1H, ^2J=10.8 Hz), 5.03 (AB m, 1H, ^2J=10.8 Hz, H-10'), 7.34 (benzene ring protons, 20H). ^{13}C NMR; 125 MHz in $CDCl_3$ δ/ppm: 17.8 ($\underline{CH_3}CH_2O$ C-7), 63.5 ($CH_3\underline{CH_2}O$ C-8), 68.7 (CH_2 C-6), 70.3 (CH C-5), 73.5 (CH C-9), 73.7 (Ar$\underline{CH_2}$ C-12), 75.4 (Ar$\underline{CH_2}$ C-11), 76.0 (Ar$\underline{CH_2}$ C-10), 78.0 (CH C-4), 80.2 (CH C-2), 82.4 (CH C-3), 96.8 (CH C-1), 130-140 (benzene ring carbons)], (β;12 mg) [^1H NMR; 500 MHz in $CDCl_3$ δ/ppm: 1.33 (t,

3H, ^{3}J=7.1 Hz, H-7), 3.50 (m, 2H, H-2, H-5), 3.60 (d, 1H, H-4), 3.65 (d, 1H, H-3), 3.66 (1H, H-8), 3.70, 3.78 (d, 2H, H-6, H-6'), 4.06 (q, 1H, ^{3}J=7.0 Hz, H-8'), 4.45 (d, 1H, ^{3}J=7.8 Hz, H-1), 4.56 (d, 1H, ^{2}J=10.9 Hz, H-11), 4.60 (d, 1H, ^{2}J=12.3 Hz, H-12) 4.65 (q, 1H, ^{2}J=12.3 Hz, H-12'), 4.75 (d, 1H, ^{2}J=10.5 Hz, H-9), 4.83 (d, 1H, ^{2}J=, H10), 4.84 (d, 1H, ^{2}J=11.0 Hz, H-11'), 4.96 (d, 1H, ^{2}J= H-10'), 4.99 (d, 1H, ^{2}J=11.0 Hz, H-9'), 7.34 (benzene ring protons, 20H). ^{13}C NMR; 125 MHz in $CDCl_3$ δ/ppm: 16.0 ($\underline{CH_3}CH_2O$ C-7), 66.0 ($CH_3\underline{CH_2}O$ C-8), 69.0 (CH_2 C-6), 73.4 (Ar$\underline{CH_2}$ C-12), 74.8 (CH C5, Ar$\underline{CH_2}$ C-9), 75.2 (Ar$\underline{CH_2}$ C-11), 76.0 (Ar$\underline{CH_2}$ C-10), 78.0 (CH C-4), 82.6 (CH C-2), 85.0 (CH C-3), 104.0 (CH C-1), benzene ring carbons: para carbons; 127.86, 127.89, 127.94, 128.03; ortho carbons: 128.05 (on CH_2 C-12), 128.18 (on CH_2 C-10), 128.27 (on CH_2 C-11), 128.47 (on CH_2 C-9), meta carbons: 128.62, 128.66, 128.67. *ipso* carbons: 138.37 (on CH_2 C-11), 138.47 (on CH_2 C-12), 138.81 (on CH_2 C-9), 138.9 (on CH_2 C-12)].

Ethyl 2,3,4,6-Tetra-O-Pentafluorobenzyl-D-glucopyranoside ***(3)***: ***(1)*** (0.0830 g; 0.397 mmol) was pentafluorobenzylated using the same procedure as described in the preparation of ***(2)***. The other reagents were scaled appropriately and were as follows: DMF under argon (5 ml), $ARCH_2Br$ (0.560 ml;3.97 mmol), sodium hydride (0.158 g, 6.58 mmol; 60% dispersion in mineral oil). ***(3)*** was obtained as a colourless oil (168 mg, 43%) by chromatography on silica gel as described above.

Further chromatographic purification using (Hexane:Ethyl acetate; 9.5:0.5 followed by 9:1) furnished separate samples of the α (38 mg) and β (25 mg) anomers.

(α; 38 mg): ^{1}H NMR; 500 MHz in $CDCl_3$ δ/ppm: 1.25 (t, 3H, ^{3}J=7.1 Hz, H-7), 3.50 (dd, 1H, ^{3}J=3.6 and 9.6 Hz, H-2), 3.54 (AB m, 1H, ^{3}J=9.7 Hz, H-4), 3.55 (AB m, 1H, ^{3}J=8.8 Hz, H-8), 3.66 (AB m, 1H, ^{2}J=11.1 Hz, H-6), 3.70 (m, 1H, ^{3}J=7.1 Hz, H-5), 3.74 (AB m, 1H, ^{3}J= 7.1 and 9.9 Hz, H-8'), 3.95 (AB m, 1H, ^{2}J=10.8 Hz, H-6'), 3.86 (t, 1H, ^{3}J=9.1 Hz, H-3), 4.61 (AB m, 1H, ^{2}J=10.0 Hz, H-11), 4.63 (AB m, 1H, ^{2}J=10.7 Hz, H-12), 4.70 (AB m, 1H, ^{2}J=12.7 Hz, H-9), 4.73 (AB m, 1H, H-12'), 4.75 (AB m, 1H, ^{2}J=11.1 Hz, H-9), 4.82 (AB m, 1H, ^{2}J=10.7 Hz, H-10), 4.92 (AB m, 1H, ^{2}J=10.5 Hz, H-11), 4.97 (AB m, 1H, ^{3}J=3.7 Hz, H-1α), 4.98 (AB m, 1H, ^{2}J=12.0 Hz, H-10'). ^{13}C NMR; 125 MHz in

$CDCl_3$ δ/ppm: 15.0 ($\underline{CH_3}CH_2O$ C-7), 59.2 (Ar$\underline{CH_2}$ C-9), 60.6 (Ar$\underline{CH_2}$ C-12), 61.2 (Ar$\underline{CH_2}$ C-11), 61.9 (Ar$\underline{CH_2}$ C-10), 63.9 (Ar$\underline{CH_2}$ C-18), 69.1 (CH_2 C-6), 70.0 (CH C-5), 77.5 (CH C-4), 80.9 (CH C-2), 82.0 (CH C-3), 95.6 (CH C-1), 110.0 – 111.9 (Ar *ipso*), 136.8, 138.9 (Ar *meta*), 140.5, 142.4 (Ar *para*), 144.7, 146.8 (Ar *ortho*). ES+MS, m/z 951.1 $[M+Na]^+$ and HRMS: $C_{36}H_{20}F_{20}O_6$.Na; mass 951.0838.

(β; 25 mg): ^{1}H NMR; 500 MHz in $CDCl_3$ δ/ppm: 1.26 (t, 3H, ^{3}J=7.0 Hz, H-7), 3.30 (t, 2H, ^{3}J=7.5 Hz, H-2, H-5), 3.45 (t, 1H, ^{3}J=9.0 Hz, H-3), 3.53 (t, 1H, ^{3}J=9.1 Hz, H-4), 3.60 (p, 1H, ^{3}J=7.0 Hz, H-8), 3.74 (dd, 2H, ^{3}J=11.0 Hz, H-6), 3.94 (p, 1H, ^{3}J=7.2 Hz, H-8'), 4.30 (d, 1H, ^{3}J=7.8 Hz, H-1β), 4.64 (d, 1H, ^{2}J=12.6 Hz, H-11), 4.66 (AB m, 1H, ^{2}J=8.7 Hz, H-12), 4.74 (d, 2H, ^{2}J=11.0 Hz, H-9, H-12'), 4.83 (AB m, 1H, ^{2}J=10.6 Hz, H-10), 4.86 (AB m, 1H, ^{2}J=10.1 Hz, H-11') 4.93 (d, 1H, ^{2}J=11.0 Hz, H-10'), 5.08 (d, 1H, ^{2}J=10.7 Hz, H-9'). ^{13}C NMR; 125 MHz in $CDCl_3$ δ/ppm: 15.2, ($\underline{CH_3}CH_2O$ C-7), 60.7 (Ar$\underline{CH_2}$ C-12), 60.8 (Ar$\underline{CH_2}$ C-9) , 61.2 (Ar$\underline{CH_2}$ C-11), 61.9 (Ar$\underline{CH_2}$ C-10), 66.0, ($CH_3\underline{CH_2}O$ C-8), 69.2 (CH_2 C-6), 74.6 (CH C-5), 77.7 (CH C-4), 82.4 (CH C-2), 84.6 (CH C-3), 103.2 (CH C-1), 110.0 – 110.9 (Ar *ipso*), 137.0, 138.8 (Ar *meta*), 140.8, 142.5 (Ar *para*), 145.0, 146.9 (Ar *ortho*) . ES+MS, m/z 951.1 $[M+Na]^+$ and HRMS: $C_{36}H_{20}F_{20}O_6$.Na; mass 951.0838.

(α anomer in C_6D_6): ^{1}H NMR; 500 MHz in C_6D_6 δ/ppm: 1.02 (t, 3H, ^{3}J=7.0 Hz, H-7), 3.23 (o, 1H, H-8), 3.33 (dd, 1H, ^{3}J=3.4, 9.4 Hz, H-6), 3.47 (dd 1H, ^{3}J=9.4 Hz, H-6'), 3.56 (o, 1H, H-8'), 3.65 (t, 1H, ^{3}J=9.3, 9.5 Hz, H-4), 3.71 (d, 1H, ^{3}J=9.3 Hz, H-6'), 3.74 (m, 1H, ^{3}J=9.3 Hz, H-5), 4.00 (t, 1H, ^{3}J=9.1 Hz, H-3), 4.13 (AB m, 2H, ^{2}J=10.9 Hz, H-9), 4.30 (AB m, 2H, ^{2}J=11.2 Hz, H-12), 4.52 (d, 1H, ^{2}J=10.6 Hz, H-11), 4.60 (d, 1H, ^{2}J=11.7 Hz, H-10), 4.77 (m, 1H, Hz, H-10'), 4.78 (m, 1H, H-11'), 4.81 (d, 1H, ^{3}J=3.4 Hz, H-1). ^{13}C NMR; 125 MHz in C_6D_6 δ/ppm: 15.0 ($\underline{CH_3}CH_2O$ C-7), 58.3 (Ar$\underline{CH_2}$ C-9), 60.0 (Ar$\underline{CH_2}$ C-12), 60.9 (Ar$\underline{CH_2}$ C-11), 61.5 (Ar$\underline{CH_2}$ C-10), 63.9 ($CH_3\underline{CH_2}$ C-8), 69.1 (CH_2 C-6), 70.6 (CH C-5), 77.7 (CH C-4), 80.9 (CH C-2), 81.9 (CH C-5), 95.8 (CH C-5), 110.-110.5 (Ar *ipso*), 134.2, 136.4 (Ar *meta*), 139.8, 141.9 (Ar *para*), 144.0, 146.4 (Ar *ortho*). ^{19}F NMR; 376 MHz in C6D6 δ/ppm: -163.47 to -162.78 (*meta*), -155.25 to -154.21 (*para*), -144.70 to -143.03 (*ortho*).

(β anomer in C_6D_6): ^{1}H NMR; 500 MHz in C_6D_6 δ/ppm: ^{1}H NMR; 500 MHz in C_6D_6 δ/ppm: 1.11 (t, 3H, ^{3}J= 7.0 Hz, H-7), 2.97 (m, 1H, ^{3}J= 1.8, 8.0 Hz, H-5), 3.28 (m, 1H, ^{3}J= 7.1, 9.0 Hz, H-2), 3.32 (o, 1H, ^{3}J= 7.0, 9.5 Hz, H-8), 3.38 (m, 1H, ^{3}J= 9.0 Hz, H-3), 3.41 (m, 1H, ^{3}J= 2.0, 11.5 Hz, H-6), 3.55 (t, 1H, ^{3}J= 9.3 Hz, H-4), 3.66 (dd, 1H, ^{3}J= 3.5, 11.5 Hz, H-6'), 3.78 (o, 1H, ^{3}J= 7.1, 9.4 Hz, H-8'), 4.05 (d, 1H, ^{3}J= 7.8 Hz, H-1), 4.28, 4.31 (AB m, 2H, ^{2}J= 11.4, 11.4 Hz, H-11), 4.40 (AB m, 1H, ^{2}J= 10.8 Hz, H-9), 4.46 (AB m, 1H, ^{2}J= 10.8 Hz, H-12), 4.66 (AB m, 1H, ^{2}J= 10.6 Hz, H-12), 4.69 (AB m, 1H, ^{2}J= 11.2 Hz, H-10), 4.80 (AB m, 1H, ^{2}J= 11.0 Hz, H-9'), 4.81 (AB m, 1H, ^{2}J= 11.2 Hz, H-10'). ^{13}C NMR; 125 MHz in C_6D_6 δ/ppm: 15.0 ($\underline{CH_3}CH_2O$ C-7), 60.3 (ARCH2 C-11), 60.4 (ARCH2 C-9), 60.8 (ARCH2 C-12), 61.6 (ARCH2 C-10), 65.4 ($CH_3\underline{CH_2}$ C-8), 68.9 (CH C-4), 74.6 (CH C-5), 77.5 (CH_2 C-6), 82.4 (CH C-2), 84.7 (CH C-3), 103.2 (CH C-1), 111.1 – 111.7 (Ar *ipso*), 136.5, 138.5 (Ar *meta*), 140.3, 142.3 (Ar *para*), 144.7, 146.7 (Ar *ortho*). ^{19}F NMR; 376 MHz in C6D6 δ/ppm: -163.31 to -162.91 (*meta*), -155.00 to -154.44 (*para*), -144.70 to -143.95 (*ortho*).

Methyl-α-D-mannopyranoside ***(4):*** ^{1}H NMR; 500 MHz in CD_3OD δ/ppm: 3.32 (s, 3H, H-7), 3.49 (o, 1H, ^{3}J= 2.0, 9.0, 11.5 Hz, H-5), 3.61 (t, 1H, ^{3}J= 9.5 Hz, H-4), 3.66 (q, 1H, ^{3}J= 3.0, 9.0 Hz, H-3), 3.72 (q, 1H, ^{3}J= 5.5, 11.5 Hz, H-6), 3.79 (q, 1H, ^{3}J= 1.4, 5.0 Hz, H-2), 3.85 (dd, 1H, ^{3}J= 2.5, 12.0 Hz, H-6'). ^{13}C NMR; 125 MHz in CD_3OD δ/ppm: 54.0 ($\underline{CH_3}O$ C-7), 61.8 (CH C-6), 67.4 (CH C-4), 70.9 (CH C-2), 71.4 (CH C-3), 73.3 (CH C-5), 101.6 (CH C-1).

4.3. Protection and deprotection of the mannopyranoside.

The protected mannopyrannoside compounds were provided by Dr. Elizabeth Grayson. The deprotection reactions were also carried out in her lab. The NMR assignments and mass spectrometry data is presented below.

Methyl 2,3,4,6-Tetra-O- benzyl-α-D-mannopyranoside ***(5)***: 96% yield. ^{1}H NMR; 500 MHz in C_6D_6 δ/ppm: 3.11 (s, 3H, H-7), 3.72 (dd, 1H, ^{3}J= 1.4, 10.8 Hz, H-6), 3.79 (m, 1H, ^{3}J= 2.3 Hz, H-2), 3.81 (d, 1H, ^{3}J= 10.9 Hz, H-6'), 3.92 (o, 1H, H-5), 4.05 (d, 1H, ^{3}J=

3.0, 9.4 Hz, H-3), 4.24 (t, 1H, ^{3}J= 9.6, 9.7 Hz, H-4), 4.42 (m, 1H, ^{2}J=10.8 Hz, H-11), 4.45 (m, 2H, ^{2}J=12.0 Hz, H-9), 4.51 (AB m, 1H, ^{2}J=12.9 Hz, H-8), 4.53 (AB m, 1H, ^{2}J=11.5 Hz, H-10), 4.56 (d, 1H, ^{2}J=11.5 Hz, H-11'), 4.62 (AB m, 1H, ^{2}J=12.3 Hz, H-8'), 4.76 (d, 1H, ^{3}J=1.3 Hz, H-1), 4.95 (AB m, 1H, ^{2}J=11.4 Hz, H-10), 7.04 -7.07 (m, 4H, *para*), 7.11 – 7.14 (m, 8H, *ortho*), 7.22 – 7.35 (m, 8H, *meta*). ^{13}C NMR; 125 MHz in C_6D_6 δ/ppm: 54.4 ($\underline{CH_3}$ C-7), 70.0 (CH_2 C-6), 72.1 (Ar$\underline{CH_2}$ C-9) C-9), 72.7 (CH C-5), 73.0 (Ar$\underline{CH_2}$ C-8), 73.4 (Ar$\underline{CH_2}$ C-11), 75.0 (Ar$\underline{CH_2}$ C-10), 75.5 (CH C-4), 75.7 (CH C-2), 80.8 (CH C-3), 99.4 (CH C-1), 127.4 – 127.6 (Ar *para*), 127.7 – 127.9 (Ar *meta*), 128.1 – 128.5 (Ar *ortho*), 139.1 – 139.5 (Ar *ipso*) . ES+ MS, m/z 577.4 $[M+Na]^{+}$, 554.5 [M].

Methyl 2,3,4,6-Tetra-O-Pentafluorobenzyl-α-D-mannopyranoside ***(6)***: 16% yield. ^{1}H NMR; 500 MHz in C_6D_6 δ/ppm: 3.04 (s, 3H, H-7), 3.49 (dd, 1H, ^{3}J= 11.0 Hz, H-6), 3.59 (dd, 1H, ^{3}J= 2.5, 10.0 Hz, H-5), 3.63 (t, 1H, ^{3}J= 2.5 Hz, H-2), 3.74 (dd, 1H, ^{3}J= 4.0, 11.0 Hz, H-6'), 3.84 (dd, 1H, ^{3}J= 2.5, 9.5 Hz, H-3), 3.99 (t, 1H, ^{3}J= 9.5,10.0 Hz, H-4), 4.22 (AB m, 2H, ^{2}J= 11.0 Hz, H-8, H-11), 4.31 (AB m, 1H, ^{2}J = 11.5 Hz, H-9), 4.37 (AB m, 2H, ^{2}J= 11.5 Hz, H-11'), 4.43 (AB m, 2H, ^{2}J= 10.5, 12.0 Hz, H-8', H-10), 4.62 (d, 1H, ^{3}J=1.5 Hz, H-1), 4.72 (AB m, 1H, ^{2}J= 11.0 Hz, H-10'). ^{13}C NMR; 125 MHz in C_6D_6 δ/ppm: 54.5 ($\underline{CH_3}$O C-7), 58.7 (Ar$\underline{CH_2}$ C-9), 59.9 (Ar$\underline{CH_2}$ C-8), 60.1 (Ar$\underline{CH_2}$ C-11), 60.9 (Ar$\underline{CH_2}$ C-10), 69.5 (CH C-6), 72.1 (CH C-5), 74.5 (CH C-4), 76.5 (CH C-2), 81.1 (CH C-3), 98.9 (CH C-1), 111.3 (Ar *ipso*), 137.0 (Ar *meta*), 141.5 (Ar *para*), 146.6 (Ar *ortho*). ^{19}F NMR; 376 MHz in C6D6 δ/ppm: -163.60 to -162.55 (*meta*), -155.22 to -154.04 (*para*), -144.72 to -144.38 (*ortho*). ES+ MS, m/z 937.6 $[M+Na]^{+}$ and HRMS: $C_{35}H_{18}O_6F_{20}.^{23}Na$; mass 937.0676.

Methyl 2,3,4,6-Tetra-O-(2',3',5',6' tetrafluoro-4-methoxy) benzyl-α-D-manopyranoside ***(7)***: 13% yield ^{1}H NMR; 500 MHz in C_6D_6 δ/ppm: 3.05 (s, 3H, H-7), 3.44 (s, 12H, 4 x H-$\underline{CH_3}$OAr), 3.65 (d, 1H, ^{3}J=11.1 Hz, H-6), 3.69 (dt, 1H, ^{3}J= 4.5, 9.8 Hz, H-5), 3.78 (t, 1H, ^{3}J= 2.0, H-2), 3.84 (dd, 1H, ^{2}J= 11.0 Hz, ^{3}J = 4.6 Hz, H-6'), 3.97 (dd, 1H, ^{3}J= 3.0, 9.39 Hz, H-3), 4.11 (t, 1H, ^{3}J= 9.6 Hz, H-4), 4.39 (AB m, 1H, ^{2}J= 12.1 Hz, H-11), 4.41 (AB m, 1H, ^{2}J= 11.0 Hz, H-8), 4.47 (AB m, 1H, ^{2}J= 11.0 Hz, H-9), 4.51 (AB m, 1H, ^{2}J=

9.4 Hz, H-10), 4.54 (AB m, 1H, ^{2}J= 11.2 Hz, H-9'), 4.54 (AB m, 1H, ^{2}J= 11.2 Hz, H-11'), 4.62 (AB m, 1H, ^{2}J= 10.8 Hz, H-8'), 4.70 (d, 1H, ^{3}J= 1.6 Hz, H-1), 4.88 (AB m, 1H, ^{2}J= 10.6 Hz, H-10'). ^{13}C NMR; 125 MHz in C_6D_6 δ/ppm: 54.5 ($\underline{CH_3}$O C- 7), 59.0 (Ar$\underline{CH_2}$ C– 9), 60.0 (Ar$\underline{CH_2}$ C- 8), 60.5 (Ar$\underline{CH_2}$ C- 11), 61.0 (Ar$\underline{CH_2}$ C-10, 4 x $\underline{CH_3}$OAr), 69.5 (CH_2 C- 6), 72.0 (CH C-5), 74.5 (CH C-4), 76.5 (CH C-2), 81.0 (CH C-3), 99.0 (CH C-1), 110.0 (Ar *ipso*), 138.4, 138.8 (Ar *para*), 139.8, 142.0 (Ar *meta*), 144.8, 147.0 (Ar *ortho*). ES+ MS, m/z 985.2 $[M+Na]^{+}$, and HRMS: $C_{39}H_{30}O_{10}F_{16}.^{23}Na$; mass 985.1476.

Methyl 2,3,4,6-Tetra-O- 2' Monofluorobenzyl-α-D-mannopyranoside ***(8)***: 88% yield. ^{1}H NMR; 500 MHz in C_6D_6 δ/ppm: 3.05 (s, 3H, H-7), 3.71 (d, 1H, ^{3}J= 9.6 Hz, H-6), 3.76 (t, 1H, ^{3}J= 2.6 Hz, H-2), 3.83 (s, 2H, H-5, H-6'), 4.02 (dd, 1H, ^{3}J= 3.0, 9.5, H-3), 4.22 (q, 1H, ^{3}J= 5.9 , 9.4 Hz, H-4), 4.57 (s, 2H, H-8, H-9), 4.62 (AB m, 1H, ^{2}J= 12.0 Hz, H-9'), 4.66 (AB m, 2H, ^{2}J= 12.9 Hz, H-11), 4.69 (s, 2H, H-1, H-10), 4.75 (AB m, 1H, ^{2}J= 12.7 Hz, H-8'), 5.04 (AB m, 1H, ^{2}J= 11.7 Hz, H-10'), 6.71 – 6.77 (m, 8H, *meta*), 6.79 – 6.83 (m, 4H, *para*), 7.3 – 7.6 (m, 4H, *ortho*). ^{13}C NMR; 125 MHz in C_6D_6 δ/ppm: 54.3 ($\underline{CH_3}$O C-7), 65.5 (Ar$\underline{CH_2}$ C-9), 66.7 (Ar$\underline{CH_2}$ C-11), 66.9 (Ar$\underline{CH_2}$ C-8), 68.6 (Ar$\underline{CH_2}$ C-10), 70.1 (CH C-6), 72.5 (CH C-5), 75.3 (CH C-4), 76.2 (CH C-2), 81.0 (CH C-3), 99.2 (CH C-1), 115.0 (Ar *ipso*), 124.2 (Ar *para*), 126.5, 130.5 (Ar *ortho* at position with H), 159.8, 161.8 (Ar *ortho* at position with F) 129.2 (Ar *meta*). ^{19}F NMR; 376 MHz in C6D6 δ/ppm: -119.55 to -118.59 (*ortho*). ES+ MS, m/z 649.4 $[M+Na]^{+}$.

Methyl 2,3,4,6-Tetra-O- 2',6'- Difluorobenzyl-α-D-mannopyranoside ***(9)***: ^{1}H NMR; 500 MHz in C_6D_6 δ/ppm: 3.03 (s, 3H, H-7), 3.82 (m, 2H, H-6), 3.83 (m, 1H, H-4), 3.91 (s, 1H, H-2), 4.05 (s, 1H, H-3), 4.07 (s, 1H, H-5), 4.58 (AB m, 1H, ^{2}J= 10.3 Hz, H-10), 4.61 (m, 3H, ^{2}J= 10.2, 11.3 Hz, H-8, H-11), 4.67 (AB m, 1H, ^{2}J= 11.1 Hz, H-9), 4.71 (d, 1H, ^{3}J= 1.7 Hz, H-1), 4.75 (AB m, 1H, ^{2}J= 10.9 Hz, H-9'), 4.97 (AB m, 1H, ^{2}J= 10.9 Hz, H-8'), 5.09 (AB m, 1H, ^{2}J= 10.3 Hz, H-10'), 6.39 – 6.45 (m, 4H, *para*), 6.49 – 6.61 (m, 8H, *meta*). ^{13}C NMR; 125 MHz in C_6D_6 δ/ppm: 54.3 ($\underline{CH_3}$O C-7), 59.4 (Ar$\underline{CH_2}$ C-9), 60.6 (Ar$\underline{CH_2}$ C-11), 60.8 (Ar$\underline{CH_2}$ C-8), 61.8 (Ar$\underline{CH_2}$ C-10), 70.4 (CH C-6), 72.5 (CH C-5), 75.7 (CH C-4), 76.8 (CH C-2), 81.5 (CH C-3), 99.5 (CH C-1), 110.1 – 11.3 (Ar *para*),

114.1 – 115.2 (Ar *ipso*), 129.6 – 130.1 (Ar *meta*), 161.2 – 163.4 (Ar *ortho*). ^{19}F NMR; 376 MHz in C6D6 δ/ppm: -115.22 to -115.05 (*ortho*). ES+ MS, m/z 721.3 $[M+Na]^+$.

Methyl 2,3,4,6-Tetra-O- 2',3',5',6'- Tetrafluorobenzyl-α-D-mannopyranoside ***(10)***: 64% yield. ^{1}H NMR; 500 MHz in C_6D_6 δ/ppm: 3.00 (s, 3H, H-7), 3.56 (d, 1H, ^{3}J= 11.1 Hz, H-6), 3.61 (o, 1H, H-5), 3.70 (t, 1H, ^{3}J= 2.3 Hz, H-2), 3.76 (dd, 1H, ^{3}J= 4.6, 11.2 Hz, H-6'), 3.90 (dd, 1H, ^{3}J= 3.0, 9.6 Hz, H-3), 4.03 (t, 1H, ^{3}J= 9.6, 9.7 Hz, H-4), 4.33 (m, 1H, H-11), 4.36 (m, 2H, H-8, H-10), 4.39 (AB m, 1H, ^{2}J= 11.2 Hz, H-9), 4.45 (AB m, 1H, ^{2}J= 10.7 Hz, H-9'), 4.48 (AB m, 1H, ^{2}J= 11.1 Hz, H-11'), 4.57 (AB m, 1H, ^{2}J= 10.9 Hz, H-8'), 4.62 (d, 1H, ^{3}J= 1.5 Hz, H-1), 4.80 (AB m, 1H, ^{2}J= 10.5 Hz, H-10'), 6.10 – 6.24 (m, 4H, *para*) . ^{13}C NMR; 125 MHz in C_6D_6 δ/ppm: 54.4 ($\underline{CH_3}$O C-7), 59.2 (Ar$\underline{CH_2}$ C-9), 60.3 (Ar$\underline{CH_2}$ C-8), 60.6 (Ar$\underline{CH_2}$ C-11), 61.4 (Ar$\underline{CH_2}$ C-10), 69.7 (CH C-6), 72.2 (CH C-5), 74.9 (CH C-4), 76.6 (CH C-2), 81.3 (CH C-3), 99.0 (CH C-1), 105.7 (Ar *para*), 117.2 (Ar *ipso*), 127.5 (Ar *meta*), 144.0, 146.0 (Ar *ortho*). ^{19}F NMR; 376 MHz in C6D6 δ/ppm: -144.80 to -144.38 (*meta*), -140.41 to -139.61 (*ortho*). ES+ MS, m/z 865.1 $[M+Na]^+$.

5 References

1. Bubb, W. A., *Concepts in Magnetic Resonance.Part A* **2003,** 19A, (1), 1-19.
2. Bruice, P. Y., *Organic Chemistry*. 3 rd ed.; Prentice Hall: New Jersey, 2001; p 878-879.
3. Maitland Jr, J., *Organic Chemistry*. 3 rd ed.; W.W. Norton and Company: New York, 1997; p 1233-1235.
4. McMurry, J., *Organic Chemistry*. 3 rd ed.; Brooks/Cole Publishing Company: California, 1992; p 916-956.
5. Barkley, A., Arya, P., *Chemistry- A European Journal* **2001,** 7, (3), 555-563.
6. Davis, B. G., Jones, J.B., *Synlett* **1999,** 9, 1495-1507.
7. Zheng, T., Peleen, D., Smith, L.M., *Journal of the American Chemical Society* **2005,** 127, 9982-9983.
8. Nilsson, C. L., *Analytical Chemistry* **2003**, 349A-353A.
9. Solis, D., Jiminez-Barbero, J., Kaltner, H., Romero, A., Siebert, H.C., von der Lieth, C.W, Gabius, H.J., *Cells Tissues, Organs* **2001,** 168, (1-2), 5-23.
10. Wong, C. H., Bryan, M.C., Nyffeler, P.T., Liu, H., Chapman, E., *Pure and Applied Chemistry* **2003,** 175, (2-3), 179-186.
11. Collins, P., Ferrier, R., *Monosaccharides*. John Wiley and Sons Ltd: Chichester, 1995; p 5-40.
12. Chai, W., Piskarev, V., Lawson, A.M., *Analytical Chemistry* **2001,** 73, (17), 651 - 657.
13. Morelle W, P. A., Michalski JC, *Rapid Communications in Mass Spectrometry* **2005,** 19 (9), 1145-1158
14. Duffin, K. L.; Welply, J. K.; Huang, E.; Henion, J. D., *Analytical Chemistry* **1992,** 64, (13), 1440-1448.
15. Claridge, T. D. W., High Resolution Techniques in Organic Chemistry. In Elsevier Ltd: Oxford, 1999; Vol. 19, pp 145-257, 117,121.
16. Friebolin, H., *Basic One and Two-dimensional NMR Spectroscopy*. Wiley: Heidelberg, 2005; p 133-138, 231-276.
17. Keeler, J., *Understanding NMR Spectroscopy*. John Wiley and Sons Ltd: Chichester, 2005; p 187-244.
18. Reynolds, W. F., McLean, S., Tay, L., Yu, M., Enriguez, R.G., Estwick, D.M., Pascoe, K.O., *Magnetic Resonance in Chemistry* **1997,** 35, 455 - 462.
19. Bernstein, M., Hall, L.D., Sukumar, S., *Carbohydrate Research* **1982,** 103, C1 - C6.
20. Agrawal, P. K., *Phytochemistry* **1992,** 31, (10), 3307 - 3330.
21. Ho, S. C., *Carbohydrate Research* **1978,** 64, 251 - 256.
22. Hall, L. D., Sukumar, S., Sullivan, G.R., *Chemical Communications* **1979**, 292 - 294.

23. Hall, L. D., Morris, G.A.,Sukumar, S., , *Journal of the American Chemical Society* **1980,** 102, 1745 - 1747.
24. Curatolo, W., Neuringer, L.J., Ruben, D., Haberkon, R., *Carbohydrate Research* **1983,** 112, 297 - 300.
25. Blundell, C. D., Reed, M.A.C., Overduin, M., Almond, A., *Carbohydrate Research* **2006,** 341, 1985 -1991.
26. Amstrong, G. S., Mandelshtam, V.A., Shaka, A.J., Bendiak, B., *Journal of Magnetic Resonance* **2005,** 173, 160 -168.
27. Uhrin, D., Jin, L., Kover, K.E., Reynolds, S. In *Cryoprobes and DNP. Utilizing the potential of C13-C13 INADEQUATE at Natural Abundance of C-13.*, Euromar 2006, York, United Kingdom, 16th - 21st July 2006, 2006; York, United Kingdom, 2006.
28. Robertson, J., *Protecting Group Chemistry*. Oxford University Press: Oxford, 2002; p 1-4, 83-94.
29. Wuts, P. G. M., Greene, T.W., *Protective Groups in Organic Synthesis*. Wiley: New York, 1999; p 1-148.
30. Tiwari, P., Misra, A.K., *Carbohydrate Research* **2006,** 341, 339 - 350.
31. Pouchert, C. J., Behnke, J., *The aldrich Library of Carbon-13 and Proton FT NMR Spectra*. Aldrich Chemical Company Inc.: 1993; Vol. 2, p 63B, 130B.
32. Kawahara, F. K., *Analytical Chemistry* 40, (13), 2073 - 2075.
33. Kawahara, F. K., *Analytical Chemistry* **1968,** 40, (6), 1009 - 1010.
34. Chambers, R. D., *Fluorine in Organic Chemistry*. Wiley: New York, 1973; p 4-7, 67-72, 85-89.
35. Sheppard, W. A., Sharts, C.M., *Organic fluorine chemistry*. W.A. Benjamin: New York, 1969; p 27-48.
36. Tennant-Eyles, R. J., Davis, B.G., Fairbanks, A.J., *Tetrahedron: Assymmetry* **2000,** 11, 231 - 243.
37. Waldmann, H., Kappes, T., *Carbohydrate Research* **1998,** 305, 341 - 349.
38. Grayson, E., In Durham University: Durham, 2006.
39. Borschberg, H. J., *Chimia* **1991,** 45, 329 - 341.
40. Hwu, J. R., Chua, V., Schroeder, J.E., Barrans Jr, R.E., Khoudary, K.P., Wang, N., Wetzel, J.M. , *Journal of Organic Chemistry* **1986,** 51, 4733 - 4734.
41. Bukard, S., Borschberg, H.J., *Helvetica Chimica Acta* **1989,** 72, 254 - 263.
42. Riley, J. G., Grindley, T.B., *Journal of Carbohydrate Chemistry* **2001,** 20, (2), 159 - 169.
43. Berger, S., Braun, S., *200 and More NMR Experiments*. Wiley-VCH: Weinheim, 2004; p 92 -102.
44. Varian, I., *VNMR Command and Parameter Reference*. Varian, Inc: California, 2001.
45. Varian, I., *User Guide: Liquids NMR*. Varian, Inc: California, 2001.
46. Girard, C. M., M.; de Solminihac, T.; Herscovivi, J.; , *Carbohydrate Research* **2002,** 337, 1769 - 1774.
47. Koto, S., Morishima, N., Miyata, Y., Zen, S., *Bulletin of the Chemical Society of Japan* **1976,** 49, (9), 2639 - 2640.

SECTION 2

"Studies of the structural, physical, and chemical properties of the lanthanide (III) complexes of DOTA… and related ligands are often complicated by the presence of two coordination isomers in solution."[1]

1 Introduction.

1.1. Lanthanide luminescence and potential applications.

Paramagnetic lanthanide (III) ions have recently diverted biomedical attention from the then popular radionuclides in cancer and tumor treatment. [2] This is because radionuclides have been found to be unacceptably toxic, and emphasis has been shifted to diagnosing tumours at the very earliest stages. The most common lanthanide elements in this regard are gadolinium and europium. Gadolinium (III) ions, having the highest electronic magnetic moment ($\mu = 63\mu_B^2$) are exploited as contrast agents for magnetic resonance imaging (MRI) due to the long electron relaxation lifetimes. Europium, on the other hand with modest electron relaxation lifetimes, finds use not in MRI imaging, but in luminescence applications (including imaging) because of its attractive and well studied emissive properties. [3]

Europium luminescence applications span a wide range; analytical, forensic, and biomedical. Under forensics, it has been used to investigate counterfeit phosphors in Euro bank notes. [4]

Europium's effective luminescence is used for structural studies of the gadolinium contrast agents. [5] Newly developed ligand systems are probed for their structural properties using europium whose physico-chemical properties are similar to those of gadolinium (emitting in the UV region), both having core like f-orbitals, minimizing interaction with surroundings and leading to electrostatic bonding and high coordination numbers. For example, the number of bound water molecules in a newly developed gadolinium complex can be determined with high sensitivity using europium luminescence. Moreover, the entire metal-ligand binding properties can also be studied. Advantages of europium in structural probing of the ligands stems from the fact that it possesses long luminescent lifetimes (milliseconds range), because there are only a few

quenching pathways in its luminescence. [6] Attractively long luminescent lifetimes are observed even in aqueous solutions, aiding its use to extend the testing of contrast agents under development *in vivo*, where biological chromophore- bearing substances like peptides and nucleotides' background emission interfere. Another attractive feature of lanthanide luminiscence is that partly filled f orbitals interact weakly with the environment, making the metal centred luminescence immune to triplet oxygen quenching found in living systems. These have advantages over development tests which yield excellent results *in vitro*, but lower intensity *in vivo*. The long luminescent lifetimes of europium makes it possible to escape background emission by time resolved measurements in which case a delay is set between excitation and measurement. [6, 7] This technique is called time gating.

Europium luminescence quenching provides an indirect method of metal ions analysis.[3] A chelated europium ion was used by Pope *et al* to determine the zinc ion concentration. Zinc binds to the metal chelate, mediating coordination changes to the ligand which in turn modulates the photophysical properties of the metal centre. The quenching of the metal centre is then used indirectly as a way of assaying the zinc ions in solution. Another way in which europium luminescence has been used in bioassays is in luminescence microscopy[8]. When conventional transmission microscopy is used, analytes are indistinguishable, and only the average concentration is determined. However, using europium luminescence affords a way of manipulating the measurements to make them time resolved so that intensities from the individual analytes are measured free from background emission and from one another's interference.

Free europium ions have similar biodistribution and physico-chemical properties to calcium. This means that they compete with calcium for calcium channels *in vivo* and in bone structures. Competition against calcium makes free europium very toxic to be used directly in living system as a result. Means have had to be devised to administer the europium to living systems when applied *in vivo*. Chelation was found to be a method of choice for safe administration of europium.[2]

Unsolicited quenching of europium is a likely but unwelcome event when luminescence studies are performed on living systems. This is because the largest proportion of biological systems are composed of water. Water is a very efficient quenching agent. Chelation is essential, not only for lowering europium toxicity but also for lowering water quenching. 1,4,7,10- tetraaza cyclododecane 1,4,7,10-tetra acetic acid, which for the sake of brevity is referred to as DOTA (Figure 1), has been used for the encapsulation of metal ligands, and has been well studied and applied in MRI contrast agents.

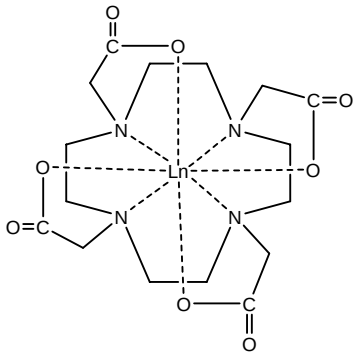

Figure 1: The structure of EuDOTA: the Europium(III) complex of 1,4,7,10-tetraaza cyclododecane 1,4,7,10-tetra acetate. Ln represents Eu^{3+}. Cationic counterions and the charge of the molecule are not shown.

1.2. Thermodynamic stability and kinetic inertness of the complexes.

The complex resulting from encapsulation of the metal by DOTA-like ligands must have several properties which make it fit for the purpose. The properties include: high thermodynamic stability and kinetic inertness, water solubility, low osmolality and rapid renal excretion when used in clinical applications. [5, 7]

Thermodynamic stability is a requirement for these complexes so as to make sure that when injected into living systems, the complex does not dissociate, with the eminent release of the toxic metal ion. Apart from that, they must be kinetically inert with respect to conformation change as it has been shown that conformation changes modulate photophysical properties [3] of the complex which lead to observation of no luminescence

or weighted average if one of the conformers in question has low quantum yield. As a result of this, it is imperative to evaluate thermodynamic stability and kinetic inertness of the DOTA-like complexes before passing the development stage onto the applications and test stages.

1.3. Structure of the DOTA-like cyclen and its possible conformations.

DOTA, is a prototype of all ligands based on cyclen with different pendant donor groups. As a result the DOTA-like ligands have more or less similar geometries to their prototype. The DOTA free ligand is predisposed to form complexes with metal ions. [2, 7, 9] The predisposition is very crucial in the determination of the stability of the macrocycle because all the donor atoms adopt a *syn* spatial arrangement with respect to the cyclen plane. This makes the donor atoms as close as possible to the orientations facilitating formation of the complex. [10]

Lanthanide DOTA complexes are composed of a cyclododecane ring forming the backbone. They have C4 symmetry perpendicular to their principal axis [11, 12], with four ethylenic groups separated by nitrogen atoms. The ethylene carbons are fully staggered, making the macrocycle ring highly puckered. The ring pucker makes the ring protons magnetically non-equivalent. The four coplanar nitrogens describe a square. Four acetate groups extend from the nitrogen atoms and they are *syn* with respect to the plane of the nitrogens.

The four acetate oxygens form a plane above the nitrogen plane. A metal ion with axial symmetry is at the centre, with octadentate coordination to the four coplanar nitrogen atoms and the four oxygens. The ninth coordination site is occupied by a water molecule. The two planes associated with the metal centre together with the capping water molecule describe a square antiprismatic structure.

The free ligand's predisposition, and ring pucker makes the DOTA complexes very stable [11]. However, it was discovered that in solution the complexes exhibit at least two forms. Solid state studies have led to observations that indeed there were two forms associated with these complexes. Possible diastereomers for the DOTA were studied from crystals developed by different methods. Desreux *et al* discovered one form in which the DOTA complex formed a shell around the metal centre. [12] Eight coordinate bonds extend to the metal centre from the nitrogen and oxygen planes above with the ninth axial position occupied by a water molecule. The metal-nitrogen and metal-oxygen bonds suggested that the coordination polyhedron in this case described a twisted square antiprism (TSAP) and nitrogen and oxygen planes twist angle of *ca* 29º. [7]

Aime *et al* [13] on the other hand, using a different crystallization method, obtained a different conformational polymorph with similar coordination to the one crystallized by Desreux *et al*. The metal-nitrogen and the metal-oxygen bonds were shorter than the polymorph studied by Desreux and suggested a square antiprism (SAP) with the nitrogen and oxygen twist angle of *ca* 40º. This is a little on the lower side of an ideal square antiprism polyhedron (45º).

The sliding movements of the ligands arms about the metal centre are responsible for the two conformers. However, another school of thought is for the view that in addition to the arm movements, the ligand is engaged in an enantiomerization in which the macrocycle ring is inverting. [14, 15] The process is thought to take place simultaneously with the arm movements or separately in which case there is a direct equilibration between the SAP and the two diastereomers.

Studies leading to observation of two isomers in DOTA led to more studies on isomerism pathways. Desreux and Jacques [16] studied YbDOTA by quantitative EXSY. They were of the view that isomerization involving scrambling of the acetate arms about the metal centre, and enantiomerization which involved inversion of the tetraaza were possible. They concluded that the energy barrier to the two processes was comparable, and they occurred in a concerted fashion.

Aime *et al* [14], were of the view that the energy barrier to enantiomerization was higher than that of isomerization, and hence enantiomerization was slower. Bandshape analysis on LuDOTA was used as they thought that the two dimensional EXSY was not adequate. Thermodynamic calculations using data from EXSY was prone to phenomenal errors since a paramagnetic metal centre was involved.

Further work was carried out by different groups to understand the isomerization pathways. Aime *et al* studied chelates of DOTA with twelve metals in the lanthanide series.[17] In addition they also studied macrocyclic tetrabenzylphosphinate chelates with metal ions from europium to yttrium. [18] They observed unusual macrocyclic rigidity when chelates were formed with yttrium, europium and ytterbium, suggesting that rigidity increased with size of pendant arm and charge to size ratio. This is consistent with Brittain and Desreux's luminescence and NMR studies on lanthanide complexes. They observed that ring rigidity varied with functional group bulk and charge to size ratios.

Bari *et al* [1]observed that when *p*-NO_2 benzyl subtituents were introduced into the ring, these bulky groups adopted a more equatorial orientation with respect to the plane of the ring and made ring inversion unfavourable. Bianchi and coworkers observed that while a gadolinium based contrast agent was developed, macrocyclic ring rigidity increased with the number of acetate groups. [10] However, this presented a combination of factors in the form of an increase in bulk as well as coordination sites.

The present study seeks to understand the thermodynamic stability and kinetic inertness of a modified Eu-DOTA complex, 1,4,7,10-tetrakis pycolyl-1,4,7,10 tetraazacyclododecane Europium(III) triflate. For brevity this will be referred to as Eu-DOTApy **(I)** and is shown in Figure 2. Interest is also on the types of isomers formed and isomerization pathways undergone by the complex.

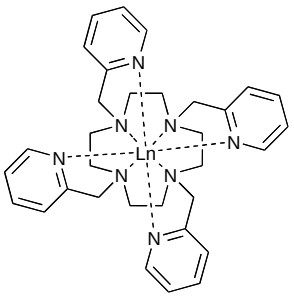

Figure 2: The structure of 1,4,7,10-tetrakis picolyl-1,4,7,10 tetraaza cyclododecane Europium(III) triflate **(I).** Ln represents Eu^{3+}. Triflate counterions and the charge of the molecule are not shown.

I is a macrocyclic complex based on DOTA. The pendant arms are appended with pyridyl groups which form antennae groups to increase luminescence intensity and quantum yields. Like all DOTA-like complexes, it has predisposed ligands forming a perfect hole for metal centre encapsulation. Unlike in DOTA, the ligands are neutral possibly leading to weaker, longer and more labile bonds.

Understanding the stability and inertness of this complex will go a long way on evaluating its safe application to living system and checking the effectiveness of the appended antenna groups in enhancing the luminescence sensitivity in assays. Since luminescence increases with molecular rigidity [19], the more stable and inert the complex, the more rigid is the whole shell around the central metal and the higher the quantum yields. With the above information at hand, it is not unreasonable to believe that energy barrier to ring inversion of **I** is very high.

1.4. Dynamic Nuclear Magnetic Resonance spectroscopy in the study of dynamic processes.

Chemical processes can be followed and characterized by physical methods. [20, 21] These processes include proton exchange reactions and others like rotations about bonds, conformation and configuration inversion. Nuclear Magnetic Resonance (NMR) spectroscopy is one of the methods which have been used for a long time to follow the processes above. The applicability of NMR stems from the fact that it is able to observe and distinguish between the different microenvironments a system can adopt. [22] The small branch of NMR used for such purposes is named Dynamic NMR (DNMR).

The ability of NMR to observe the differences in the microstructure is based on the interaction between spin magnetic moments and the applied external magnetic field. This leads to different chemical shifts of chemically different systems. Chemical shifts are also determined by spatial orientation of the spin system in the molecule. Factors such as temperature can cause the two spin systems to exchange orientations. If the spins exchange orientations at a rate higher than the NMR timescale (10^{-1} -10^{3} Hz), they become indistinguishable and a single resonance is observed at an average chemical shift. The fact that the rate of rotation about bonds, configuration and conformer inversion is within the NMR timescale, is exploited to study exchange processes.

Exchange processes timescales are subdivided into the slow, intermediate and fast regimes. [23] Measurements in the slow exchange regime exploit *z*-magnetization manipulations and are able to provide information about rate constants for slow exchange processes (10^{-1} – 10^{1} Hz). Spin lattice-relaxation times (T_1) are a core parameter in this range. Experiments exploiting measurements of the spin-spin relaxation time (T_2) are ideal for probing the intermediate and fast exchange regimes. At this point broadening and coalescence are observed and used in lineshape analysis. However, this is subject to high magnetic field homogeneity.

A number of methods are available to study the exchange processes. Among them is the lineshape analysis. [24, 25] Spectra are recorded in a range of temperatures beginning at temperatures were there is virtually no exchange up to the point beyond coalescence of exchanging spins. A number of parameters like linewidths and peak separations are extracted from the limiting spectrum. A guess of the rate constant is made and values extracted from the limiting spectrum (linewidth, peak separation) are combined to simulate the spectrum. The simulated spectrum is compared to the observed spectrum and the comparison is the basis for accepting the value of the rate constant as a true representation of the exchange process. This can be a long process as a number of iterations may be necessary.

In the present study selective inversion recovery or selective polarization transfer was employed to study the exchange processes. Exchange processes are very slow and selective inversion, which involves manipulating the *z*-magnetization, was used. This makes use of the fact that for a system displaced from equilibrium, spin-lattice relaxation and exchange processes are responsible for restoring equilibrium. [23, 26] For a molecule with two conformers, A and B, the spin system has access to two magnetic environments. If the conformers are equally energetically favourable, the spin states are equally accesible and vice versa. The two conformers give rise to two distinct chemical shifts.

Selectively inverting one of the spins, say A, displaces the magnetisation of spin state A away from equilibrium into an inverted non-equilibrium spin state A*. The return to equilibrium can be through spin lattice relaxation processes at a rate R_1. Another option would be for spin A* to return equilibrium by exchanging the non-equilibrium magnetisation with spin B at a rate determined by their mutual exchange rate constant, *k*, giving rise to the non-equilibrium spin state B*. The amount of exchange depends on the amount of time allowed for exchange to take place. Spin B* then returns to equilibrium state by spin lattice relaxation processes. The balance between spin lattice relaxation and chemical exchange processes are shown in Scheme 1.

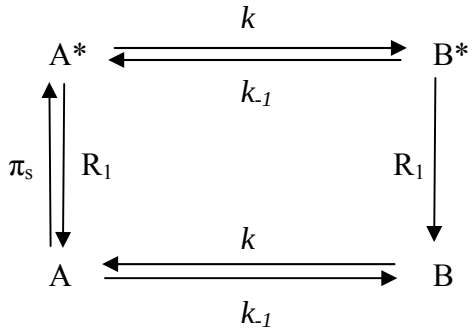

Scheme 1: A schematic showing the balance between spin lattice relaxation processes and chemical exchange processes. π_s is the selective inverting pulse. R_1 is the spin lattice relaxation rate constant and k is the chemical exchange rate constant.

If exchange is faster than T_1 relaxation, then exchange rates can be successfully measured by observing the system's return to equilibrium, up to a point where T_1 relaxation becomes faster than exchange and dominate equilibration. The pulse sequence for selective inversion is shown in Figure 3.

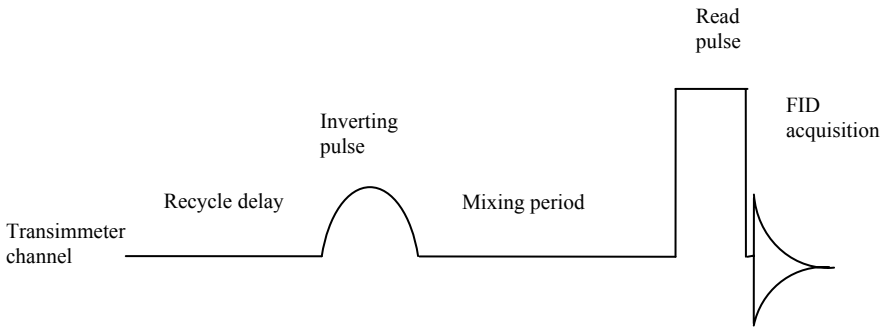

Figure 3: Simplified schematic of a selective inversion pulse sequence. Other channels and pulses not shown. Diagram is not to scale.

In the sequence the *z*-magnetization of one of the exchanging spins is perturbed away from equilibrium by selective 180º soft, shaped inverting pulse. A mixing time during which the inverted pulse returns to equilibrium by exchange follows the inversion pulse.

A hard 90º pulse (read pulse) flips the magnetization onto the transverse plane to be recorded (FID acquisition). A recycle delay is necessary to let the *z*-magnetization restore to equilibrium conditions before repetition of the sequence. For exchange to be measured by this method, the exchange rates must be faster or comparable to the spin-lattice relaxation rates.

The data extracted from NMR experiments can be transformed into meaningful information which characterizes processes. Kinetic and thermodynamic parameters are some of the properties of a system that can be studied in this way. Rate constants are a handy tool to asses how fast reactions take place. Another parameter related with rates is the activation energy, which presents alternative routes taken from the reactants to the products side. The route with a higher value of activation energy is usually the slower. Plots of logarithms of rate constants against reciprocal absolute temperatures yields Arrhenius and Eyring parameters from which reaction enthalpies, entropies and activation energies are derived.

For more accurate work, especially in DNMR, Eyring parameters are preferred. [25] Although the Arrhenius equation pioneered the field which related kinetics to thermodynamics, it has fallen in disfavour. Approximations in the Arrhenius equation make it liable to errors in that it is based on oversimplified classical thermodynamics. The equation has a frequency factor term, A, interpreted as the number of 'effective' collisions per unit time and volume needed to drive the reaction to completion, and neglects the crucial geometry of the collision. On the other hand, the Eyring equation is based on statistical thermodynamics and the absolute rate theory which advocates a transmission coefficient (κ) rather than a frequency factor. This is interpreted as the number of all reacting molecules reaching the transition state. The Arrhenius (1a), Eyring (1b) and the Gibb's free energy (1c) equations are shown below.

$$k = A \cdot e^{-\frac{E_a}{RT}} \qquad 1a$$

$$k = \kappa \cdot \frac{k_B T}{h} e^{-\frac{\Delta G^{\#}}{RT}} \qquad 1b$$

$$\Delta G^{\#} = \Delta H^{\#} - T\Delta S^{\#} \qquad 1c$$

$$E_a = \Delta H^{\#} + RT \qquad 1d$$

κ is the transmission coefficient, A is the frequency factor. Other symbols bear their usual meaning.

1.5. Structure determination by two dimensional techniques.

Heteronuclear and homonuclear two dimensional NMR experiments are useful for spectral assignments. They rely on the evolution of coupling between spin coherences to generate the cross peaks used for mapping out correlations. [27, 28] Generally two dimensional experiments are divided into three periods, the preparation, the evolution and the mixing period (Figure 4). During the preparation period, equilibrium *z*-magnetization is subjected to a pulse which perturbs it from equilibrium. The perturbation modifies coherences which are simply magnetizations. Coherences are observable only for components of the magnetization which are in the transverse plane. Following this period is the evolution period during which coupling between coherences takes place. The last is the mixing period during which the evolved coupling and the coherences associated with the evolution are transformed back into observable form.

The evolution period is systematically incremented in a series of scans, to create varying amounts of coupling which are then used to generate two dimensional spectra with diagonal and cross peaks. An important factor governing observance of cross peaks (correlations) is the size of the coupling constant that develops between the spins in

comparison to linewidth of the peaks in their one-dimensional spectra. Coupling constant values must be larger or comparable to the linewidths. Linewidths greater than coupling constants mean that coherences (magnetization) that lead to correlation do not live long enough to be transformed into observable coherences during the mixing period. Coupling constants are intrinsic properties of spin systems but linewidths are a function of many factors.

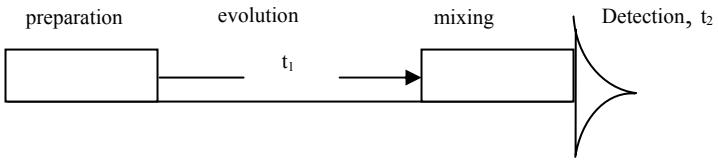

Figure 4: A generalized diagram of two dimensional experiments. Adapted from Undertanding NMR Spectroscopy.

2 Experimental

2.1. Materials and Instrumentation.

Eu-DOTApy was used as supplied by Dr. Louise Natrajan of Manchester University. Approximately 10mg was dissolved in 1 ml water-d_2 (99.9 atom % D) manufactured by Aldrich Chemical Company Inc. to constitute a solution used in selective inversion experiments. A saturated solution of the above was prepared and used for carbon-13 variable temperature experiments.

A 2-channel Varian Inova spectrometer (software VNMR 6.1C) operating at a proton frequency of 500MHz and a carbon-13 frequency of 125 MHz was used for spectral acquisition.

2.2. Spectral assignment and chemical structure determination.

Spectra assignments were done by a combination of ^{1}H, ^{13}C, COSY, HSQC, EXSY and selective decoupling techniques. The paramagnetic effect causes unusual chemical shifts, making it difficult to do assignments by comparison to well documented look up tables available, unlike in complexes with diamagnetic metal centres.[14] Coupling patterns are obscured by extensive broadening. Assignment was therefore done by a less straight-forward back and forth reference to the different techniques named above.

2.3. Spin-lattice relaxation time constant determination and probe temperature calibration.

Spin lattice relaxation time constant (T_1), was determined by non-selective inversion recovery pulse sequence experiments. [24, 29-31] A fairly dilute solution (~10 mg in 1ml) was used in this case to minimize extremely high relaxation rates due to concentration effects.

High concentrations cause rapid spin-lattice relaxation rates and cause *z*-magnetizations to decay rapidly with substantial error introduction to the T_1 measurements.

Dialed probe temperatures were calibrated at the lower temperature regime (2 to 22°C) by the methanol method and by the ethylene glycol method at the higher temperature regime (26 to 38°C).

Nitrogen gas passing through liquid nitrogen bath was used as the carrier gas for the probe calibration and T_1 determinations to ensure a constant and stable sample environment.

2.4. Selective inversion and the exchange rate constants.

A local macro, "selinv_amk" was used to invoke selective excitation pulse sequence shown in Figure 3 above and was used to study exchange processes. Hyperbolic secant inversion pulse was used for its high bandwidth selectivity, homogeneity and short pulse durations using less RF energy.[32] The pulse is short enough not to allow magnetization decay while the pulse is being applied, yet sufficiently selective to invert only the *z*-magnetization of the chosen resonance.

The peak at the lowest frequency was selectively inverted by placing the inverting pulse on resonance with its bandwidth. The peak to be inverted was chosen from normal gradient selected EXSY spectrum which showed that its exchanging partner was at the other extreme of the spectrum and free from overlap. Overlap had to be kept to a minimum so as to be able to selectively invert any resonance and study its return to equilibrium while simultaneously studying the behaviour of the exchanging partner under the influence of exchange. In addition, at the end of exchange, we have to be able to measure peak intensities as accurately as possible, which is only possible in the absence of overlap and crowding.

The mixing time, which allows the two exchanging spins to exchange magnetization, was incremented systematically. To make each experiment of reasonable length, and avoid magnetic drift with time, the mixing time was arrayed at 1ms increments for the 0 – 40 ms; 2ms for the 40 – 80 ms; 4 ms for the 80 – 128 ms and 8 ms for the 128 – 240 ms intervals. Using constant increments made the experiment long and at higher regions (80-240 ms) of the array, spin lattice relaxation effects dominated exchange effects as the exponential growth from exchange was flattening off. Little exchange information could be tapped from this region but this was gathered to make it easier for the fitting program to define the exponential growth.

Exchange rate constants were simulated using the CIFIT-2 program as developed and made available on request by Professor Alex Bain of Mc Master University, Canada. [33, 34] The parameters fed to the program from the spectra included, the major and minor peak equilibrium and initial magnetizations, spin lattice relaxation rates and a guess of the rate based on the spin-lattice relaxation time constant.

Variable temperature C-13 NMR spectra were acquired from a saturated solution of **(I),** using the parameters given in Table 1.

The carbons are in the vicinity of a paramagnetic centre whose effect is through dipolar interactions. The acquisition time and recycle delay were set to 0.100 and 0.900 s respectively. The transverse relaxation rate is very fast and there was no need to acquire data points when the transverse magnetization had all relaxed in case more noise was incorporated. Spin lattice relaxation time constant (T_1), which determine the length of recycle delays, is considerably short for nuclei in paramagnetic environments hence why a very short T_1.

Table 1 Carbon-13 acquisition parameters.

Acquisition parameter	Value
Spectral width	~30 kHz
Number of points	6010
Transmitter power	52 dB
Transmitter offset	2000 Hz
Number of transients	1024

The unusually wide proton sweep width (~29 kHz) called for very high decoupler power to achieve effective decoupling across the whole spectrum. The decoupler power was set to 48 dB, and to match the high decoupler power, the decoupler modulation frequency was doubled to 20.6 kHz. To avoid the risk of probe damage and lock level fluctuations,[35] due to heat resulting from high decoupler settings, the decoupler duty cycle was set to 10%, that is 'off' during the recycle delays and 'on' only during the FID acquisition period. A GARP decoupler modulation mode whose effective bandwidth ($4.8\gamma B_2$) is twice that of WALTZ ($2\gamma B_2$) was used. γB_2 is the decoupling field strength.

A line broadening value of 10 Hz was applied in order to improve the signal-to-noise ratio of the carbon lines.

3 Results and discussion.

3.1. Assesment of the simulation program and the errors using a model system.

CIFIT-2 programme was used for the simulation of the rate constants. It was therefore imperative to assess sources of errors of the local system with respect to the programme. First, selective inversion experiments were done using dimethylacetamide (DMA), a well studied and understood model compound for exchange experiments. The value of the rate constant, (0.450±0.003 Hz) at ambient temperature (20.0ºC), turned out to be very comparable to the literature value of 0.447±0.013 Hz at 20.0ºC. [26] Slight deviations may be due to the fact that temperature calibrations were not performed, as a rough idea of the rate was enough to give an idea of error sources to expect and their extent.

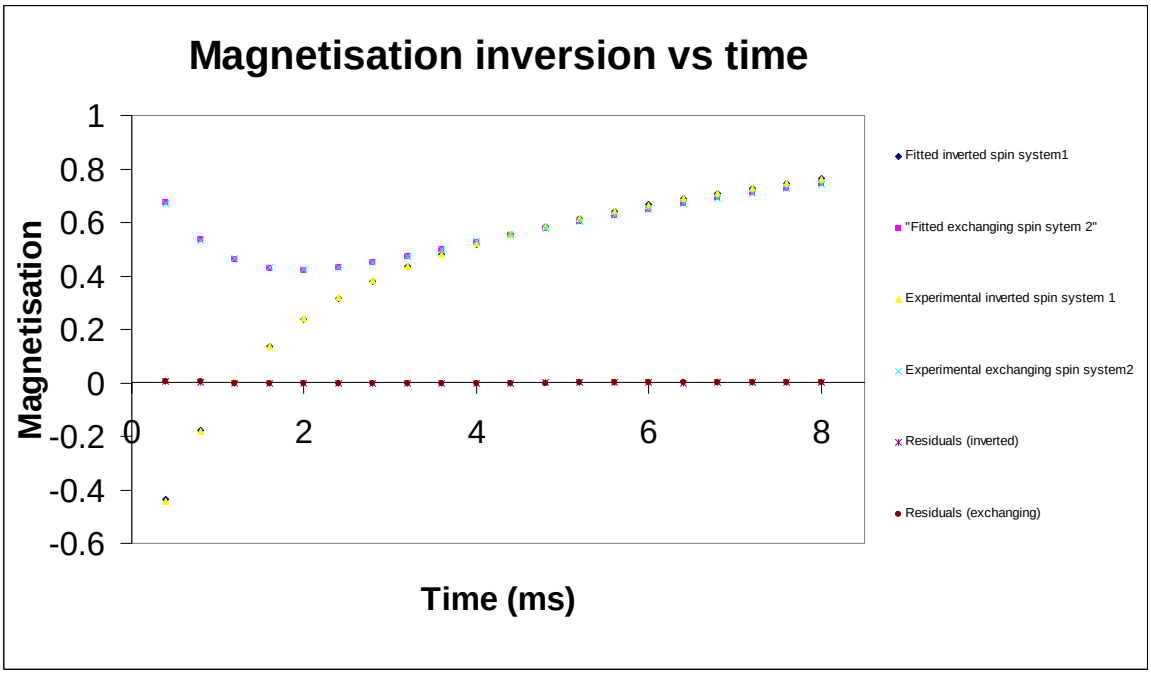

Figure 5: Plot showing selective Inversion results of DMA to determine exchange rate constant. Residuals are overlaid.

Figure 5 presents results of a selective inversion experiment on DMA. The plot shows the experimental and fitted magnetization inversion of spin 1 and its exchange with spin 2 together with the residuals. The fitted and experimental results are in good agreement within experimental error. This is further clarified by the residuals plot, in which the residuals lie close to zero. However, careful scrutiny of the residuals shows a somewhat periodic oscillation around zero, instead of a random walk. Immediately after inversion, residuals are greater than zero. At around 1 ms they go below zero and remain so till after 4 ms when they become greater than zero. Clearly this shows some form of systematic error although the error magnitudes are very minimal. A blown up residuals plot is shown in Figure 6.

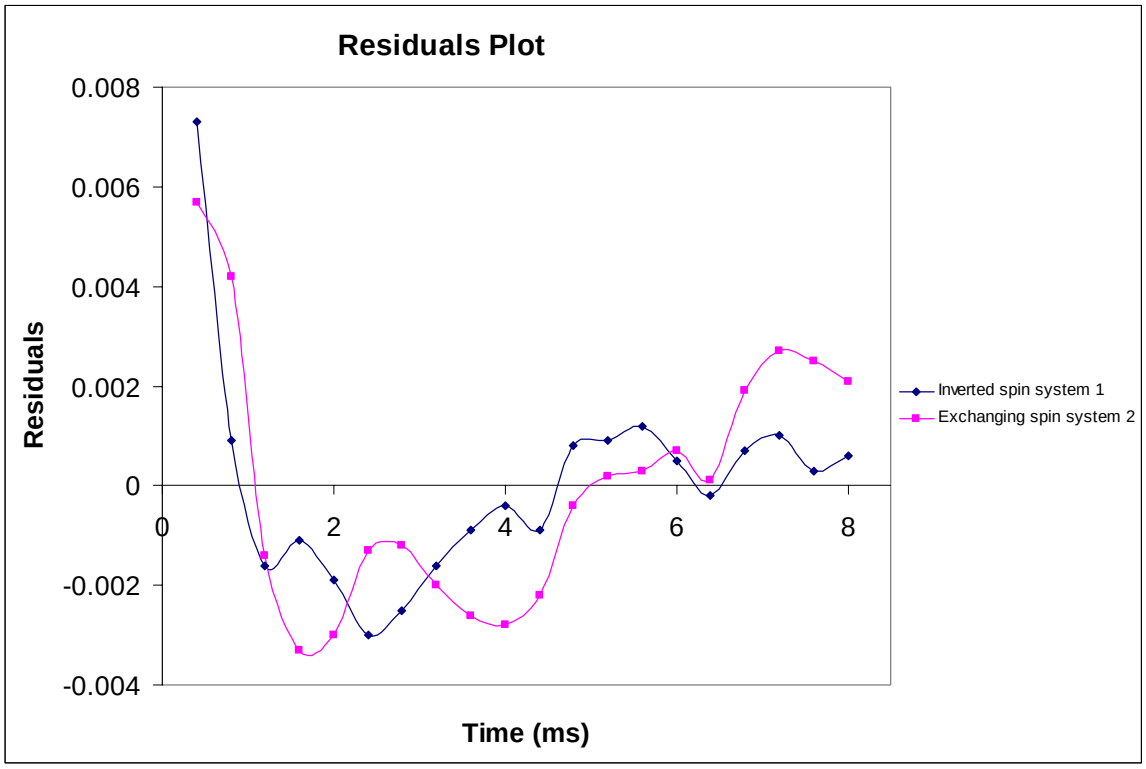

Figure 6: Residuals plot (blown up) of DMA at ambient temperature.

A similar treatment was done on the title compound to study sources of error and their extent and make a comparison with the model system. The spectra were acquired at constant and calibrated temperature (22.5ºC) *vide infra*. The plots are presented in

Figures 7 and 8. In a similar manner, systematic variation of the residuals was observed. Residuals are generally greater than zero immediately after inversion and tend towards zero and below, and continue with a periodic excursion about the zero line with time.

From the residual plot of the major form (Figure 7), a stronger periodic variation is observed than in the minor form (Figure 8). However, the magnitude of deviation in the major form is slightly less than in the minor form. This therefore shows that the minor form has larger amounts of error. The major form, although with a smaller amount of error, is much more affected by systematic errors. All in all, the amount of error is very small (within experimental error), but the systematic nature of the error observed means that doing replicate measurements will do little to improve the results and the only option left is to set up the experiment as carefully as possible to minimize errors. Temperature will have to be carefully controlled and calibrated.

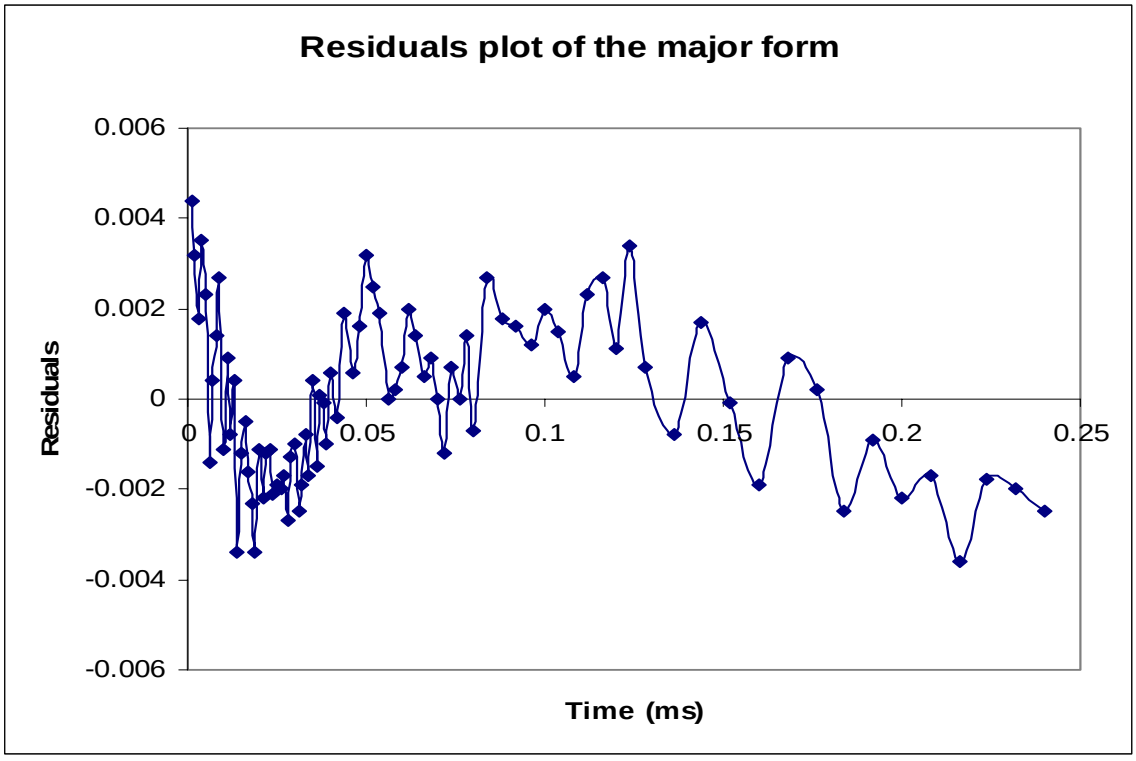

Figure 7: Residuals plot of the major form at 22.5º.

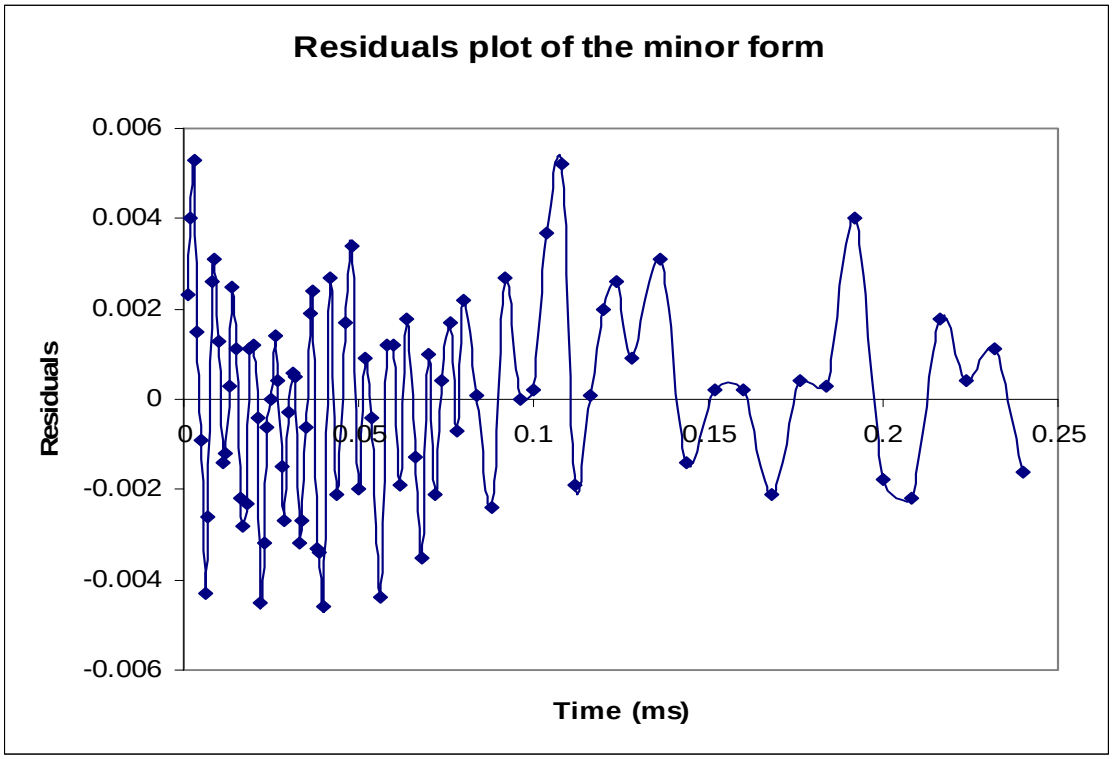

Figure 8: Residuals plot of the minor form at 22.5º.

3.2. Temperature Calibration and linewidth studies.

The temperature dialed in during the experimental set up is not always equal to the probe temperature. For this reason temperature calibration was done to get a fairly accurate temperature. A plot of actual temperature against set temperature (2 - 30ºC) yielded an equation of the form:

$$y = 1.1198x - 2.1855 \qquad 2$$

The plot of actual against set temperature, covering the temperature range (2 - 30ºC) used to quantify rotational and isomerisation thermodynamic parameters, is reported in the appendix section (Figure A5). The plot has a good linear fit, with a correlation coefficient of r = 0.9996.

Assuming that the actual temperature varied linearly with the set, the line was extrapolated to determine the actual temperatures at higher ranges. The extrapolated temperatures were only used for qualitative purposes; to have an idea of the actual temperatures to avoid boiling or freezing of the solution. All measurements used for the quantitative determination of exchange rates and activation energies were carried out at temperatures which had been accurately calibrated in the range 2 to 30ºC.

The behavior of linewidth with temperature was also studied so as to be able to decide the limits to which temperature variation subjects this system. The plot is shown in Figure 9. For a successful selective inversion experiment, the inverting pulse has to be highly selective. When the inversion has been done, the integral region of the inverted line and its exchange partner must have minimum spectral overlap so as to be able to measure the integrals as accurately as possible. Figure 9, reveals that the linewidths vary with temperature in which case they become broader as temperature increases. The minor form has stronger temperature dependence. This implies that at higher temperature the integrals measurement accuracy diminishes. Peak bases cannot be accurately determined so as to be able to set integral regions. Some peaks actually overlap.

The relaxation broadened peaks of the paramagnetic system is further broadened by temperature. This has far-reaching negative effects on the NMR of this system. This means that at higher temperatures, 2-D experiments would not be possible. For example, for a COSY correlation to be possible, the linewidths of the scalar coupled spins have to be not significantly greater than the coupling constant. [27] For argument's sake, the linewidth of the minor peak at 3.18 (41.3ºC) was compared with the proton homonuclear coupling constant necessary to generate a COSY. This linewidth at *ca* 191 Hz compared to the largest proton homonuclear coupling constant of the order of 20 Hz, means there is no probability of generating a COSY correlation in this system at this temperature. The same applies to HMBC ($^3J_{H\text{-}C}$ ~ 3-7, 4-11Hz). Chances of an HSQC ($J_{H\text{-}C}$ ~ 140-180 Hz) tend towards zero. The major peak with linewidth of *ca* 54 Hz can barely afford an HSQC only, however, peak overlap that develops with temperature may make following the proton signals difficult.

All the linewidth presented on the plot goes through a minimum at around 3.54 (9.2ºC) and broaden as temperature goes down. The broadening in this case is due to the increased solvent viscosity dominance from low temperatures.

The linewidth variation with temperature limits 2-D experiments to a narrow temperature window (-0.2 to 41.3ºC) although the solvent and dynamics allow a much wider range (-0.2 to 107.6ºC).

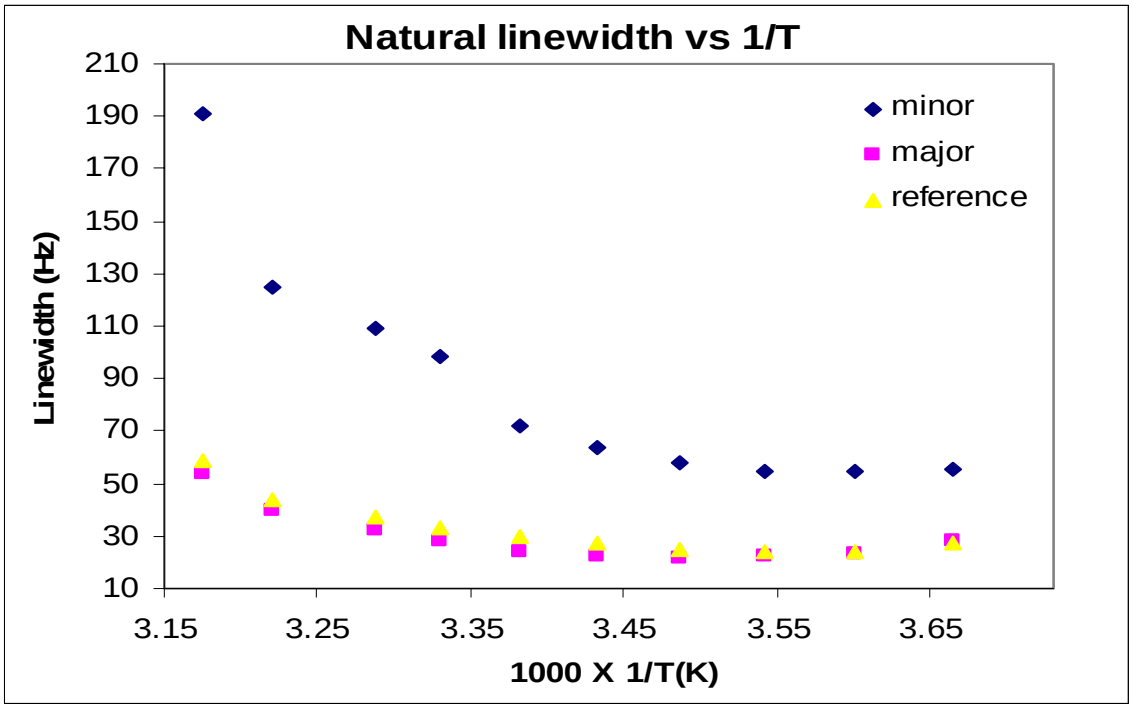

Figure 9: Variation of natural linewidth with inverse temperature.

3.3. Simulation results, errors, and their sources.

The barriers to rotation and exchange between isomers were studied as a function of temperature. Since the parameters used to determine the rates are temperature dependent, it is very important to study the behavior of these parameters as a function of

temperature. The parameters used to simulate the rate constant are the T_1, equilibrium and non-equilibrium *z*-magnetization (integrals), and the linewidths.

The dependence of T_1 on temperature is shown in Figure 10 as a plot of T_1 versus reciprocal of absolute temperature. The T_1 values are dependent on temperature; falling as the temperature decreases.

The experimental T_1 of the minor form is higher than the major form at high temperature and they both fall as temperature drops, crossing over at 3.29 (31.4ºC). The plot shows a stronger temperature dependence of the minor form T_1. It rapidly falls as temperature decreases and continues to do so even at the lower limiting temperature. The experimental major form gently falls as temperature falls, going through a minimum at 3.55 (9.2ºC).

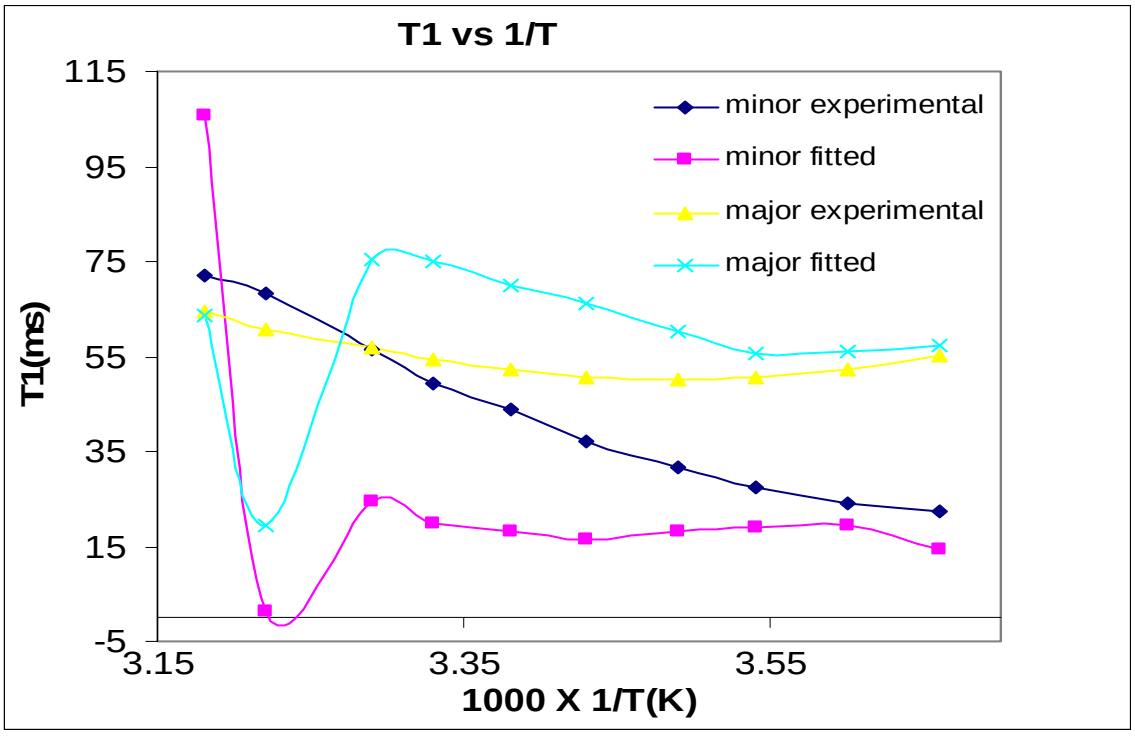

Figure 10: Plot of longitudinal relaxation time, T_1 (ms) against reciprocal absolute temperature.

Except for the glitch at 3.22 (37.4ºC), the fitted T_1 plot falls with decreasing temperature. Both minor and major forms follow a similar trend. The glitch is poorly understood but is acceptable because, when simulating the rate constant, T_1 values were allowed to vary to let the program converge and return the lowest chi squared values. If the T_1 values are held constant as fed from the experiment, the program does not converge. Letting the program vary all parameters including the T_1 attains a global minimum. The value of rate constant returned at this temperature and this glitch falls within the trend of others. An uninvestigated hypothesis would be that there may be some bond rearrangement. [1]

T_1 behavior is very critical because in a selective inversion experiment, the *z*-component of magnetization is measured at different time increments (mixing time) to simulate the rate constant of an exchange process. Thus as this component of magnetization is perturbed away from equilibrium and allowed to exchange, the exchanging spin magnetizations are expected to vary according to exchange and mixing time set. It is a requirement that the T_1 lifetime is long enough in order to probe the *z*-magnetization and so that the magnetization equilibration (relaxation) is affected by exchange processes. If the T_1 is very short (T_1 relaxation rate is faster than exchange), it may dominate the behaviour and mask any effects due to exchange. Because of this, its behavior at different temperatures needs to be quantitatively established. Residual plots at different temperatures were made to study the effect of temperature on errors associated with T_1.

An ideal situation would be when the T_1 values of the exchanging spin systems are comparable [26] and are long enough not to interfere with exchange. A closer examination of temperature variation of T_1 in Figure 10 reveals the T_1's of the exchanging spins to be comparable at 3.29 (31.4ºC). It would be thought that at this temperature systematic errors from T_1 relaxation would be negligible. However magnetization residual plots (Figures 13-14) show that there is still some periodic variation of the deviations, implying some systematic error. This was compared with residuals plots at 3.38 (22.5ºC) (Figures 7-8) and 3.66 (-0.2ºC) (Figures 11-12). The patterns of periodic oscillations around zero are similar but small. This therefore says that T_1 is not the only source of systematic

errors in this case. There are other sources intrinsic to the exchanging system which are not very apparent.

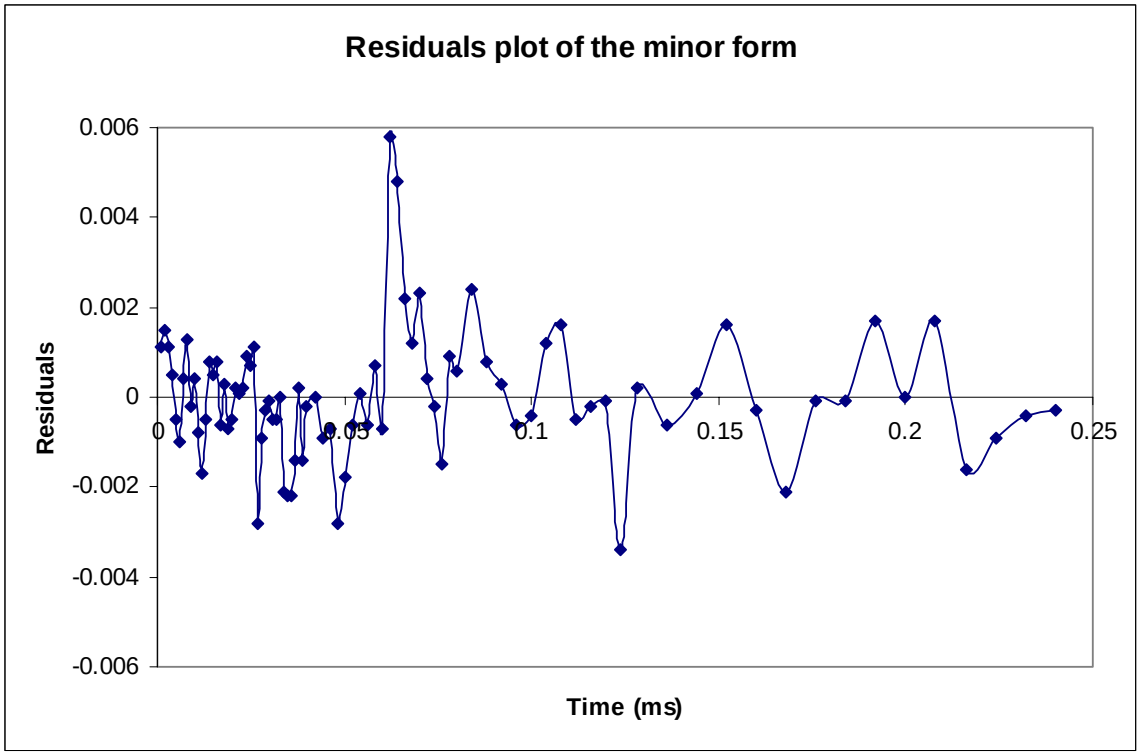

Figure 11: Residuals plot of the minor form at -0.2ºC.

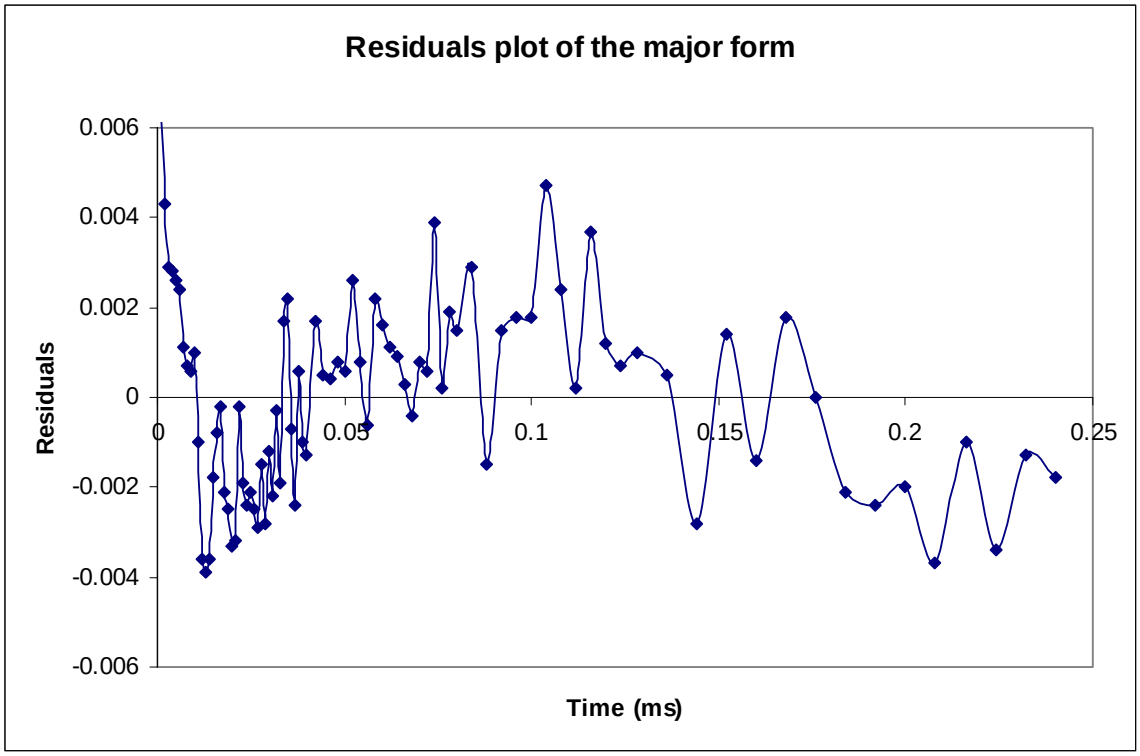

Figure 12: Residuals plot of the major form at -0.2ºC.

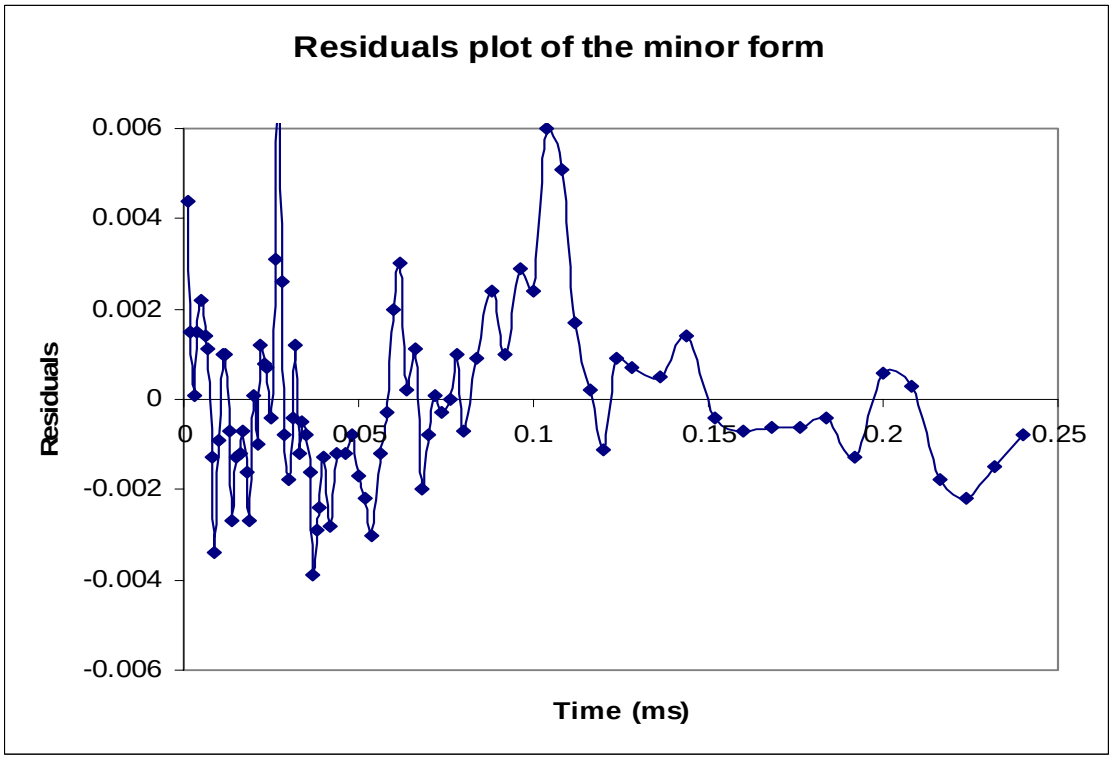

Figure 13: Residuals plot of the minor form at 31.4ºC.

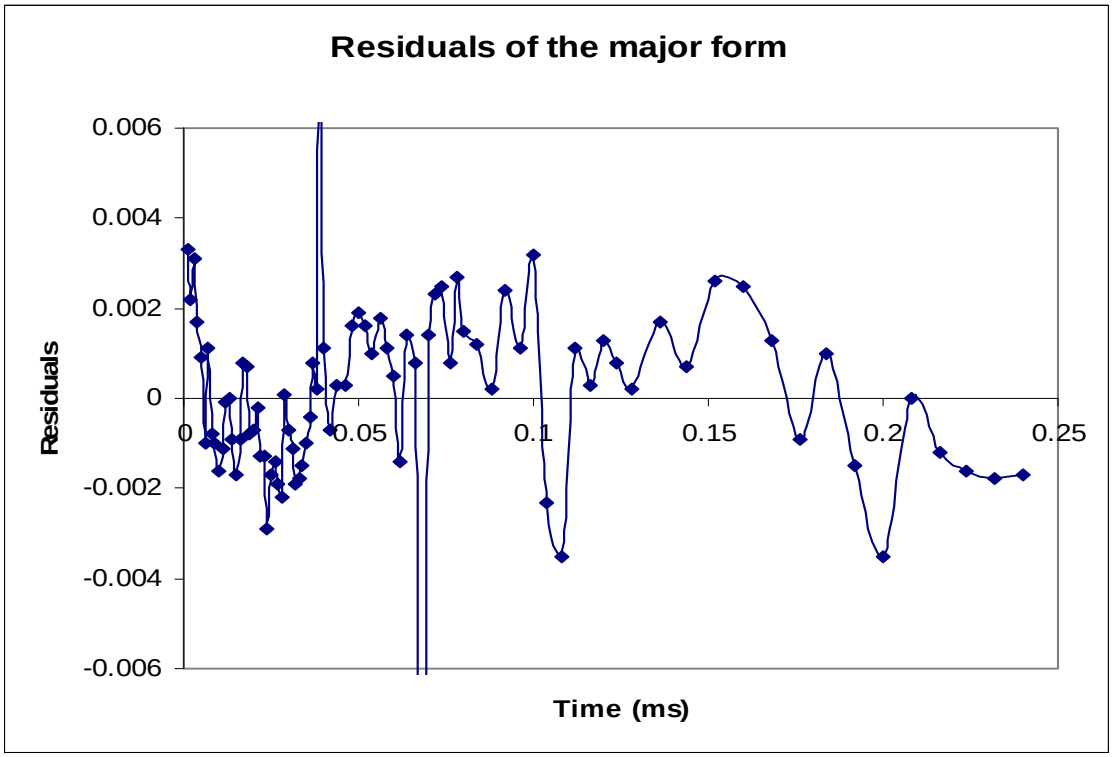

Figure 14: Residuals plot of the major form at 31.4ºC.

3.4. ^{1}H and ^{13}C assignments from the limiting temperature spectra.

Spectral assignment of the proton and carbon-13 spectra was done from a combination of one dimensional and two-dimensional homonuclear and heteronuclear as well as the selective decoupling experiments. These included COSY, EXSY and HSQC. The spectra acquired at -0.2 to 3.4ºC were mostly used as at these temperatures broadening is at its minimum. However, the assignments were not limited to the lowest temperature regime as in other instances some peaks shifted beneath others as peak positions are strongly temperature dependent.

Figure 15 shows the numbering scheme used. The complex has C4 symmetry and in the scheme is presented the asymmetric unit. The ethylene diamine carbons are puckered. One of the two ethylene diamine carbons was arbitrarily assigned position number 1. The protons attached are diastereotopic and would be referred to as axial if they point along the paramagnetic tensor (the *z* direction from the metal centre and perpendicular to the plane formed by the cyclen ring). Protons sticking outwards from the ring are equatorial.

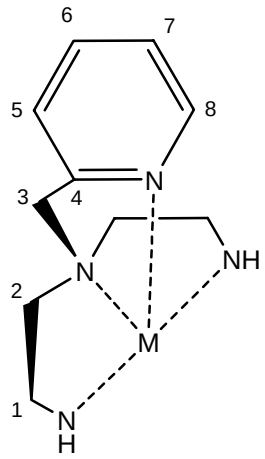

Figure 15: Mirror image about the axis of symmetry of the cyclen ring.

Since europium is known to cause lower frequency paramagnetic shifts, the peak at the lowest frequency (-17.91 ppm) in the proton spectrum (Figure 16) was assigned the axial position on carbon 1, assuming that the metal centre is above the plane formed

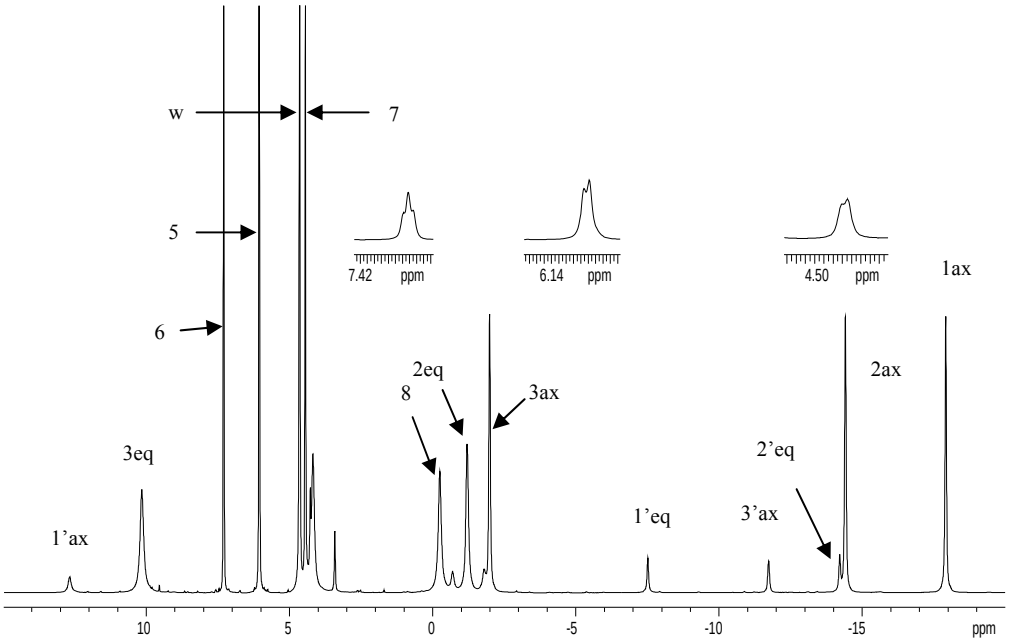

Figure 16: One dimensional proton spectrum of **(I)** at -0.2ºC, (500MHz, D_2O). A prime (‘) symbolize minor form. [*ax* = axial; *eq* = equatorial]

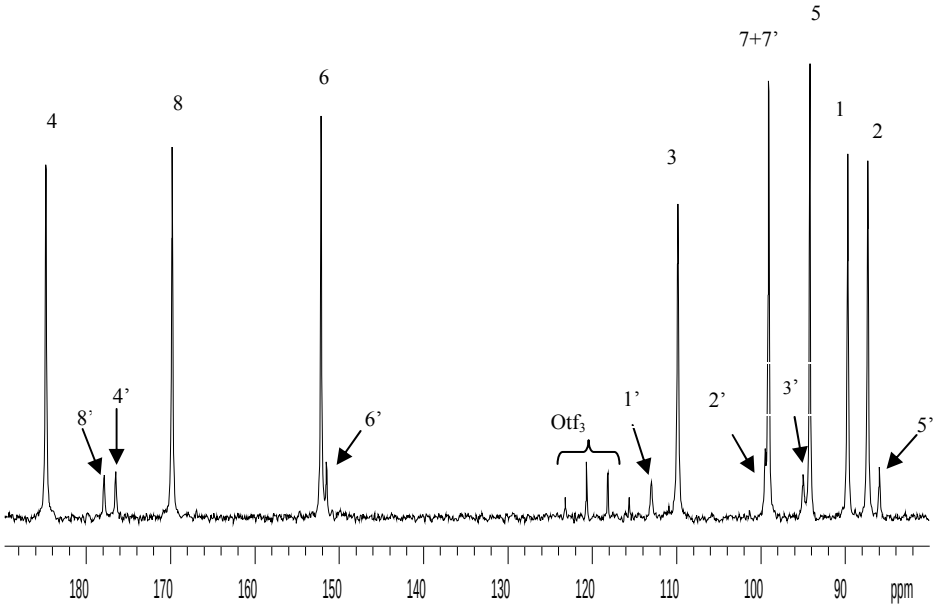

Figure 17: One dimensional carbon-13 spectrum of **(I)** at -0.2ºC, (125MHz, D_2O)

by the ring (or the page). The closer to the paramagnetic centre and the more axial, the more shielded the nuclei and hence the lower the frequency. The next peak would then be the axial proton at carbon 2. The two peaks belong to the major form of the complex. Figure 18 is an HSQC spectrum. The axial proton at 1 has a one bond correlation with carbon at 89.70 ppm, this is carbon 1. Carbon 1 in addition to a one bond correlation to axial proton 1 correlates to another proton at 4.19 ppm. This would be equatorial proton one; pointing away from the paramagnetic centre and being on a carbon next to an electronegative group it exhibits normal shift range for CH_2 group protons. By the same token axial proton 2 has a one bond correlation with a carbon 2 at 87.31 ppm, which in turn correlates with a proton at -1.20 ppm and is assigned equatorial proton 2.

A COSY spectrum (Figure 19) confirms the assignment. Axial proton 1 exhibits a homonuclear scalar coupling to equatorial proton 1, which in turn couples to equatorial proton 2, and equatorial proton 2 couples to axial proton 2. This network forms a closed loop, demonstrating that the first two proton lines at the lowest frequencies indeed belong

to an ethylene diamine fragment. In addition the network does not extend to proton 3 as the proton there is four bonds away. A maximum of three bond coupling is normal for COSY.

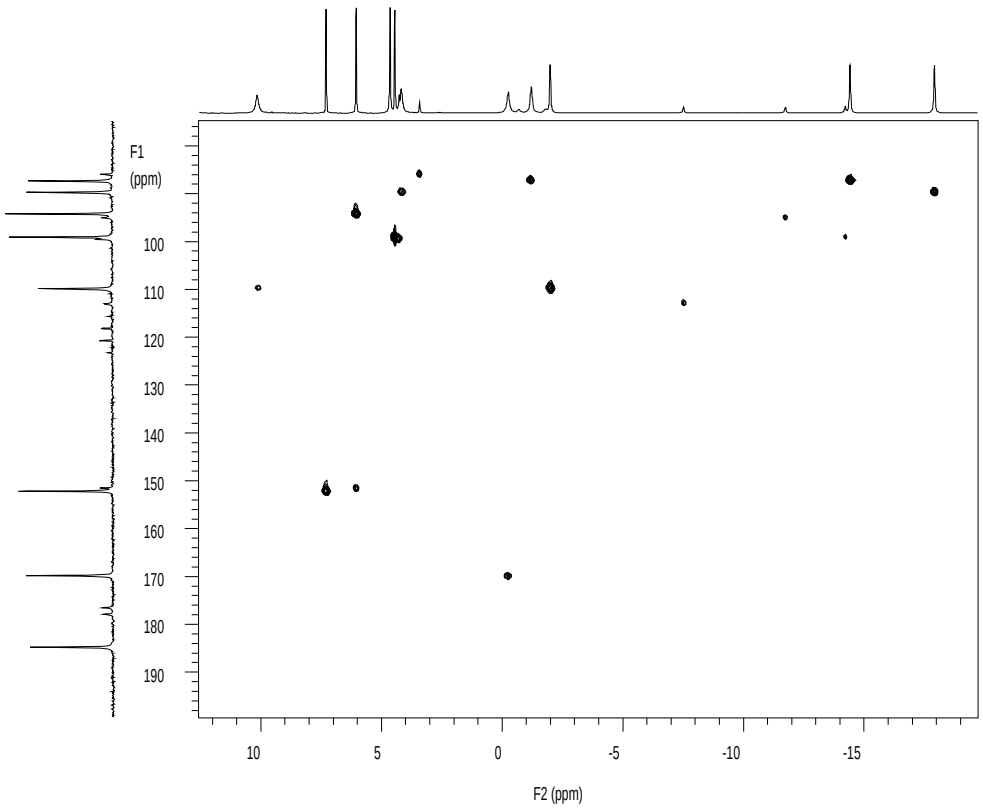

Figure 18: HSQC plot of **(I)** at -0.2ºC (500MHz, D_2O).

A strange observation is that a scalar coupling between axial 1 and axial 2 is not seen on the spectra. However, these can be seen only when the threshold of the plot is taken very low. The problem with taking the threshold too low is that even the noise appears in the spectrum making it look messy and complicated. The cross peak has very low intensity and there is no need to worry about it as the network can be seen without it.

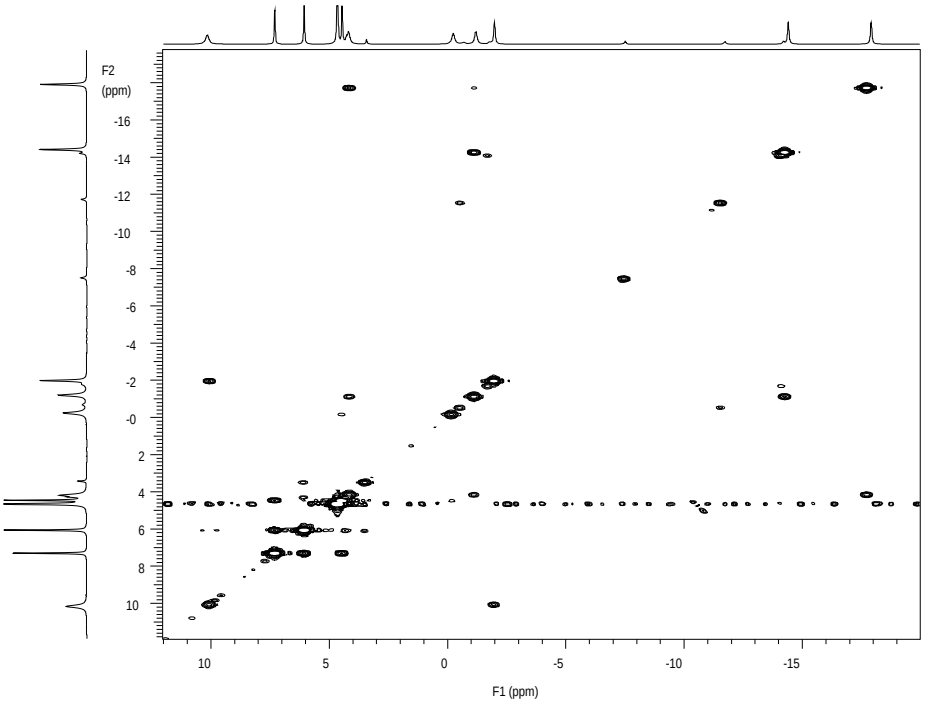

Figure 19: COSY spectrum of **(I)** at 3.4ºC (500MHz, D_2O).

The major peak at -1.98 ppm was assigned as axial proton 3 on the assumption that it is also a highly shielded CH_2 group. A one bond correlation is seen with carbon at 109.85 ppm and in addition, this carbon has a one bond correlation with another proton peak at 10.17 ppm. This was assigned equatorial proton 3 as a result. The fact that the axial proton 3 and equatorial proton 3 have a COSY correlation between themselves only confirms the assignment as the next carbon is quaternary.

The line at 184.82 ppm in the carbon spectrum corresponds to a quaternary carbon 4 by virtue of being highly deshielded from lack of protons attached. In addition, it does not have a one bond correlation with any proton.

COSY and coupling constants were used to assign the pyridyl ring protons. Multiplets are shown as insets in Figure 16. The peak at 7.30 ppm shows a COSY correlation to both 6.06 and 4.46 ppm. The peak at 4.46 ppm further shows a correlation to one at -0.24 ppm.

Assuming the M-N coordination bond of the pyridyl ring causes the proton labeled 8 to point towards the metal centre; this is expected to result in a shift of 8 to low frequency. Hence the line at -0.24 ppm is assigned to proton 8. The line at 4.46 ppm is assigned to proton 7. The proton labeled 6 on the pyridyl ring is the only one expected to have COSY correlation to two other protons. The splitting into a doublet of doublets (^3J = 6.2, 7.1 Hz) of the line at 7.30 ppm is consistent with assigning it to 6 because of its two neighbours. The doublet at 6.06 ppm (^3J = 7.1 Hz) is then assigned to 5. HSQC then provides the carbon assignments for the pyridyl ring.

Minor form peak assignment followed from the major peak assignment, and EXSY was especially useful. The axial proton 1 at -17.91 ppm exchanges with one at 12.69 ppm. This peak was then assigned minor axial 1. Axial proton 2 at -14.41 ppm is in exchange with one at -1.80 ppm thus assigned minor axial 2. HSQC shows correlation of this peak with a minor form at 99.51 ppm. Equatorial proton 2 at -1.20 ppm is in exchange with one at -14.21 ppm and is assigned minor equatorial 2. From HSQC, this minor peak has a one bond correlation with minor form at 99.51 ppm. Therefore peak at 99.51 ppm on the carbon spectrum is the minor form of carbon 2.

Axial proton 3, exchanges with one at -11.73 ppm which is the minor form. A one bond HSQC correlation between the minor axial proton and a carbon at 95.01 ppm means that this is minor carbon 3.

Proton 5 exchanges with a minor form at 3.42 ppm. An HSQC correlation is seen between this peak and one at 85.96 ppm. Proton 6 exchanges with something embedded under proton 5, which is very difficult to notice. From an HSQC this minor form of 6 forms a correlation with a minor carbon line at 151.54 ppm.

Minor forms of carbon 1, 4, 7 and 8 were assigned with the help of selective decoupling. A non decoupled carbon-13 spectrum was acquired after which low power selective decoupling was done on each proton peak in turn. Applying the selective decoupling at minor axial proton 1, the carbon line at 113.00 ppm was enhanced, showing that it is the

minor form of carbon 1. Selectively decoupling minor proton 7, the small multiplets at the base of major proton 7 disappeared, with intensity enhancement, a clear indication that the minor form occurred with the major form of 7. When proton 8 was selectively decoupled, the minor form at 177.87 ppm was enhanced, indicating that this is minor carbon 8. An assumption made was that the minor form of proton 8 was beneath the major form, and the response of one of the minor form in the carbon spectrum confirms the assumption. The carbon line at 176.53 ppm did not respond at all, a clear indication that it is the minor form of carbon 4. This is much expected as this is a quaternary carbon, with no protons to decouple. In addition, the positions of the major and minor forms of 4 are consistent with the normal resonances of quaternary carbons which are also in the vicinity of electronegative groups. [36]

From the above treatment, it can be shown that there are eight major carbon lines consistent with the structure of the highly symmetrical complex. Seven carbon lines corresponding to the minor form are distinctly seen, with the eighth beneath a major one. Ten major proton resonances can be clearly counted in agreement with the proton count on the structure. Three minor proton resonances are buried beneath major ones.

3.5. Thermodynamic parameters determination.

Figure 20, shows the variation of *lnk* with temperature. The rate constants as simulated from the CIFIT program were plotted as *lnk* against reciprocal absolute temperature, and afforded a straight line with a negative slope. The plot describes Eyring equation (equation 1b) from whose slope free enthalpy of reaction was determined to be 76.2 ± 3.0 kJ mol^{-1}. The transmission factor was assumed to be equal to one, as the major isomer dominates and the process is adiabatic. [25]

Other thermodynamic parameters are reported at 298K in table 2. The range of temperatures used was limited (4.6 -22.6ºC) to avoid complications at the lower limiting temperature brought in by decreasing values of T_1, especially the minor form, which increases chances of systematic errors as shown in section 3.3 above. At the higher end of

the temperature the data begin to show deviation from the trend as integral intensity measurements become less accurate due to broadening.

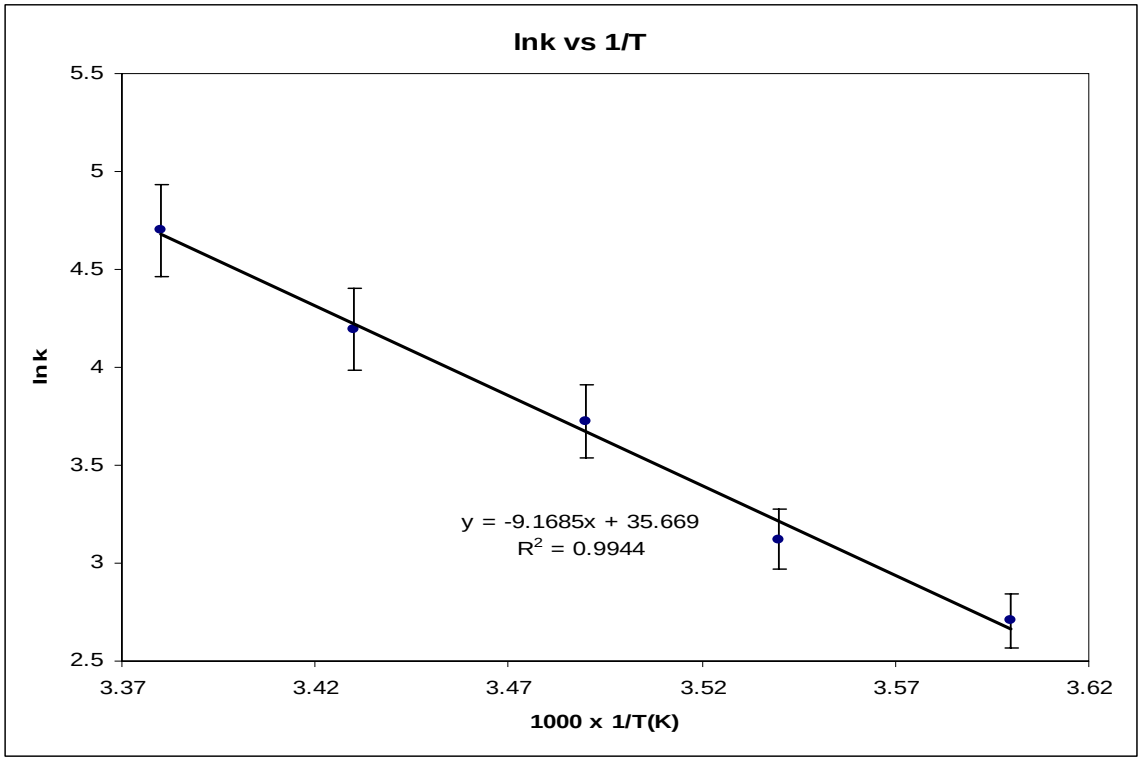

Figure 20: Plot of *ln k* against reciprocal of absolute temperature.

Table 2: Thermodynamic parameters of **I** at 298 K.

Process	E_a (kJmol^{-1})	$\Delta H^{\#}$ (kJmol^{-1})	$\Delta S^{\#}$ (Jmol^{-1})	$\Delta G^{\#}$ (kJmol^{-1})
Isomerization	78.7 ± 3.0	76.2 ± 3.0	60.0 ± 2.3	58.4 ± 3.7

Equilibrium constants are also a good measure of how far a process goes. [37] The equilibrium constants at different temperatures were determined from equilibrium intensities and are listed in table 3. The values of the equilibrium constants are all less than unity, showing that the isomerisation from the major to the minor form is not an energetically favoured process, or it is endothermic.

The values determined above indicate that the isomerization process is not energetically favourable. Exchange between the isomers is therefore unfavourable and does not occur on the NMR timescale.

Table 3: Variation of equilibrium constant with temperature.

T (ºC)	1000/T (K)	K
-0.2	3.66	.136 (.007)
4.6	3.60	.131 (.007)
4.2	3.54	.181 (.010)
13.6	3.49	.178 (.009)
18.2	3.43	.196 (.010)
22.6	3.38	.216 (.012)
27.1	3.33	.218 (.012)
31.0	3.29	.217 (.012)
37.4	3.22	.253 (.014)
41.8	3.18	.232 (.012)

3.6. Carbon-13 Variable Temperature study of the complex.

Variable temperature carbon-13 stacked plot of the title compound is presented in Figure 21. The limiting temperature spectrum (-0.2ºC) shows all the lines from the eight carbons, together with their minor forms (see Figure 17 for the assignments). Although major lines are separated from their exchanging partners by values equal to or less than *ca* 3000Hz, coalescence (major-minor) is completely achieved at around 76.2ºC. This is expected since around room temperature, the minor forms are substantially broadened, and shifted towards the major forms, showing strong chemical shift temperature dependence. The wide spectral width associated with paramagnetic system poses a challenge to the rate at which coalescence is approached.

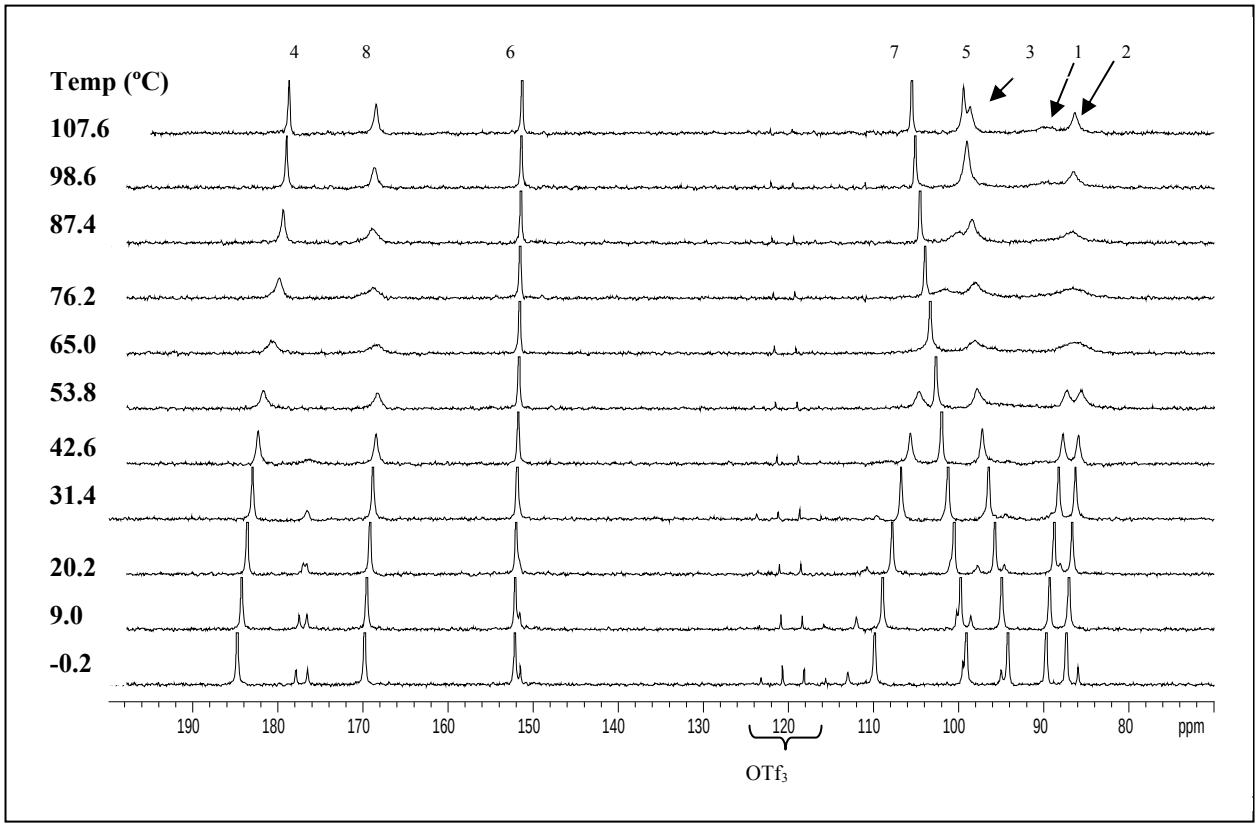

Figure 21: Stacked carbon-13 spectra of **(I)**,(125 MHz, D2O) for temperature range -0.2 to 107.6ºC.

The shift dependence on temperature is clearly illustrated by the major bridge carbon line (3), starting out at 110 ppm at the lower limiting temperature. The line rapidly shifts to lower frequencies with each temperature increment, substantially broadening and probably coalescing with its minor form at 53.8ºC, and ends up at about 99 ppm at the upper limiting temperature. The new chemical shift is not at the population weighted average shift, an anomalous behavior. Under normal circumstances, the shift would be population weighted towards the more populated spin shift, in this case, the major form.

Pyridyl carbon lines (4, 6, 8) exhibit fairly limited temperature dependence of their shifts. Carbon 6 is the least shifted, coalescing the earliest with its minor form as they are the least separated. The shifting pattern of the rest of the lines is not well defined and as a result not well understood.

Carbons 1 and 2 are the cyclen ring carbons and are chemically equivalent with a 1:1 population ratio. Broadening of these lines sets in at around 53.8ºC, further broadening with temperature occurs until the lines are averaged. Further temperature increase causes the lines to be distinctly observed as they appear to become sharper.

This does not seem to be coalescence. Coalescence would mean that there is cyclen ring flipping, causing the two carbons which are magnetically inequivalent (from a puckered configuration) to be equivalent. Observation of the separate cyclen carbons shows that there is no rapid ring flip.

An interesting observation worth mentioning is that despite the fact that the shift patterns are poorly understood, at the upper limiting temperature, the lines associated with the different common chemical environments of carbon-13 are clearly seen. The methylene carbons (1, 2) appear at the lowest frequencies because of high shielding from two protons. These are followed by the bridge methylene and at higher frequencies there are the less shielded aromatic carbons. Carbon 4 appears at the highest frequency by virtue of

being quaternary and 8 comes next to and lower than 4 as it is attached to an electronegative nitrogen atom.

The condition for equally populated spins coalescence and hence cyclen ring flip is given by equation 3:

$$k_c = \frac{\pi \Delta \nu}{\sqrt{2}} \qquad \textbf{3}$$

where $\boldsymbol{k_c}$ is the rate constant at coalescence, $\boldsymbol{\Delta\nu}$ is the chemical shift separation of the spin systems in question, and $\boldsymbol{\pi}$ has its usual meaning.

Since carbon 1 and 2 are separated by 300.87 Hz, the expected $\boldsymbol{k_c}$ is 668.37 Hz, a value much higher than the rate constants attainable in the NMR time scale and temperature window imposed by the solvent system and wide spectral width system under study. The cyclen carbons therefore do not appear to coalesce within the conditions at hand, and this shows that there is no ring flip.

The title complex (**I**) has bulky pyridyl groups appended on all the four arms. Such appendage lends a large amount of steric constraint, and hence rigidity on the cyclen carbons. The high rigidity of the cyclen ring will not easily allow ring flipping. It has been observed that with large pendant ligands, only one isomer at the ring is generally observed in temperature ranges 5 - 80ºC.[18] In addition, the coordination to the metal center is formed through eight (8) highly polarisable N atoms at the cyclen ring and the pyridyl aromatic system. The pyridyl N atoms polarisability is further stabilized by the aromatic system. This observation corresponds well with a review [7] by Parker and Williams in which they alluded to the fact that highly polarisable donor atoms form more stable and rigid metal-N atom bonds. As metal charge to size ratio increases, ring rigidity increases. [14] The system under study has high charge to size ratio, conferring cyclen rigidity. Earlier studies[38, 39] on metal-EDTA complexes, including lanthanides, have shown that charge density determines lability of the metal-nitrogen bonds. For EDTA

complexes, it was determined that a nuclear radius of 1Å was one above which the metal-nitrogen bond lability sets in. Careful scrutiny of these arguments, and taking into consideration that the DOTA cyclen is predisposed to form relatively rigid complexes with the metal [7], it is expected that with the more rigid and strain free cyclen used here, the benchmark value would be higher. In addition, the lability decreases as the charge density increases. [22] This is in support of the notion that the metal-nitrogen bonds do not invert in the NMR timescale.

Moreover, the four bulky pyridyl ligands adopt a more equatorial configuration with respect to the ring plane for steric reasons. It is argued that this configuration is biased towards one isomer[1] rather than the other, supporting the idea that the ring is not flipping.

Ring flip is ruled out based on the aforementioned facts. If ring flip took place, this would mean that the bulky pendant ligands would be in an energetically unfavorable axial orientation. Since the polarisable Eu-N is very strong, a ring flip would require some of the bonds to stretch, an unlikely event given the networked bond strengths.

3.7. Most probable isomers observed.

Dissolution of the complex in water gives rise to two isomeric forms in dynamic equilibrium as shown by the proton and carbon-13 NMR. The two possible diastereomers are a square antiprimatic (SAP) and twisted square antiprismatic (TSAP) geometries. [12, 13] From the peak intensities, it is clear that one isomer is dominant. A challenging task is to postulate which one of the two; SAP or TSAP; is the dominant isomer.

It has been shown that with larger pendant groups, the TSAP is the more thermodynamically favoured diastereomer. [18] The complex in the present study is appended with four pyridyl arms instead of the acetate arms as found in the usual DOTA. In a bid to minimize steric factors borne from the fact that DOTA-like macrocycles are already crowded, the metal-nitrogen (pyridyl) bonds are longer (2.668 Å on average) [40] than the bonds in DOTA TSAP (2.680 Å) and SAP (2.641 Å), 2.661 Å on average . [12, 13]

This would imply that the arms tend more towards an equatorial spatial arrangement with respect to the cyclen plane.

A solution of **I** was also prepared in acetone-d_6. The results were very similar to the ones for the solution in water- d_2, having major and minor peaks. The proton spectrum indicated ten proton peaks in both solutions. On introducing a drop of water into the acetone solution, the minor forms' intensities increased in favour of the major forms. Further introduction of water led to development of other peaks, a confusing observation. One possible explanation might be that although steric effects exclude water, the fact that water is more polar than acetone may mean that water has a competitive edge for the high charge density at the metal centre. This may lead to another equilibrium being set up.

Several workers have shown that pendant arm bulk favours one of the isomers [1, 10, 18]. It was also shown that with the TSAP geometry, crowding expels water molecules.[41] The acetone results suggest that the predominant isomer is TSAP, which picks up a water molecule, but with a limit to the number which can be incorporated. This leads to the minor form increasing. Moreover, Natrajan *et al* [40] observed that the complex exhibited slow (luminescence timescale) water exchange, consistent with crowding and leading to water expulsion. The observation of both the water-free and mono-aquo ions in the NMR spectrum implies that water exchange is slow on the NMR timescale.

3.8. Limitations presented by the system studied.

Complete band shape (CBS) method is a superior method for exchange studies. [25] Studies with this method encompass wider temperature ranges and measurement error effects are kept to a minimum because all the parameters are used for the simulation. Use of all the parameters associated with the exchange compensates for the errors.

In this experiment, CBS could not be used to follow and verify the ring flipping from the proton spectra. This is because of the limits imposed by the system itself. The huge paramagnetic line broadening causes line overlap at lower temperatures, precluding

chances of extending to higher temperatures where ring flip could possibly be observed. As a result, line shape broadening means that the temperature range at which peak parameters could be accurately determined is narrowed. Peak shifts are strongly temperature dependent as they shift with any small temperature increment, while they are expected to shift only when substantial broadening has taken place.

The carbon lines are narrow and the carbon lines variation can be followed over a wider range than the proton, making them better candidates for CBS studies. A problem to optimally implement CBS on the carbon-13 is caused by signal to noise limitations. CBS requires good signal to noise ratios. The wide proton spectral width, in excess of 15 kHz, causes decoupling problems. No standard decoupling procedure is able to effectively perform a broadband proton decoupling at this width.

Changing decoupler power levels from 42 to 48 dB, equivalent to doubling the decoupler channel power was the only solution. This risked burning and damaging the probe head. Decoupler duty cycle minimization to 10% (see experimental section) meant that NOE's were lost, resulting in poor signal to noise. Therefore although the solution was chemically saturated, enough signal to noise could not be obtained to apply CBS effectively.

Solution freezing and temperature settings of the instrument meant that sufficiently low the temperatures (limiting temperatures) could not be established. As a result, chemical shift separations ($\delta\nu$), limiting linewidths, and coupling constants could not be accurately determined to be fed in as data required by the CBS. All these were determined at temperatures near the limiting ones as the solution froze before getting to the limiting temperatures. This would mean that many assumptions and approximations would be made of the data leading to huge amounts of systematic errors.

Chemical shift and spin populations strong temperature dependence is another problem. The major-minor shift patterns are not clear, especially in the carbon-13 variable temperature study. Normal population weighted average shifts could not be accurately

established as they did not follow the normal trend where the shifts are weighted towards the more populated spin system for unequally populated systems. This information would be anomalous for the CBS even for the pyridyl isomerisation process (see 3.6, discussion of carbon 3 line shift)

The solvent system, temperature window and δν also limited the range. As shown in 3.6, k_c of this system was well beyond the upper temperature limit. CBS requires that all the parameters be used to compensate for errors. That is parameters at the low temperature limit, at coalescence and beyond coalescence must be determined accurately and used. In addition, it seems that coalescence of this system due to wide spectral widths is beyond the NMR timescale corresponding to $k = 10^{-1}$ - 10^{3} Hz (10 -100 kJmol^{-1}). Although CBS can extend the regime to higher values, the solvent system is a decisive limit. Thus no access to parameters at the range from coalescence and beyond means CBS cannot be fruitfully implemented.

4 Conclusion and future outlook.

4.1. General conclusions on stability and isomerism of the complex.

Based on the above results and literature, we conclude that the cyclen ring is rigid on the NMR timescale. Ring flip is not observed at least under the experimental conditions we investigated. Involvement of four highly polarizable nitrogen atoms, the high charge to size ratios, and the bulky picolyl ligands together ensure a highly rigid macrocycle ring.

The only isomerization process that is apparent in this case is the arm rotation about the axial symmetry of the metal centre. High activation energies of this process are a clear hint that the activation energy associated with the ring flip must be considerably high. It has been proved by a number of workers that increasing bulk on the macrocycle ring increases rigidity, making ring flipping a highly unlikely occurrence.

The bulky picolyl ligands, luminescence studies and the spectra in acetone support the unsolvated TSAP dominance in the isomer equilibrium of **(I)**.

4.2. Future activities.

Having seen that solvent system limits further studies of dynamics of the complex, efforts should be directed toward finding a solvent system which will enable the temperature range to be increased. However, care should be taken that the new solvent system does not undergo a chemical reaction with the system yielding a completely different chemical species. Since signal to noise ratios are crucial in CBS, high solubility of the complex in the solvent must be ensured. This done, CBS can be used on the carbon-13 spectrum to study the system and determine the rate constants at the fast exchange regime. The proton spectra would not be good candidates for CBS because of the extensive paramagnetic broadening of the system and peak overlap.

Another parameter that needs careful attention is the T_1 variation with temperature. It was observed that at 37.4ºC, the fitted T_1 value did not follow a trend followed by other temperatures' T_1 values. An investigation into the behavior of the fitting program at this temperature must be clearly established or the behaviour of the complex at this temperature must be well studied. It is tempting to think that at this temperature, there is a possibility of rapid bond breaking and reformation as the system enters the intermediate exchange regime.

The same system can be tried on other spectrometers, whose temperature settings are thought to be highly reliable. However, this will not yield overly better results as hardware drift with temperature is a universal problem which is very far from being solved. All spectrometer temperature setting hardware suffer this drift as temperatures depart from ambient values and the best compromise is temperature calibration.

More solid state studies should be done to determine the parameters of possible isomers present in **(I).**

5 References.

1. Bari, L., Pescitelli, G., Sherry, A.D., Woods, M., *Inorg. Chem.* **2005**, 8391-8398.
2. Delgado, R., Costa, J., Krassimira, P.G., Lima, L.M.P, *Pure Appl. Chem.* **2005,** 77, (3), 569-579
3. Pope, S. J. A., Laye, R.H., *Journal of the Chemical Society, Dalton Transactions* **2006**, 3108-3113.
4. http://www.smarterscience.com/eurosandeuropium.html (11 August 2006),
5. Long, N. J., Bottrill, M., Kwok, L., *Chem. Soc. Rev.* **2006,** 35, 557-571.
6. Faulkner, S., Pope, S.J.A., Burton-Pye, B.P., *Applied Spectroscopy Reviews* **2005,** 40, 1-35.
7. Parker, D., Williams, J.A.G, *Journal of the Chemical Society. Dalton Transactions* **1996**, 3613-3628.
8. Faulkner, S., Mathews, J.L., *Comprehensive Coordination Chemistry*. 2nd ed.; Elsevier Pergamon: Oxford, 2004; Vol. 9.
9. Hancock, R. D.; Maumela, H.; deSousa, A. S., *Coord. Chem. Rev.* **1996,** 148, 315-347.
10. Bianchi, A., Calabi, L., Corana, F., Fontana, S., Losi, P., et al, *Coord. Chem. Rev.* **2000,** 204, 309-393.
11. Desreux, J. F., *Inorg. Chem.* **1980,** 19, 1319-1324.
12. Desreux, J. F., Spirlet, M.,, *Inorg. Chem.* **1984,** 23, 359-363.
13. Benetollo, F., Bombieri, G., Aime, S., Botta, M., *Acta Crystallography* **1999,** C55, 353-356.
14. Aime, S., Barge, A., Botta, M., Fasano, M., Ayala, J.D., Bombirei, G., *Inorg. Chim. Acta* **1996,** 246, 423-429.
15. Aime, S., Botta, M., Fasano, M., Marques, P.M.P., Geraldes, C.F.G., Pubanz, D., Merbach, A.E.,, *Inorg. Chem.* **1997,** 36, 2059-2068.
16. Jacques, V., Desreux, J.F., *Inorg. Chem.* **1994,** 33, 4048-4053.
17. Aime, S., Botta, M., Ermondi, G., *Inorg. Chem.* **1992,** 31, 4291-4299.
18. Aime, S., Batsanov, A.S., Botta, M., Howard, J.A.K., Parker, D., Senanayake, K., Williams, G., *Inorg. Chem.* **1994,** 33, 4696-4706.
19. Skoog, D. A., Holler, F.J., Nieman, T.A, *Principles of Instrumental Analysis*. Harcourt Brace College Publishers: Florida, 1998; p 363.
20. Forsen, F., Hoffman, R.A.,, *J. Chem. Phys.* **1963,** 39, 2892-2901.
21. Hoffman, R. A., Forsen, F., *Prog. Nucl. Magn. Reson. Spectrosc.* **1966,** 1, 15-204.
22. Ba, Y., Han, S., Ni, L., Su, T., Garcia, A. , *J. Chem. Educ.* **2006,** 83, (2), 296-298.
23. Bain, A., Duns, G.J., Rathgeb, F., Vanderkloet, J., *J. Phys. Chem.* **1995,** 99, 17338-17343.
24. Friebolin, H., *Basic One-and Two-Dimensional NMR Spectroscopy*. Wiley-VCH: Weinheim, 2005; p 162-166, 305-316.
25. Sandstrom, J., *Dynamic NMR Spectroscopy*. Academic Press inc.: London, 1982; p 77-123.
26. Jarek, R. L., Flesher, R.J., Shin, S.K., *J. Chem. Educ.* **1997,** 74, 978-982.

27. Keeler, J., *Understanging NMR Spectroscopy*. John Wiley and Sons Ltd: West Sussex, 2005; p 187-243.
28. Roberts, J. D., *ABC's of FT-NMR*. University Science Books: Carlifonia, 2000; p 182-210.
29. Varian, I., *VNMR Command and Parameter Reference*. Varian, Inc: California, 2001; p 561-565.
30. Varian, I., *User Guide: Liquids NMR*. Varian, Inc: California, 2001; p 37-40.
31. Berger, S., Braun, S., *200 and More NMR Experiments*. Wiley-VCH: Weinheim, 2004; p 140-164.
32. Warnking, J. M., Pike, G.B., *Magnetic Resonance in Medicine* **2004,** 52, 1190-1199.
33. Bain, A., Fletcher, D.A., *Mol. Phys.* **1998,** 95, 1091-1098.
34. http://www.chemistry.mcmaster.ca/bain/ (17 August 2006),
35. Claridge, T. D. W., *High Resolution NMR Techniques in Organic Chemistry*. Elsevier Science Ltd: Oxford, 1999; Vol. 19, p 116-124, 346-347.
36. Breitmaier, E., *Structure Elucidation by NMR in Organic Chemistry: A Practical Guide*. 3rd Revised ed.; John Wiley and Sons Ltd: West Sussex, 2002; p 12-14.
37. Atkins, P., De Paula, J., *Atkin's Physical Chemistry*. 8th ed.; Oxford University Press: Oxford, 2006; p 791-829.
38. Baisden, P. A., Choppin, G.R., Garret, B.B., *Inorg. Chem.* **1977,** 16, 1367-1372.
39. Gennaro, M. C., Miriti, P., Casalino, C., *Polyhedron* **1983,** 2, (1), 13-18.
40. Natrajan, L., In University of Manchester: 2006.
41. Polasek, M., Rudovsky, J., Hermann, P., Lukes, I., Ander Elst, L., Muller, R.N., *Chemical Communications* **2004**, 2602-2603.

Appendix A

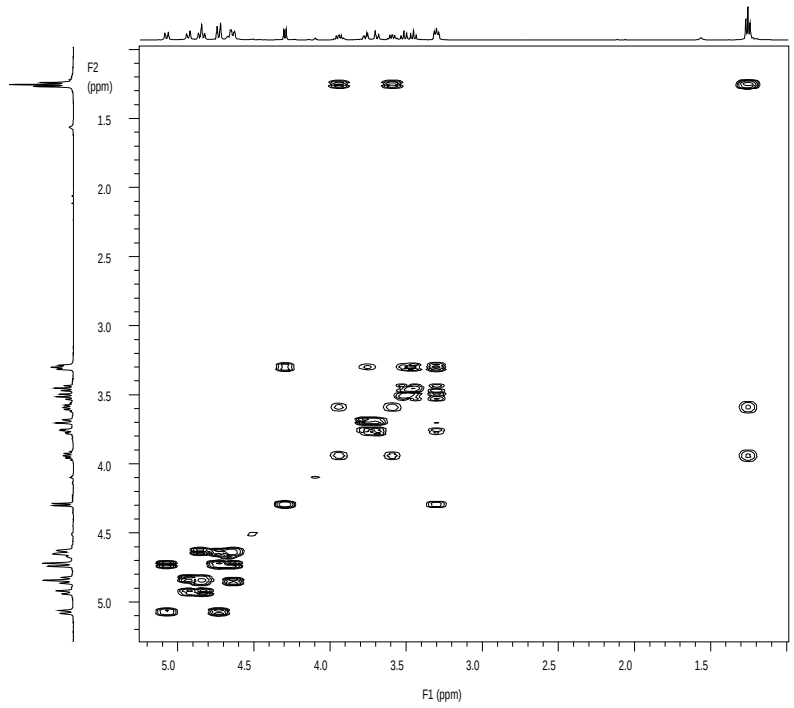

Figure A1: Full COSY spectrum of **(3).** (500 MHz, $CDCl_3$)

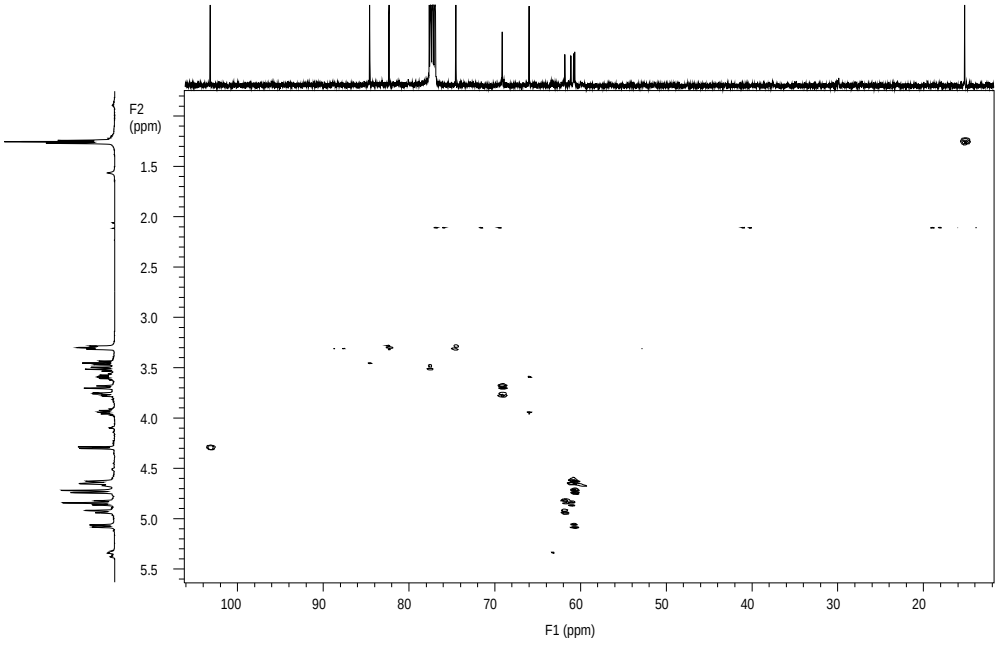

Figure A2: Full HMQC spectrum of **(3)**. (500 MHz, $CDCl_3$)

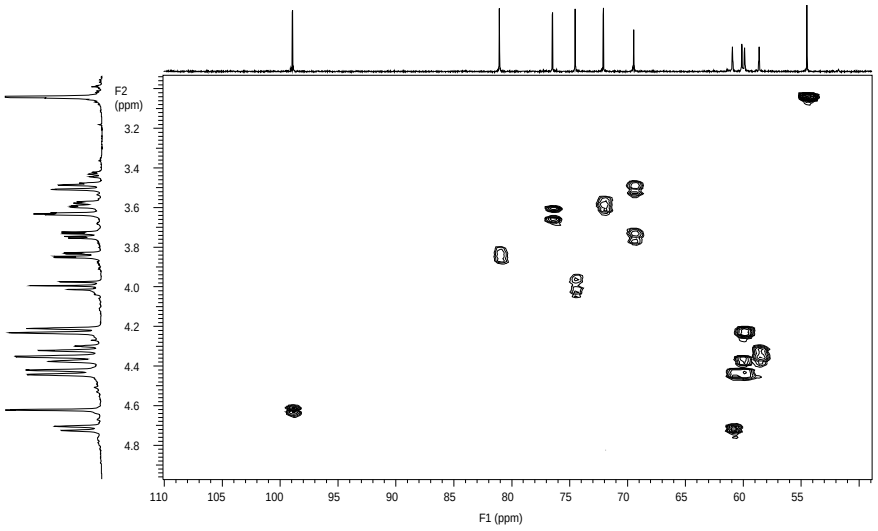

Figure A3: Full HSQC spectrum of **(6).** (500 MHz, C_6D_6)

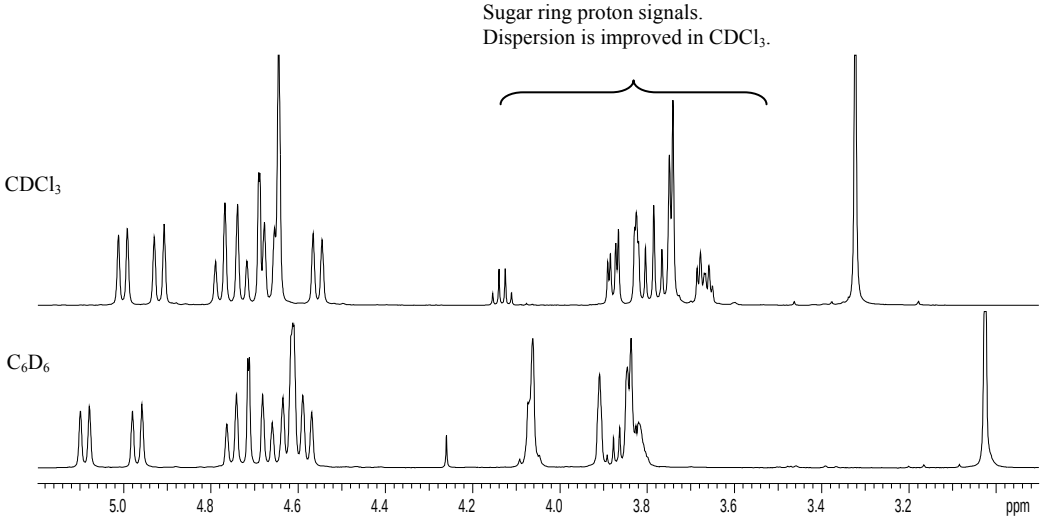

Figure A4: Proton spectrum of the DFBn mannopyranoside derivative showing the unexpected dispersion improvement when $CDCl_3$ is used as a solvent. (500 MHz).

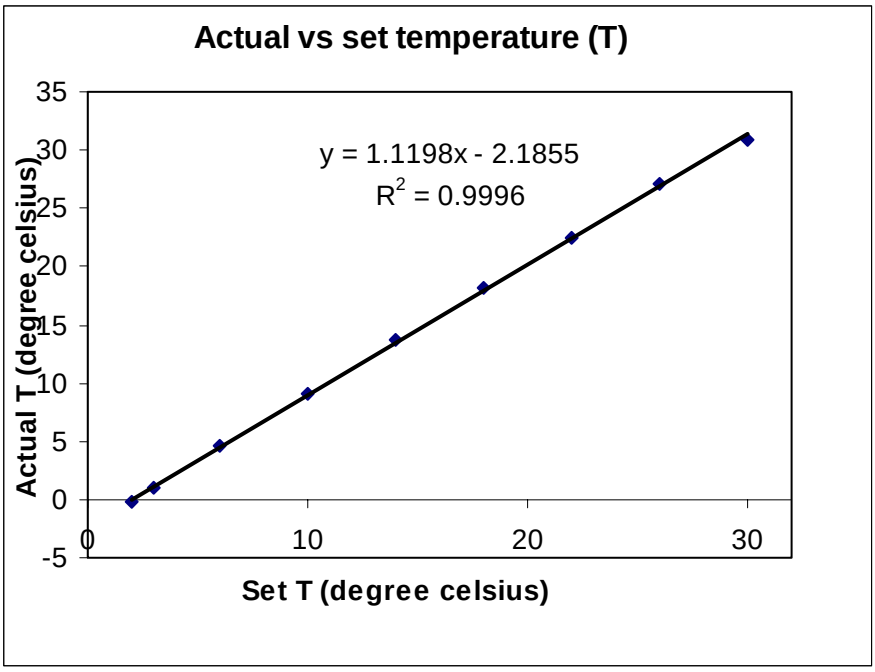

Figure A5: A plot of actual versus set temperature (degrees Celsius).

Appendix B

Lectures and seminars from Invited speakers attended.

1. Asymmetric Organocatalysis with Amines and Amino Acids; Prof. B. List (26/10/05)
2. New chemistry of Oxides and microporous materials; Prof. M.J. Rosseinsky, (09/11/05)
3. Mass spectrometry: the analytical challenge of the post-genomic era; Prof. J. Thomas-Oates, (30/11/05).
4. Using Biomolecules to assemble Nanoscale Wires; Prof. D. Fitzmaurice, (25/01/06)
5. Applications of NMR to heterogenous systems; Prof. P. Belton, (01/02/06).
6. The Message in the molecule: Probing Polymer Sequences with a molecular tweezer, (08/02/06).
7. New Biophysical tools to study biomolecules and living cells based on a single molecule fluorescence and a scanned nanopipette, Dr. D. Klenerman, (15/02/06).
8. Transition metal complexes: where experiments and theory meet; Prof. R. Perutz, (01/03/06).
9. Enzymatic C-F bond formation. The isolation and application of a fluorination enzyme, Prof. D. O'Hagan, (08/03/06).
10. Olefin Metathesis: Fundamental Science to Commercial Applications; Prof. R.H. Grubbs, (20/06/06).

Conferences and Meetings.

1. NMR Discussion Group Christmas Meeting; University of London, Birkbeck College, (15/12/05).
2. Euromar Conference; University of York, (16 – 21/07/06). I presented a poster titled: “Evaluation of a novel protecting group as an aid in assigning spectra of saccharides.”